AD-A092 399 NAVAL POSTGRADUATE SCHOOL MONTEREY CA F/G 8/14
LOW FREQUENCY GEOMAGNETIC FLUCTUATIONS (.04 TO 25 HZ) ON LAND A--ETC(U)
JUN 80 G R MCDEVITT, B B HOMAN

UNCLASSIFIED NL

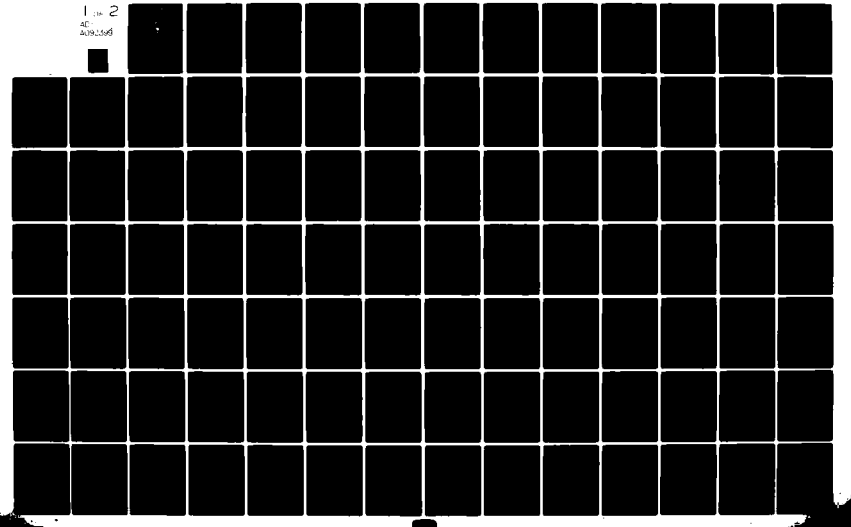

NAVAL POSTGRADUATE SCHOOL

Monterey, California

THESIS

LOW FREQUENCY
GEOMAGNETIC FLUCTUATIONS (.04 TO 25 Hz)
ON LAND AND ON THE FLOOR OF MONTEREY BAY

by

Gerald R. McDevitt
and
B. Bert Homan

June 1980

Thesis Advisor: O. Heinz

Approved for public release; distribution unlimited

SECURITY CLASSIFICATION OF THIS PAGE (When Data Entered)

REPORT DOCUMENTATION PAGE

READ INSTRUCTIONS BEFORE COMPLETING FORM

1. REPORT NUMBER	2. GOVT ACCESSION NO. AD-A092399
3. RECIPIENT'S CATALOG NUMBER (9)	
4. TITLE (and Subtitle) (6) Low Frequency Geomagnetic Fluctuations (.Ø4 to 25 Hz) on Land and on the Floor of Monterey Bay.	5. TYPE OF REPORT & PERIOD COVERED Masters Thesis, June 1980
	6. PERFORMING ORG. REPORT NUMBER
7. AUTHOR(s) (10) Gerald R./McDevitt B. Bert/Homan	8. CONTRACT OR GRANT NUMBER(s) (12) 112
9. PERFORMING ORGANIZATION NAME AND ADDRESS Naval Postgraduate School Monterey, California 93940	10. PROGRAM ELEMENT, PROJECT, TASK AREA & WORK UNIT NUMBERS
11. CONTROLLING OFFICE NAME AND ADDRESS (11) Naval Postgraduate School Monterey, California 93940	12. REPORT DATE June 1980
	13. NUMBER OF PAGES 111
14. MONITORING AGENCY NAME & ADDRESS(if different from Controlling Office) Naval Postgraduate School Monterey, California 93940	15. SECURITY CLASS. (of this report) Unclassified
	15a. DECLASSIFICATION/DOWNGRADING SCHEDULE

16. DISTRIBUTION STATEMENT (of this Report)

Approved for public release; distribution unlimited.

17. DISTRIBUTION STATEMENT (of the abstract entered in Block 20, if different from Report)

18. SUPPLEMENTARY NOTES

19. KEY WORDS (Continue on reverse side if necessary and identify by block number)

Low frequency geomagnetic measurements
Geomagnetic fluctuations in an ocean environment

20. ABSTRACT (Continue on reverse side if necessary and identify by block number)

A coil antenna consisting of approximately 6000 turns of copper wire was ~~utilized~~ used to measure the horizontal component of fluctuations of the earth's magnetic field on the floor of Monterey Bay in water depth of approximately 50 meters. The results indicate that the power spectral density of the fluctuations varies from $10nT^2/Hz$ at 0.04 Hz to $10^{-6}nT^2/Hz$ at 25 Hz, a monotonic decrease of about 6 dB/ octave, except in the 8-20 Hz region where the Schumann resonances occur. While the sensitivity of the equipment was insufficient

DD FORM 1 JAN 73 1473 (Page 1) EDITION OF 1 NOV 65 IS OBSOLETE S/N 0102-014-6601

251450

SECURITY CLASSIFICATION OF THIS PAGE (When Data Entered)

to measure the vertical component of the fluctuation we can put an upper limit of 10^{-3} nT^2/Hz at 1 Hz and 10^{-6}(nT)^2/Hz at 10 Hz on the magnitude of this component. The same sensor was also used to measure various components of the field fluctuations at a remote land site (Chew's Ridge). In the frequency range observed the general shape of the spectra was similar to those obtained at sea. However, a strong azimuthal variation at certain frequencies was noted in the land data. The possibility that these directional signals are of man made origin cannot be excluded at this time.

Approved for public release; distribution unlimited

Low Frequency Geomagnetic Fluctuations (.04 to 25 Hz) on Land and on the Floor of Monterey Bay

by

Gerald R. McDevitt
Lieutenant Commander, United States Navy
B.S. in Computer Science, North Carolina State University

and

B. Bert Homan
Lieutenant, United States Navy
B.S. in Physics, Clemson University

Submitted in partial fulfillment of the
requirements for the degree of

MASTER OF SCIENCE IN PHYSICS

from the

NAVAL POSTGRADUATE SCHOOL
June 1980

Authors _____

_____

Approved by: _____
Thesis Advisor

_____
Second Reader

_____
Chairman, Dept. of Physics and Chemistry

_____
Dean of Science and Engineering

ABSTRACT

A coil antenna consisting of approximately 6000 turns of copper wire was utilized to measure the horizontal component of fluctuations of the earth's magnetic field on the floor of Monterey Bay in water depth of approximately 50 meters. The results indicate that the power spectral density of the fluctuations varies from $10nT^2/Hz$ at 0.04 Hz to $10^{-6}nT^2/Hz$ at 25 Hz, a monotonic decrease of about 6 dB/octave, except in the 8-20 Hz region where the Schumann resonances occur. While the sensitivity of the equipment was insufficient to measure the vertical component of the fluctuation we can put an upper limit of $10^{-3}nT^2/Hz$ at 1 Hz and $10^{-6}(nT)^2/Hz$ at 10 Hz on the magnitude of this component.

The same sensor was also used to measure various components of the field fluctuations at a remote land site (Chew's Ridge). In the frequency range observed the general shape of the spectra was similar to those obtained at sea. However, a strong azimuthal variation at certain frequencies was noted in the land data. The possibility that these directional signals are of man made origin cannot be excluded at this time.

TABLE OF CONTENTS

I. INTRODUCTION ---------- 11

II. BACKGROUND ---------- 12

A. SOURCES OF GEOMAGNETIC FLUCTUATIONS ------- 12

B. EM PROPAGATION IN LAYERED CONDUCTING MEDIA ---------- 15

C. GEOMAGNETIC FORECASTS ---------- 21

D. REVIEW OF EARLIER WORK ---------- 22

III. EXPERIMENTAL EQUIPMENT AND TESTS ---------- 24

A. EQUIPMENT CONFIGURATION ---------- 24

1. DATA ACQUISITION EQUIPMENT ---------- 24

2. DATA ANALYSIS EQUIPMENT ---------- 28

3. UNDERWATER EQUIPMENT ---------- 30

B. SENSOR SENSITIVITY ---------- 33

1. THEORETICAL ---------- 33

2. EXPERIMENTAL ---------- 36

C. SYSTEM TRANSFER FUNCTION ---------- 43

D. SYSTEM NOISE ---------- 48

IV. EXPERIMENTAL RESULTS ---------- 52

A. UNDERWATER DATA ---------- 52

B. LAND DATA ---------- 52

C. DISCUSSION AND CORRELATION OF DATA -------- 74

V. EQUIPMENT/SYSTEM IMPROVEMENT AND RECOMMENDATIONS ---------- 77

APPENDIX A EQUIPMENT SCHEMATICS ---------- 81

APPENDIX B EQUIPMENT USAGE ---------- 86

APPENDIX C BOULDER PAPERS ---------- 90
APPENDIX D TRANSFER FUNCTION USAGE ---------- 105
LIST OF REFERENCES ---------- 107
INITIAL DISTRIBUTION LIST ---------- 109

LIST OF ILLUSTRATIONS

1. Power Spectrum of Geomagnetic Disturbances Observed on the Earth's Surface ---------- 13

2. Electromagnetic Propagation in a Three Layer Medium (Plane Waves) ---------- 17

3. Induced Magnetic Field in Terms of Incident Field (Bi) on the surface ---------- 20

4. General Hookup of Data Taking Equipment --------- 25

5. Sensor Dimensions ---------- 25

6. General Hookup of Data Analysis Equipment ------- 28

7. Schematic of Experimental Layout for at Sea Measurements ---------- 31

8. Graphical Depiction of Theoretical Sensor Sensitivity ---------- 35

9. Calculation of the Magnetic Field on the Axis of a Current-Carrying Ring ---------- 39

10. Hookup for Measuring Sensor Sensitivity ---------- 39

11. Helmholtz Coil Schematic for Measuring Sensor Sensitivity ---------- 39

12. Theoretical and Experimental Sensor Sensitivity (Method I) ---------- 41

13. Theoretical and Experimental Sensor Sensitivity (Method II) ---------- 42

14. Preamplifier Gain Characteristics Curve --------- 45

15. Lowpass Gain Characteristics of the VCO/FVC Combination ---------- 46

16. System Transfer Function Curve ---------- 47

17. Total rms Noise Voltage Referred to Preamplifier Input ---------- 51

18. Horizontal Magnetic Field Fluctuations 4/14/80 .04-1 Hz 1020-1100 ---------- 54

19. Horizontal Magnetic Field Fluctuations
4/14/80, 1-25 Hz 1020-1100 ---------- 55

20. Horizontal Magnetic Field Fluctuations
4/18/80, .04-1 Hz, 0840-0925 ---------- 56

21. Horizontal Magnetic Field Fluctuations
4/18/80, 1-25 Hz,0840-0925 ---------- 57

22. Horizontal Magnetic Field Fluctuations
4/18/80, .04-1 Hz, 0955-1040 ---------- 58

23. Horizontal Magnetic Field Fluctuations
4/18/80, 1-25 Hz, 0955-1040 ---------- 59

24. Horizontal Magnetic Field Fluctuations
4/18/80, .04-1 Hz, 1130-1215 ---------- 60

25. Horizontal Magnetic Field Fluctuations
4/18/80, 1-25 Hz, 1130-1215 ---------- 61

26. Horizontal Magnetic Field Fluctuations
4/18/80, .04-1 Hz, 1250-1340 ---------- 62

27. Horizontal Magnetic Field Fluctuations
4/18/80, 1-25 Hz, 1250-1340 ---------- 63

28. Horizontal Magnetic Field Fluctuations
4/18/80, .04-1 Hz, 1410-1500 ---------- 64

29. Horizontal Magnetic Field Fluctuations
4/18/80, 1-25 Hz, 1410-1500 ---------- 65

30. Magnetic Field Fluctuations
5/1/80, .04-1 Hz, 1100-1130 ---------- 66

31. Magnetic Field Fluctuations
5/1/80, 1-25 Hz, 1100-1130 ---------- 67

32. Magnetic Field Fluctuations
5/1/80, 1-25 Hz, 1140-1210 ---------- 68

33. Magnetic Field Fluctuations
5/1/80, 1-25 Hz, 1215-1245 ---------- 69

34. Magnetic Field Fluctuations
5/1/80, 1-25 Hz, 1250-1320 ---------- 70

35. Magnetic Field Fluctuations
5/1/80, 1-25 Hz, 1330-1400 ---------- 71

36. Magnetic Field Fluctuations
5/1/80, 1-25 Hz, 1415-1445 ---------- 72

37. Magnetic Field Fluctuations
5/1/80, 1-25 Hz, 1500-1530 ---------- 73

38. Schematic of Preamplifier Circuit ---------- 82

39. Schematic of Mixer Circuit ---------- 83

40. Schematic of 2 KHz Reference
Oscillator Circuit ---------- 84

41. Schematic of Voltage-Controlled
Oscillator Circuit ---------- 85

ACKNOWLEDGEMENT

Many persons were contributors to this endeavor, both directly and indirectly. We would like to take this opportunity to express our gratitude to the many people who made this small part of a continuing project a success. First, to Professors Heinz, Moose, and Fraser-Smith who offered and gave support, guidance, and viable information throughout the research.

We thank the personnel of the Research Department for their diligent efforts in design and construction of electronic components, which made the project possible. Their support in other areas is also appreciated.

A special thanks is due Mr. Thomas Maris of the Physics and Chemistry Department who always seemed to have the right solution for the problem at hand.

Much thanks is owed to the Master and Crew of the Research Vessel ACANIA. If not for their expertise, patience, and understanding of the deployment of the data taking equipment, much less data would have been gathered.

Finally, we owe a special thanks to our wives, Dee Dee Homan and Sandra McDevitt for their patience, support, and understanding when long hours demanded our energies.

I. INTRODUCTION

This thesis research is a part of an ongoing effort, at the Naval Postgraduate School, to obtain improved long term data and interpretations of the electromagnetic noise on the ocean floor. The overall project objectives are to study and interpret signals covering 5 decades of frequency from .001 Hz to 100 Hz through the combined use of total field magnetometers and ULF/ELF receivers. The overall project emphasizes the importance of obtaining measurements of geomagnetic noise fluctuations on the sea floor and on land over a period of several years and at various locations.

The particular objectives of this thesis research are 1) to collect local magnetic field fluctuation data at a relatively quiet land site near Monterey, California for comparison with data obtained from the floor of Monterey Bay and 2) to test a coil type antenna specifically designed for deep sea use, as well as the required electronics and data recording equipment.

II. BACKGROUND

A. SOURCES OF GEOMAGNETIC FLUCTUATIONS

Geomagnetic fluctuations result from sources internal and external to the earth's surface. Internal sources, which account for approximately one-third of the variations in earth's magnetic field, are referred to as secular variations, having periods of thousands of years. Geomagnetic storms, diurnal variations, and micropulsations are due to external sources and have periods on the order of days and less.

Probably the best known sources of geomagnetic fluctuations are those generated by the interaction of charged particles with the magnetic fields of the magnetosphere. Figure 1 indicates an approximate power spectrum of variations measured on the earth's surface having periods of a day or shorter. Although this phenomenon is not fully understood, much effort has been expended in studying the sources and predicting the occurrences of these variations. The high frequency fluctuations, referred to as micropulsations, fall into two general classes: Pi or irregular pulsations and Pc or continuous pulsations and are believed to result from wave- particle interaction in the magnetosphere (Jacobs 1970).

Of particular interest are long and short term predictions of the Pc 1 geomagnetic pulsations (.2-5 Hz). A

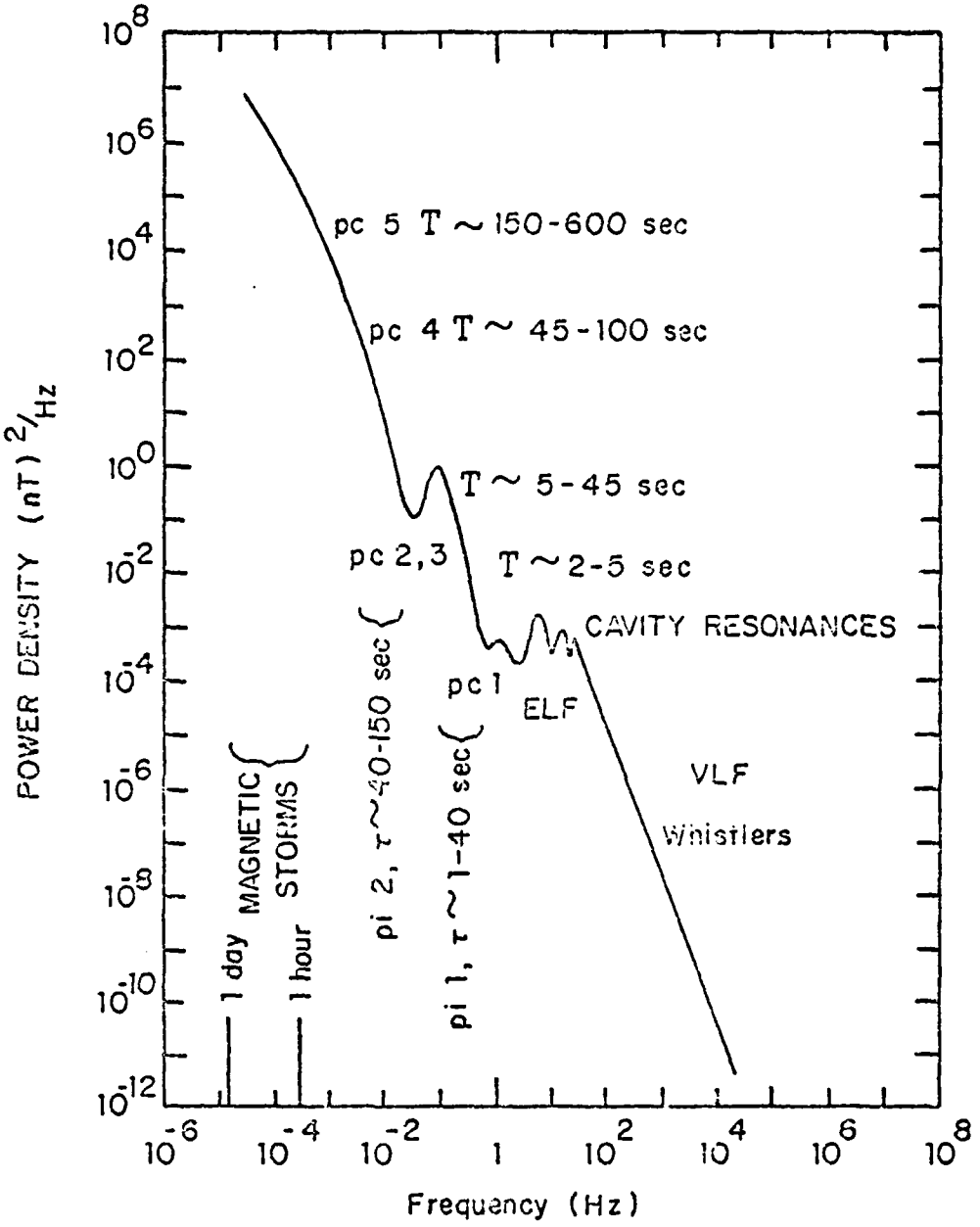

Figure 1

Power Spectrum of Geomagnetic Disturbances Observed on the Surface of the Earth.

[Cladis, Davidson, and Newkirk 1971]

number of methods are available for the forecasting of long-term (Fraser-Smith, 1972 and Matyeyeva et al., 1972) and short-term (Fraser-Smith, 1980) geomagnetic pulsation occurances. However, the accuracy of these methods must eventually be determined by comparison with the observed data for both research and operational reasons.

Thus a better understanding of the time dependent component of the geomagnetic field is of considerable interest both in geophysical and naval applications. Prediction of geomagnetic fluctuations is especially valuable in Navy operational and projected systems such as extremely low frequency (ELF) communications, submarine detection (Magnetic Anomaly Detection), and weapon deployment (mines, particle beams, and torpedoes).

In addition to the information about magnetospheric processes which can be deduced from a study of time variations of the geomagnetic field, these fluctuationa also serve as an important tool in the study of other geophysical quantities. Thus both conventional and naval magnetotelluric techniques make use of the variable geomagnetic field in the measurement of ocean floor conductivities. Similar measurements are employed in the study of earthquake faults, the location of aquifers and geophysical prospecting in general.

B. ELECTROMAGNETIC PROPAGATION IN LAYERED CONDUCTING MEDIA

To describe electromagnetic propagation in layered conducting media, a three layer model was selected (see figure 2). Note that plane wave propagation is assumed. This model was used to predict the expected geomagnetic variations in the media and at their interfaces. Before proceeding with an explanation of the model and its use, the following definitions are presented:

λ = Wavelength, meter

v_p = Phase velocity, meter/second

$\Gamma = \alpha + j\beta$, Complex propagation constant, meter^{-1}

ω = Angular frequency, radian/second

μ = Permeability, henry/meter

ε = Dielectric constant, farad/meter, $\varepsilon = \varepsilon_r \varepsilon_0$ where $\varepsilon_0 = 10^{-9}/36\pi$ farad/meter

ε_r = Relative dielectric constant, for air $\varepsilon_r = 1$ and for sea water $\varepsilon_r = 81$

σ = Conductivity, siemens/meter, for sea water $\sigma_2 = 4$ siemens/meter and for sea floor $\sigma_3 = .1$ siemens/meter

E = Electric field strength, volt/meter

B = Magnetic flux density, tesla

δ = Skin depth, $1/\alpha$, meter

f = Frequency, hertz

η = Intrinsic impedance, ohm

The media are assumed to be non-magnetic with $\mu_1 = \mu_2 = \mu_3 = \mu_0 = 4\pi(10^{-7})$ henry/meter. Sea water and the ocean floor

are assumed to be good conductors in the frequency of interest (.04 to 25 Hz), i.e., $\sigma/\omega\varepsilon>>1$ (conduction current dominates). On the other hand, air is assumed to be a good insulator, i.e., $\sigma/\omega\varepsilon<<1$ (displacement current dominates). For these conditions the following equations for the propagation constants and intrinsic impedances along with their numerical values are valid:

Region 1: (air)

$\Gamma_1=j\omega(\mu_0\varepsilon_1)^{\frac{1}{2}}$ $\quad|\Gamma_1|=1.9(10^{-8})f$ meter^{-1}

$\eta_1=(\mu_0\varepsilon_1)^{\frac{1}{2}}$ $\quad|\eta_1|=377$ ohm

Region 2: (sea water)

$\Gamma_2=(j\omega\mu_0\sigma_2)^{\frac{1}{2}}$ $\quad|\Gamma_2|=5.6(10^{-3})f^{\frac{1}{2}}$ meter^{-1}

$\eta_2=(j\omega\mu_0/\sigma_2)^{\frac{1}{2}}$ $\quad|\eta_2|=1.4(10^{-3})f^{\frac{1}{2}}$ ohm

Region 3: (sea floor)

$\Gamma_3=(j\omega\mu_0\sigma_3)^{\frac{1}{2}}$ $\quad|\Gamma_3|=8.9(10^{-4})f^{\frac{1}{2}}$ meter^{-1}

$\eta_3=(j\omega\mu_0/\sigma_3)^{\frac{1}{2}}$ $\quad|\eta_3|=8.9(10^{-3})f^{\frac{1}{2}}$ ohm

For simplicity, only the theory for a normally incident, plane polarized wave is considered. The modification for the general case of oblique incidence is easily made. It can be shown that the direction of propagation in the sea is vertically downward, regardless of the angle of incidence.

Use of Maxwell's equations and the above assumptions results in the following wave equations for the media of interest:

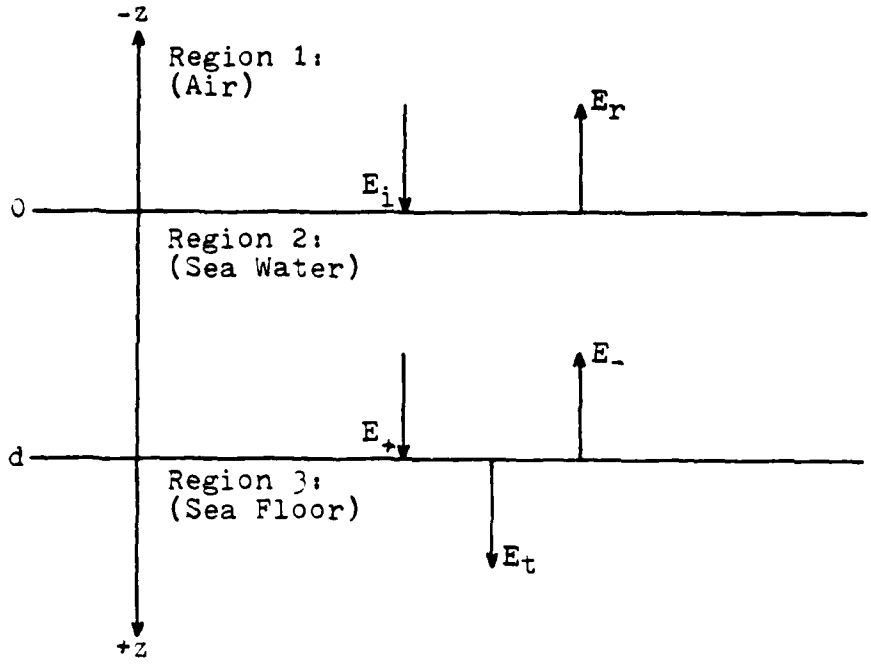

Figure 2. THREE-LAYER MODEL

Region 1: (air)

$$E_{x_1} = E_i e^{-\Gamma_1 z} + E_r e^{\Gamma_1 z}$$

$$B_{y_1} = (\mu_0/\eta_1)\{E_i e^{-\Gamma_1 z} + E_r e^{\Gamma_1 z}\}$$

Region 2: (sea water)

$$E_{x_2} = E_+ e^{-\Gamma_2 z} - E_- e^{\Gamma_2 z}$$

$$B_{y_2} = (\mu_0/\eta_2)\{E_+ e^{-\Gamma_2 z} - E_- e^{\Gamma_2 z}\}$$

Region 3: (sea floor)

$$E_{x_3} = E_t e^{-\Gamma_3 z}$$

$$B_{y_3} = (\mu_0/\eta_3) E_t e^{-\Gamma_3 z}$$

The boundary conditions require that the electric and magnetic fields be continuous at each interface, i.e., at

the air-sea water and sea water-sea floor boundaries. These conditions are:

$$z=0: \quad E_i+E_r = E_+ + E_-$$

$$(\mu_0/\eta_1)\{E_i-E_r\} = (\mu_0/\eta_2)\{E_+-E_-\}$$

$$z=d: \quad E_+ e^{-\Gamma_2 d}+E_- e^{\Gamma_2 d} = E_t e^{-\Gamma_3 d}$$

$$(\mu_0/\eta_2)\{E_+ e^{-\Gamma_2 d}-E_- e^{\Gamma_2 d}\} = (\mu_0/\eta_3) E_t e^{-\Gamma_3 d}$$

We have here five unknowns with only four relations between them. To obtain a meaningful result from the above equations, the various E components are expressed as ratios, normalized to E_i. The form of the ratios are:

$\underline{E}_r = (E_r/E_i)$, $\underline{E}_+ = (E_+/E_i)$, $\underline{E}_- = (E_-/E_i)$, and $\underline{E}_t = (E_t/E_i)$

Algebraic calculations result in the following expressions:

$$\underline{E}_+ = \frac{2\eta_2(\eta_2+\eta_3)}{(\eta_3+\eta_2)(\eta_1+\eta_2)+(\eta_2-\eta_1)(\eta_3-\eta_2)e^{-2\Gamma_2 d}}$$

$$\underline{E}_- = \frac{2\eta_2(\eta_3-\eta_2)}{(\eta_2+\eta_3)(\eta_1+\eta_2)e^{2\Gamma_2 d}+(\eta_2-\eta_1)(\eta_3-\eta_2)}$$

$$\underline{E}_t = \underline{E}_+ e^{-(\Gamma_2-\Gamma_3)d}+\underline{E}_- e^{(\Gamma_2+\Gamma_3)d}$$

$$\underline{E}_r = \underline{E}_+ + \underline{E}_- - 1$$

Using the above equations for region 2 (sea water), an expression for the induced-to-incident magnetic field on the sea floor is obtained.

$$B_{y_2}(z) = E_{x_2}/\eta_2 = E_i(\underline{E}_+ e^{-\Gamma_2 z}-\underline{E}_- e^{\Gamma_2 z}) \text{ since } E_i=(\eta_1/\mu_0)B_i$$

$$B_{y_2}(z) = (\eta_1/\mu_0)B_i\{\underline{E}_+ e^{-\Gamma_2 z}-\underline{E}_- e^{\Gamma_2 z}\}$$

$$\underline{B}_{y_2}(z) = B_{y_2}/B_i = (\eta_1/\mu_0)\{\underline{E}_+ e^{-\Gamma_2 z}-\underline{E}_- e^{\Gamma_2 z}\}$$

Now assuming that η_2 and η_3 are much less than η_1, we define

$q = \eta_3/\eta_2 = \{\sigma_2/\sigma_3\}^{\frac{1}{2}}$. After some algebraic manipulations, we obtain:

$$\underline{B}_{y_2}(z) = 2\{\frac{(q+1)e^{\Gamma_2(d-z)} - (q-1)e^{-\Gamma_2(d-z)}}{(q+1)e^{\Gamma_2 d} - (q-1)e^{-\Gamma_2 d}}\}$$

For z=d and substituting the numerical values of η_2, η_3, Γ_2 into the above equation at a specified frequency, one can obtain a plot of the induced-to-incident magnetic field versus depth. See Figure 3. Clearly, if one is to detect magnetic field variations in sea water at any appreciable depth, then the variations must be of low frequency.

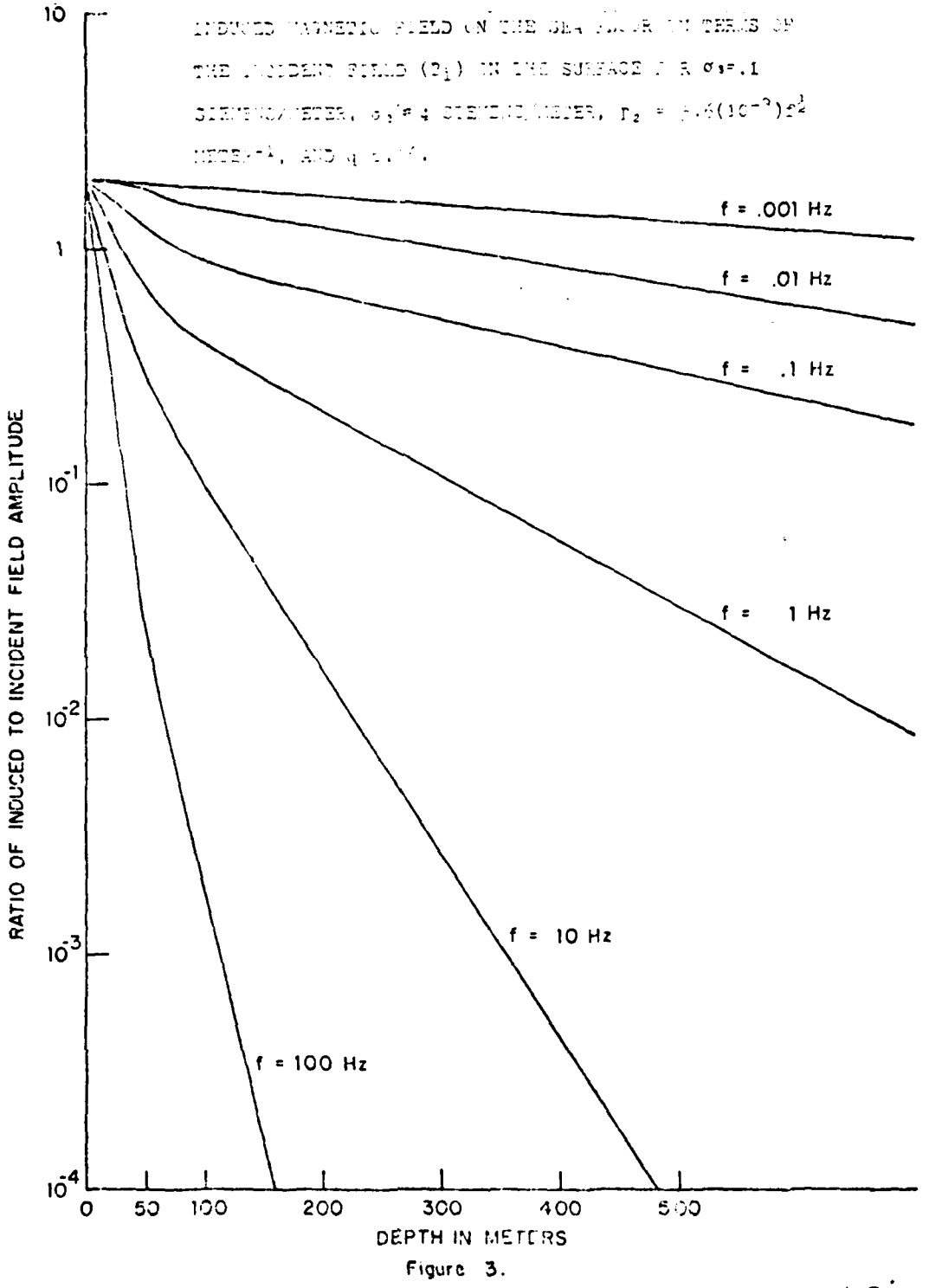
INDUCED MAGNETIC FIELD ON THE SEA FLOOR IN TERMS OF
THE INCIDENT FIELD (B_1) IN THE SURFACE LAYER σ_1=.1
SIEMENS/METER, σ_2=4 SIEMENS/METER, Γ_2 = 1.6(10^{-3})$f^{\frac{1}{2}}$
METER^{-1}, AND μ = μ_0.
f = .001 Hz
f = .01 Hz
f = .1 Hz
f = 1 Hz
f = 10 Hz
f = 100 Hz
RATIO OF INDUCED TO INCIDENT FIELD AMPLITUDE
10
1
10^{-1}
10^{-2}
10^{-3}
10^{-4}
0
50
100
200
300
400
500
DEPTH IN METERS

Figure 3.

C. GEOMAGNETIC FORECASTS

The Space Environment Services Center located in Boulder, Colorado publishes a Preliminary Report and Forecast of Solar Geophysical Data, including geomagnetic activity. A more detailed synopsis of geophysical data is contained in the environmental data services monthly publication "Solar-Geophysical Data". Of importance to the research effort here at Naval Postgraduate School are the reports of the A and K-indices for the mid-latitude region containing Monterey. The major monitoring station for the mid-latitude areas in the U.S. is located in Fredericksburg, Virginia.

A and K-indices reported by Fredericksburg are of interest to NPGS, since this station lies approximately on the same latitude as Monterey. The A-indices indicate a 24-hr daily variation in the earth's magnetic field while the K-indices indicate a 3-hr period of variation within the 24-hr A-index. The K-indices vary in range from 0 (very quiet) to 9 (extremely disturbed) with an A-index of 30 or greater indicating geomagnetic storm conditions.

The above information was utilized to correlate geomagnetic predictions and forecasts with geomagnetic data obtained in Monterey Bay. This correlation concept is utilized below in Section V, experimental results. (See Appendix C for a further description of geomagnetic forecasts).

D. REVIEW OF EARLIER WORK

A fair amount of research has been and is being done in the detection and prediction of low frequency variations (less than 100 Hz) of the earth's magnetic field, both on land and in the sea. Earlier experiments by Horton and Hoffman (1962), Santirocco and Parker (1963), and Davidson (1964) revealed that the power spectral density of background geomagnetic activity in the frequency range 10^{-4}- 1 Hz decreased monotonically with a slope of approximately -6 dB/octave. The spectrum then levels off and is dominated by the Schumann resonances in the frequency range 1-40 Hz (Schumann and Konig, 1954). Measurements indicate a general increase in background activity between 20 and 70 Hz as reported by Campbell (1966), with a continued sharp decrease in slope above 80 Hz.

Spectrums obtained by Larsen and Egeland (1968) indicate that the general decline observed at frequencies below 5 Hz continues through 70 Hz and probably to higher frequencies (Maxwell and Stone, 1963; Westerlund, 1970) with the Schumann resonance activity being superimposed on the declining background as a form of fine structure. Hence, there is a remarkably steady decline of the background fluctruations at a rate of approximately 6 dB/octave covering almost 6 decades of frequency (10^{-4} - 10^{2} Hz) (Fraser-Smith and Buxton, 1975).

Recent measurements conducted by Fraser-Smith and Buxton in the .1 - 14 Hz frequency range confirmed earlier predictions and detections. They discovered that the general decline in background activity continued for frequencies up to 5 Hz, but for frequencies above 5 Hz the decline appeared to be suppressed by the occurence of the Schumann resonances.

More recent work was accomplished in the low frequency ranges at La Mesa in Monterey. Barry (1978) and Clayton (1979) investigated geomagnetic fluctuations in the frequency ranges .1-10 Hz and .4-40 Hz, respectively. Their results are in general agreement with earlier measurements.

Chaffee (1979) measured geomagnetic variations of the earth's magnetic field on the floor of Monterey Bay in 100-200 meters of sea water and covering the frequency range .01-3 Hz. Chaffee observed the power spectrum of typical geomagnetic fluctuations to vary from 1 nT^2/Hz at .01 Hz to approximately 10^{-5} nT^2/Hz. Most low frequency studies made in sea water have been performed to detect geomagnetic fluctuations produced by surface waves. Since little data is available on actual geomagnetic noise at low frequencies, the project at Naval Postgraduate School is a continuing effort to create a reliable data base for future reference and correlation.

III. EXPERIMENTAL EQUIPMENT AND TESTS

A. EQUIPMENT CONFIGURATION

Most of the equipment utilized for this project was either designed and/or manufactured at the Naval Postgraduate School, while test equipment used was mostly of commercial origin. Much effort was expended in testing and ensuring that the experimental equipment operated as concieved and predicted. It was important for all equipment to be dc coupled to avoid loss of low frequency signals. A discussion of the equipment and its configuration follows:

1. Data Acquisition Equipment

SENSOR

The general hookup of the data acquisition equipment is depicted in Figure 4. The sensor is a self-supporting, continuously wound, non-center-tapped coil antenna manufactured from approximately 6000 turns of 18 gauge copper magnet wire. The sensitivity of the coil is established in Section III. B. Its weight is approximately 100 pounds. Its overall dimensions (.15m by .37m) were determined by the largest glass sphere commercially manufactured by Benthos, Incorporated. Refer to Figure 5. The coil resistance is 120 ohms and its self-inductance is approximately 9.31 henries.

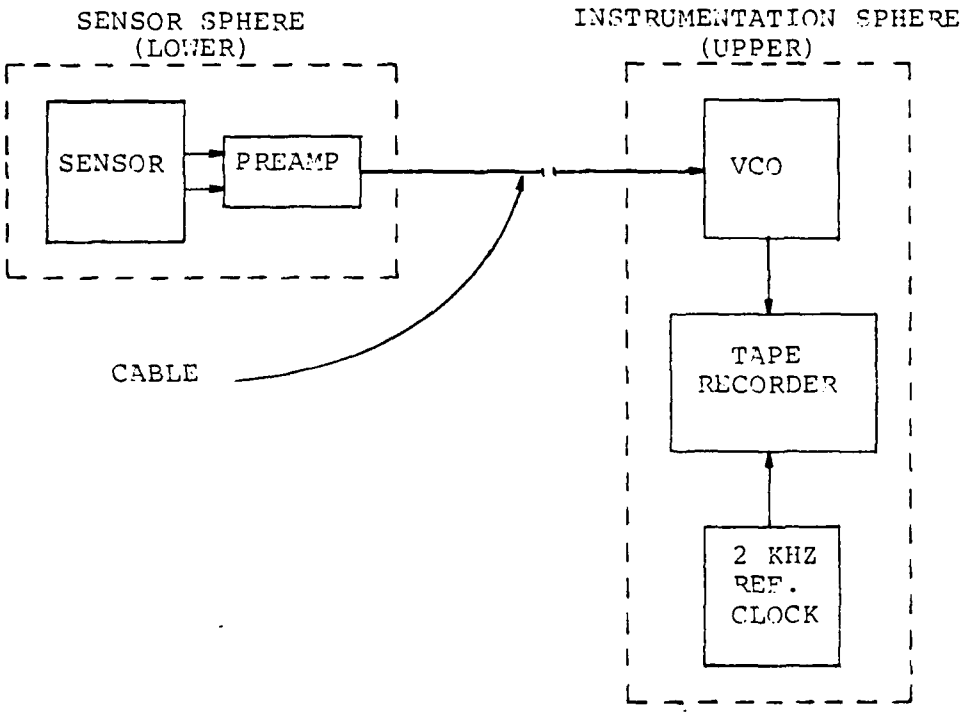

Figure 4 Data Taking Equipment

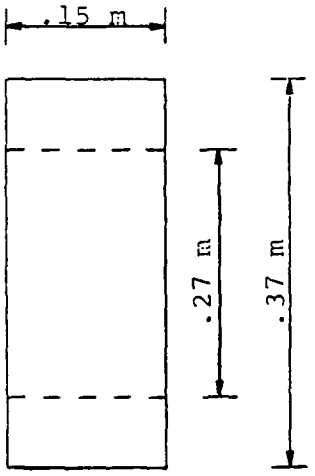

Figure 5 Sensor Dimensions

PREAMPLIFIER

Various differential preamplifiers were tested and used including the PAR-113 amplifier manufactured by Princeton Applied Research Corporation. This preamplifier was selected because of its higher signal to noise ratio, low power requirements, and compactness. The preamplifier itself is packaged as an integral part of the sensor, i.e., it is housed in the glass sphere with the sensor. Attempts to separate the preamplifier from the sensor resulted in additional noise caused by cable motion.

The front end of the preamplifier utilized a low-noise, "state of the art" differential device (LH 0038 C) manufactured by National Semiconductor Corporation. It has a single-ended output which is connected to additional stages of amplification. The final stage of the preamplifier contains an active filter which is set to a cutoff frequency of 20 Hz. The overall preamplifier gain, including filters, is approximately 66 dB. A graph of the preamplifier gain characteristics is included as Figure 14. A schematic diagram of the preamplifier circuit is contained in Appendix A.

VOLTAGE CONTROLLED OSCILLATOR

The schematic diagram of the voltage controlled oscillator (VCO) is included in Appendix A. The function of the VCO is to convert low frequency analog voltages received from the sensor through the preamplifier into a

varying frequency, centered at 1500 Hz. The output level of the VCO is approximately 0.2 volt (zero to peak) square wave of varying frequency which is recorded on an analog cassette tape recorder. The conversion factor for the VCO is 1.25 Hz/mV.

REFERENCE OSCILLATOR

A 2 KHz reference oscillator signal is recorded simultaneously with the VCO signal on a separate channel. The schematic diagram of the reference oscillator is also included in Appendix A. The primary purpose of the reference oscillator is to reduce tape recorder noise (wow and flutter) during playback.

TAPE RECORDER

The tape recorder employed for this project is a portable stereo cassette type (Marantz Superscope, Model CD-330), powered by a 6 Vdc battery. The Superscope was selected to meet the size constraints imposed by the glass spheres. Additional characteristics are:

(1) Tape Speed: 1-7/8 in/s

(2) Frequency response: 40 Hz to 12 KHz

(3) Signal-to-noise ratio: 50 dB

(4) Wow and flutter: .12%

POWER SUPPLIES

Gould Gelyte lead batteries are utilized to meet dc power requirements. They are sealed, rechargeable, and virtually maintainance free batteries, containing no free

electrolyte. Various sizes are used to meet the power specifications of all data taking and analysis equipment, except test equipment.

2. Data Analysis Equipment

Refer to Figure 6 for the general hookup of the data analysis equipment. The tape recorder and power supplies (discussed above) were employed in data analysis as well as in data taking. A description of the additional analysis equipment follows:

MIXER

Appendix A contains the schematic for the mixer circuit. The mixer is powered by ± 12 Vdc and accepts the recorded sensor data and reference oscillator signals at its

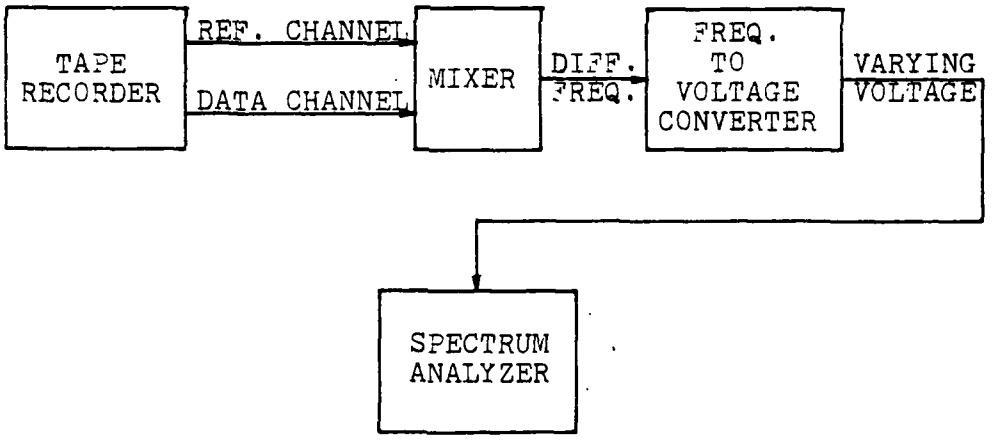

Figure 6 DATA ANALYSIS EQUIPMENT

inputs from the tape recorder. The difference frequency of the mixer is the input to a frequency-to-voltage converter. The mixer circuit also contains a low pass filter with a

cutoff frequency at approximately 1200 Hz. The purpose of the low pass filter is to elimate unwanted harmonics of the difference frequency.

FREQUENCY-TO-VOLTAGE CONVERTER (ANADEX PI-375)

The purpose of the frequency-to-voltage converter (FVC) is to convert the difference frequency from the mixer into an analog voltage. The varying voltage is an exact representation of the geomagnetic fluctuations detected by the sensor. The FVC is powered by 24 Vdc and has the following additional characteristics:

(a) Input frequency range: 0-2000 Hz

(b) Output dc voltage: 0-10V full scale

(c) Conversion factor: 4.91 mV/Hz

The output of the converter is analyzed with a spectrum analyzer.

SPECTRUM ANALYZER (S/A)

Numerous spectrum analyzers were used for data analysis: The Schlumberger Model 1510-03, The Ubiquitos Model UA-500, The Mini-Ubiquitos Model 440, and the Hewlett Packard Model 3582A. Each of these analyzers has inherent advantages and disadvantages revealed during their operation.

The Schlumberger S/A does not provide for dc coupling and hence was not adequate for low frequency applications. The Ubiquitos has dc coupling and limited low frequency capabilities. Also an external display had to be provided to obtain a power spectral density read out which

would be highly inaccurate. The Hewlett Packard Analyzer was capable of dc coupling and provided for a digital display of the power spectrum. However, it does not have a logarithmic scale for frequency.

The most adequate S/A utilized was the Mini-Ubiquitos Model 440. It provides for dc coupling, has a digital display of the power spectrum, and has a logarithmic as well as a linear frequency scale.

Since the discriminator output is a positive dc voltage, it was necessary to provide for dc offset in order to increase the input sensitivity of the spectrum analyzer. The Tertronix Model AM 502 differential amplifier was utilized with its gain set to X1.

3. Underwater Equipment

Underwater equipment included the following (see Figure 7):

(a) Benthos vacusealed glass spheres with associated hard hats, penetrators, and sealant strip.

(b) Cable and connectors

(c) Anchor and nylon line

The particular spheres employed during this project were a low expansion borosilicate type, having a 0.404 meter inside diameter. The actual spheres used in the tests were two hemispherical shells specially matched to guard against leakage. They are pressure tested by the manufacturer, to 1000 atmospheres, which is equivalent to a sea water depth

SCHEMATIC OF EXPERIMENTAL LAYOUT

FOR AT SEA MEASUREMENTS

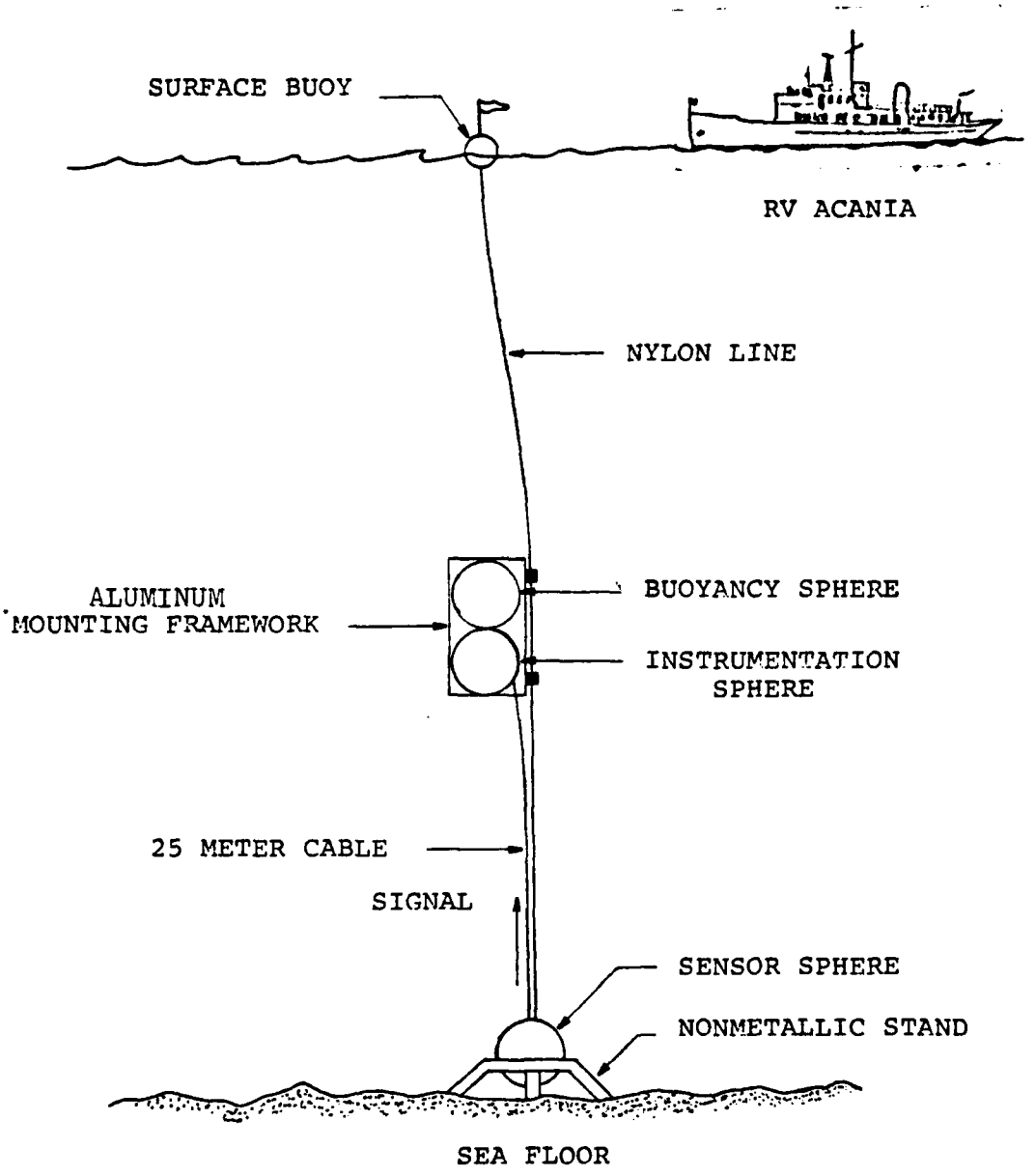

FIGURE 7

of 10,000 meters. Before the spheres are placed in the hardhats, which provide protection against breakage, the hemispherical seam is sealed with sealant strip and taped.

Penetrators were installed in the wall of the Benthos Glass Housings to provide electrical connections to enclosed equipment. A pressure type penetrator is used to activate the tape recorder when the instrumentation sphere is at a depth of approximately 10 meters.

Signals from the sensor to the instrumentation sphere are propagated through a twisted-pair, shielded, rubber coated, 25 meters long cable with Brantner type sea connectors. The connectors are made from a special molded neoprene material; they have brass, hard gold plated contacts and are pressure rated to greater than 1000 atmospheres when mated.

An anchor supports the sensor sphere and provides added negative buoyancy to prevent the system from floating. It was designed and constructed from PVC piping, filled with sand, and neoprene-coated lead bricks were strapped to the piping for additional weight. Extreme care was taken to ensure that any exposed metallic surface which might induce unwanted currents into the sea water are eliminated.

B. SENSOR SENSITIVITY

1. Theoretical Sensor Sensitivity

The use of wire coils to measure magnetic field changes is not new. Faraday's Law of Induction states that the electromotive force (emf) induced in a single-turn circuit is equal to minus the rate of change of flux:

$$\text{emf} = -\frac{\partial \Phi}{\partial t} \qquad (3\text{-}1)$$

The flux is that which passes through a surface bounded by the conductor and is defined as:

$$\Phi = \int \bar{B} \cdot d\bar{a} \qquad (3\text{-}2)$$

If we consider N turns of wire connected in series, then the total induced emf is the sum of the emf induced in each separate turn, or for a loop:

$$\text{emf} = -N \frac{\partial \Phi}{\partial t} \qquad (3\text{-}3)$$

In this work it shall be assumed that magnetic fields vary sinusoidally with time and may be written as:

$$\bar{B} = \bar{B}_o e^{-j\omega t} \qquad (3\text{-}4)$$

Where $\bar{B}_o$ is a magnetic vector field and only a function of spatial coordinates and not of time. By substituting equation (3-2) into (3-3) and with equation (3-4) we have:

$$\text{emf} = -NB_o j\omega A \qquad (3\text{-}5)$$

where A is the area enclosed by the coil. The magnitude of this emf is;

$$emf = NB_o(2\pi f)A \qquad (3\text{-}6)$$

If the output of the sensor is connected to a high input impedance amplifier, then negligible current can flow through the sensor which might otherwise produce a back emf and reduce the magnitude of the field to be measured. The sensor's open circuit voltage or sensitivity can be calculated from the parameters given in Section III. A. 1 for a 1 nT field at a frequency of 1 Hz; emf = 3.1117 μV, thus 20 log (emf) = -110.14 dB. (re: 1 Volt)

The area used in calculating the emf for a single turn of wire is easier to visualize than the area of a finite width coil. It was decided that an average area obtained from the area within the inner radius and the area within the outer radius would be used. This method appears to be more accurate than using an average radius to compute the area. Figure 8 depicts the expected sensitivity of the sensor.

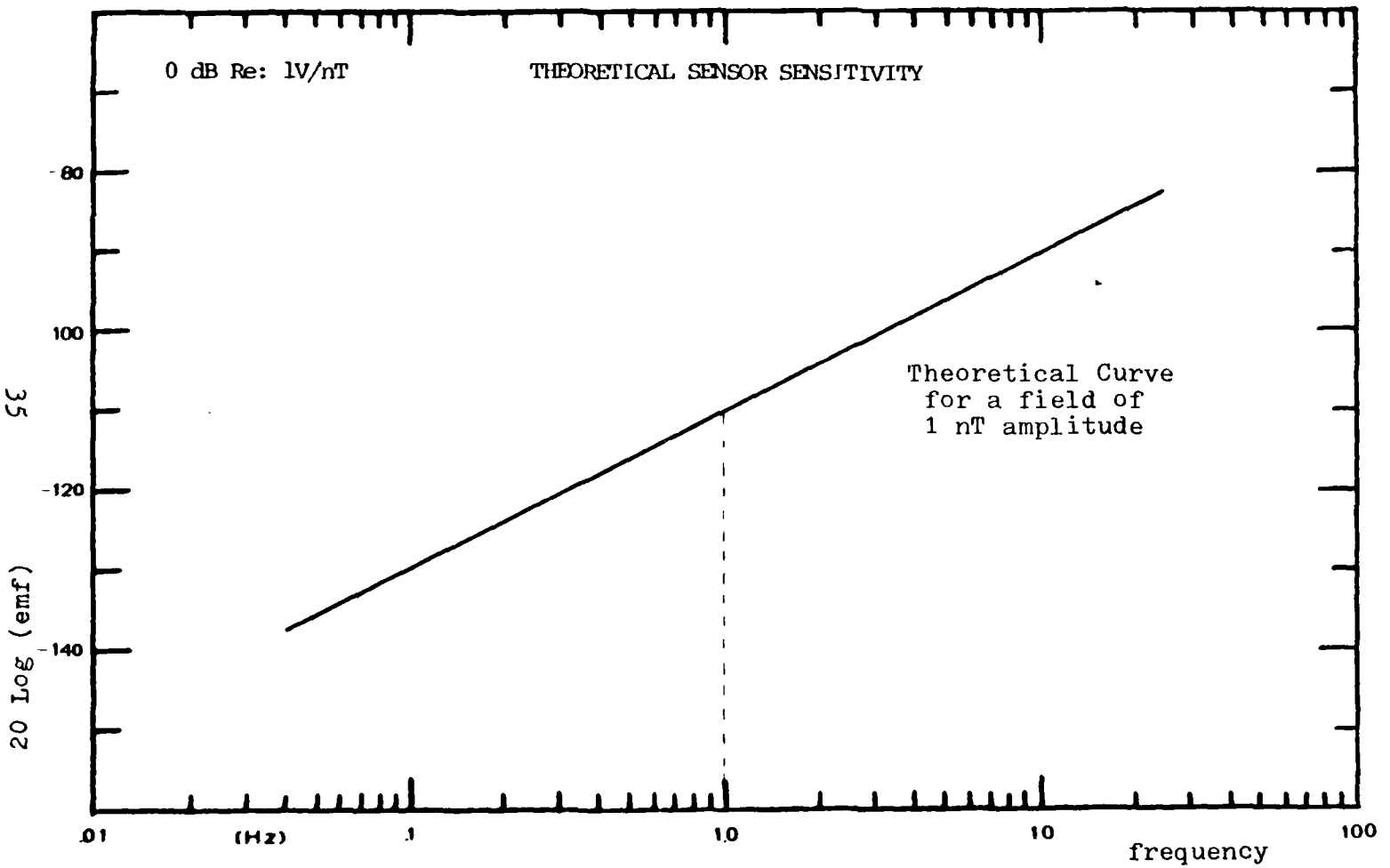
0 dB Re: 1V/nT
THEORETICAL SENSOR SENSITIVITY
-80
-100
-120
-140
20 Log (emf)
35
Theoretical Curve
for a field of
1 nT amplitude
.01
(Hz)
.1
1.0
10
100
frequency

Figure 8

2. Experimental Determination Of Sensor Sensitivity

Two methods were utilized to determine the sensor's actual sensitivity. The first method consisted of producing a known field at a specified distance from an 84 turn copper coil and measuring the electromotive force or voltage signal produced by the sensor. The second method was similar to the first, but a .61 meter radius Helmholtz coil was used to establish a more uniform magnetic field in the central region.

METHOD I.

The magnetic field produced by a circular ring of N turns at a point Z along the symmetry axis is given by:

$$\vec{B}(z) = \frac{2\pi NIr^2(10^2)}{(z^2 + r^2)^{3/2}} \hat{k}. \qquad (3\text{-}7)$$

Equation (3-7) is obtained from the Biot-Savart Law using the units of I (ampere), r (meters), Z (meters), and B (nanotesla) as depicted in Figure 9. Test coil specifications were as follows:

r = .1577 m

N = 84 turns

r inner = 15 cm

r outer = 16.5 cm

where r was computed from the average area of the coil. Rearranging equation (3-7) we have:

$$Irms = \frac{(z^2 + r^2)^{3/2}}{1.68(10^{-6})r^2\pi} B. \qquad (3\text{-}8)$$

Specifying the desired field strength and distance determines the current through the coil at different frequencies. To produce the required current a 110Ω resistor was placed in series with the coil of 4Ω depicted in Figure 10, and the signal voltage was set according to:

$$V_{a,b} = I(R_1 + R_2). \qquad (3\text{-}9)$$

The current was determined to be within ± 1.0% of one mA and the field produced along the central axis of symmetry was determined to within ± 10.% of a nT.

The data obtained on the sensor's sensitivity for a 5 nT and 66.4 nT signal, when compared to the theoretical curve, revealed that a more uniform field in the vicinity of the sensor was needed and that the test should be performed in an area remote from metallic structures such as in a laboratory. The data obtained was within 6 dB of the theoretical values as can be seen in Figure 12.

METHOD II.

The second method, that of using a pair of Helmholtz coils, produced a more uniform field over a larger area. Figure 11 illustrates how the coil was designed to produce an easily accessible, almost homogeneous magnetic field in the central region between the coils.

Expressions for the magnetic induction vector for the axial and radial componets are:

$$B_z = \frac{\mu_o\, 8NI}{5\sqrt{5}\ R}\left[1 - \frac{144}{125}\left(\frac{z}{R}\right)^4 + \frac{54\ z^2 r'^2}{125\ R^4} + \ldots\right] \qquad (3\text{-}10)$$

$$B_{r'} = \frac{\mu_o 8NI}{5\sqrt{5}\ R}\left(\frac{12zr'}{125R^4}\right)\left(3z^2 + 10r'^2 + \ldots\right) \qquad (3\text{-}11)$$

as given in (Jefemenko, 1966).

So, in the central region:

$$B_z = \frac{\mu_o 8NI}{5\sqrt{5}\ R} \qquad (3\text{-}12)$$

$$B_{r'} = 0 \qquad (3\text{-}13)$$

to the terms of the order $(L/R)^4$, where L is the linear dimensions of the region. Using the same method to determine the current in the loops, as explained above, the data shown in Figure 13 indicates that the actual sensitivity was about one dB less than the theoretical value for the entire frequency band of interest. It was determined that the accuracy of the measured sensitivity was well within the expected theoretical limits. The major source of error in the theoretical computuation was determining accurately the area enclosed by the conductor due to the finite width of the coil.

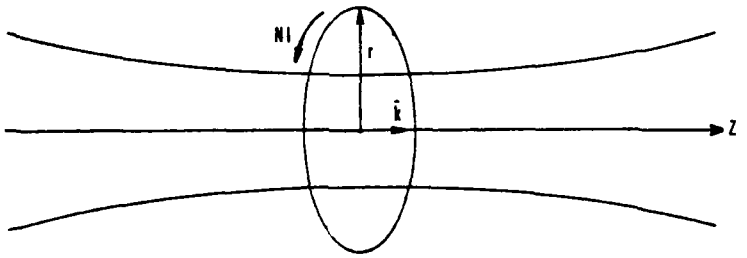

Figure 9 Magnetic Field Along Axis of a Current Carrying Ring

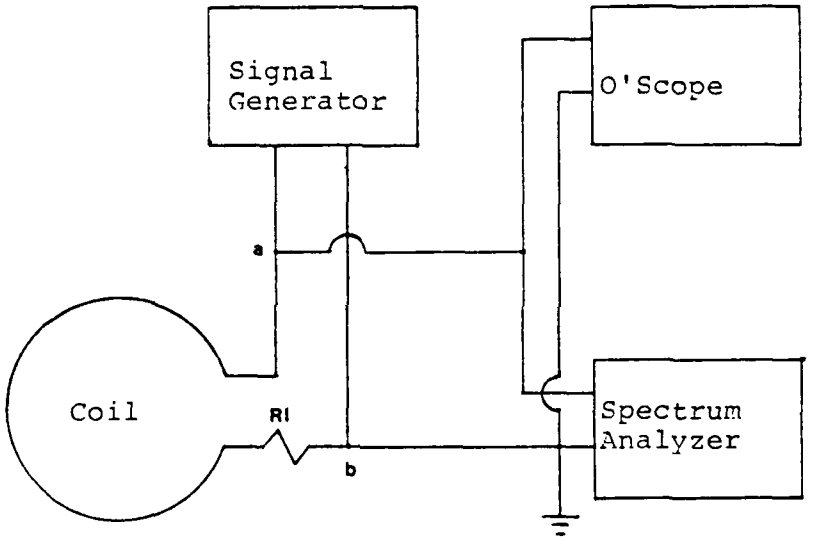

Figure 10 Hookup for Establishing a Known Field

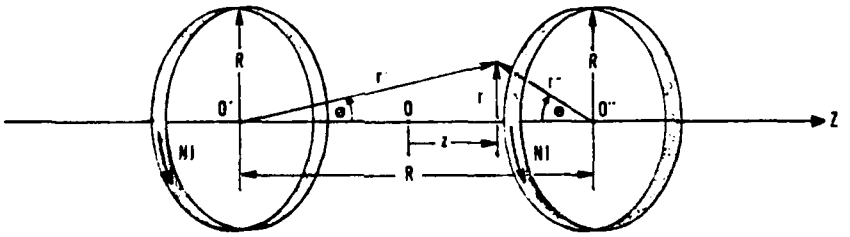

Figure 11 Helmholtz Coil Schematic

To obtain the corrected power spectral density referenced to 1 nT^2/Hz, the following procedure (derived in Appendix D) was used:

N dB = The Spectrum Analyzer reading in dB volts.

(A) = The Hanning window bandwidth correction for the particular Spectrum Analyzer used.

(B) = The transfer Function defined above.

(C) = The corrected power spectral density where 0 dB is referenced to $1nT^2/Hz$.

(C) = N dB - (B) - (A).

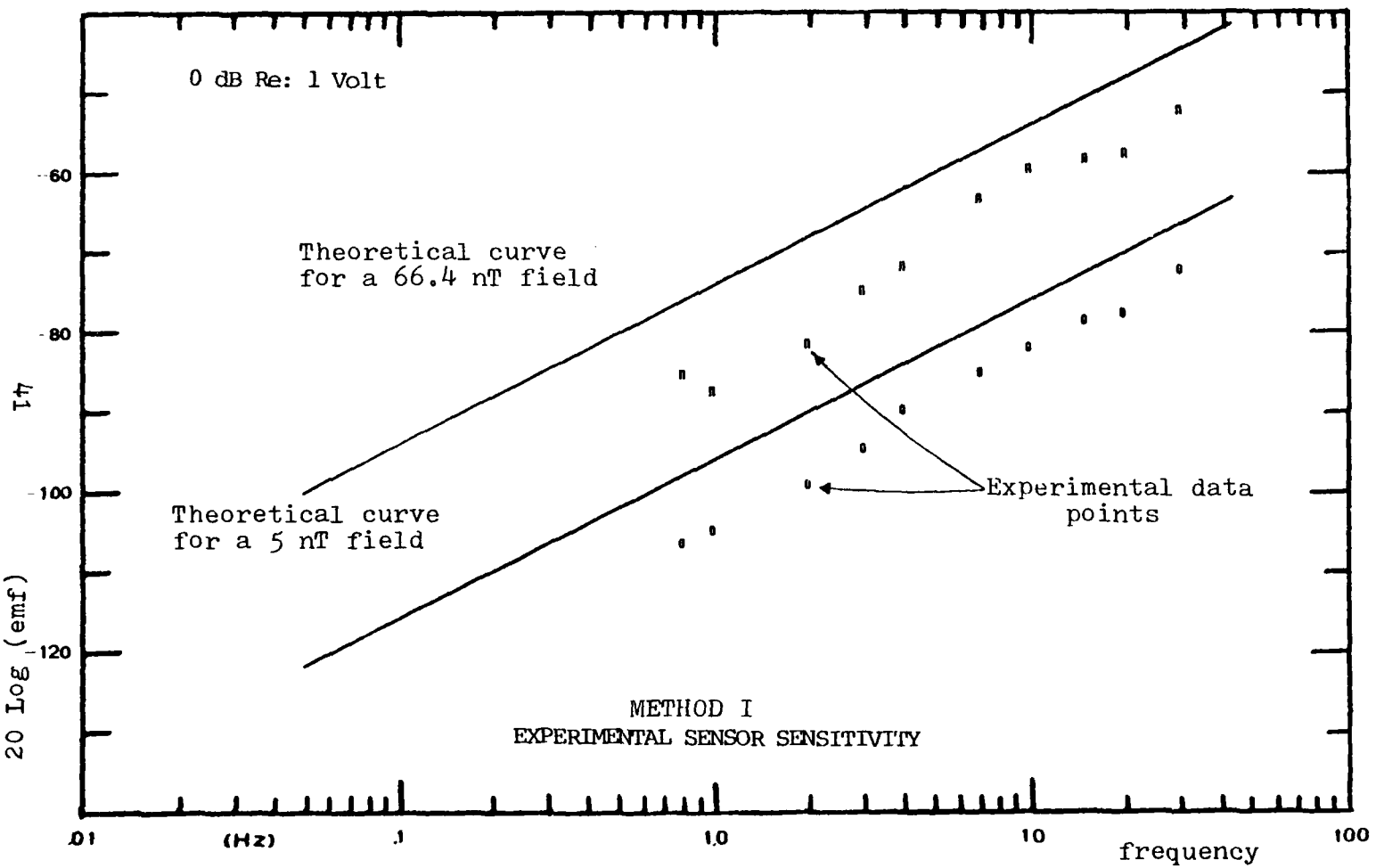
0 dB Re: 1 Volt
Theoretical curve
for a 66.4 nT field
Theoretical curve
for a 5 nT field
Experimental data
points
METHOD I
EXPERIMENTAL SENSOR SENSITIVITY
20 Log (emf)
-60
-80
-100
-120
.01
(Hz)
.1
1.0
10
100
frequency

Figure 12

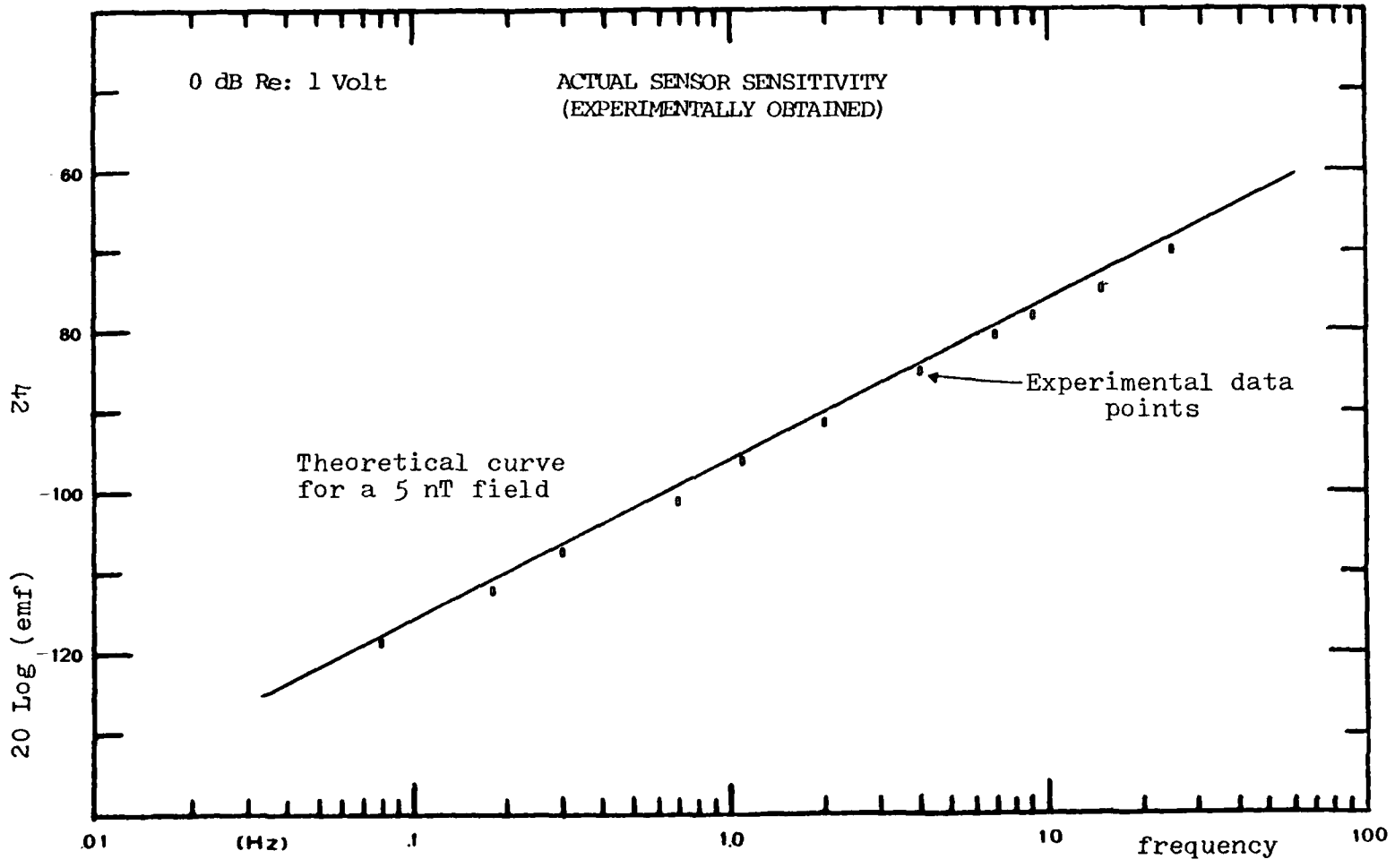
0 dB Re: 1 Volt
ACTUAL SENSOR SENSITIVITY
(EXPERIMENTALLY OBTAINED)
-60
-80
-100
-120
20 Log (emf)
Theoretical curve
for a 5 nT field
Experimental data
points
.01
(Hz)
.1
1.0
10
100
frequency

Figure 13

C. SYSTEM TRANSFER FUNCTION

The system can be represented by a simple block diagram that converts a varying magnetic field into a voltage that can be displayed and whose power spectral density can be measured with a Spectrum Analyzer:

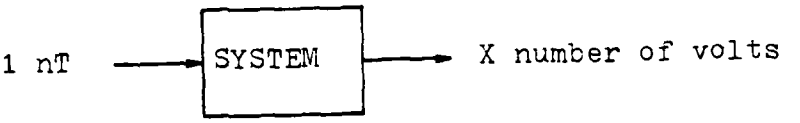

The transfer function is frequency dependent. It was calculated by separating the system into its components as follows:

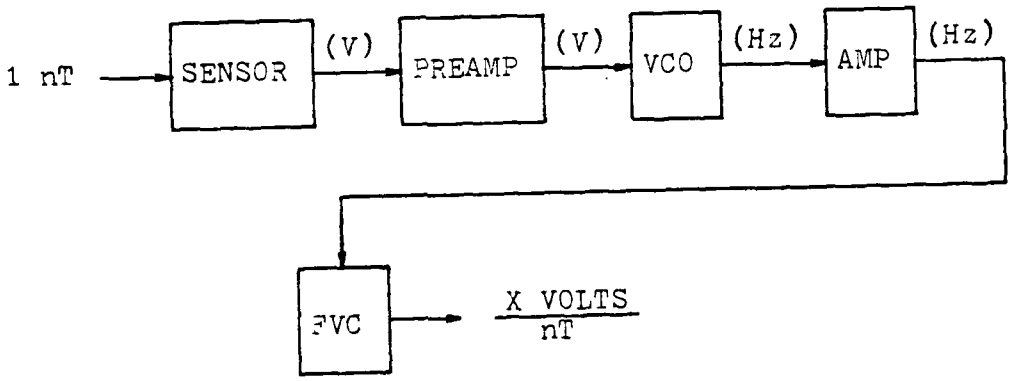

Once the sensor sensitivity was determined using the Helmholtz coils it remained to compute the gains and conversions of the electronic components to determine the overall system transfer function.

The preamplifier was designed to be a low pass, low noise amplifier with a very sharp cutoff frequency at 20 Hz. This cutoff frequency is necessary to attenuate the 60 Hz

fields present at all land sites. As can be observed in Figure 14 the gain characteristics are flat to 10 Hz with a gain of 66.5 dB. The sharp cutoff at 20 Hz was obtained with a final stage active filter network which added slightly to the gain prior to cutoff.

The voltage controlled oscillator (VCO) was designed to have a center frequency of 1500 Hz with an output voltage level of .4 volts (Peak to Peak). The purpose of having a low output voltage at 1500 Hz is to minimize crosstalk between tape recorder channels and to operate well within the frequency response of the tape recorder. Since the tape recorder and mixer (described in Section III. A) have unity gain, the overall gain of the VCO and frequency-to-voltage converter (FVC) was measured by amplifying the 1500 Hz signal to the required level to drive the FVC with a low noise, PAR-113 amplifier. The low pass gain characteristics of the VCO/FVC combination can be seen in Figure 15. The response is similar to that of the preamplifier and is characterized by a constant gain of 34.7 dB from dc to 4 Hz and a slight decrease after 10 Hz as required for additional 60 Hz filtering.

The system transfer function was calculated by adding the gain of the preamplifier to the gain of the VCO/FVC combination and to the sensor sensitivity at equivalent frequencies. This can be seen in Figure 16. The data presented in this research is referenced to 1 nT rather than 1 volt.

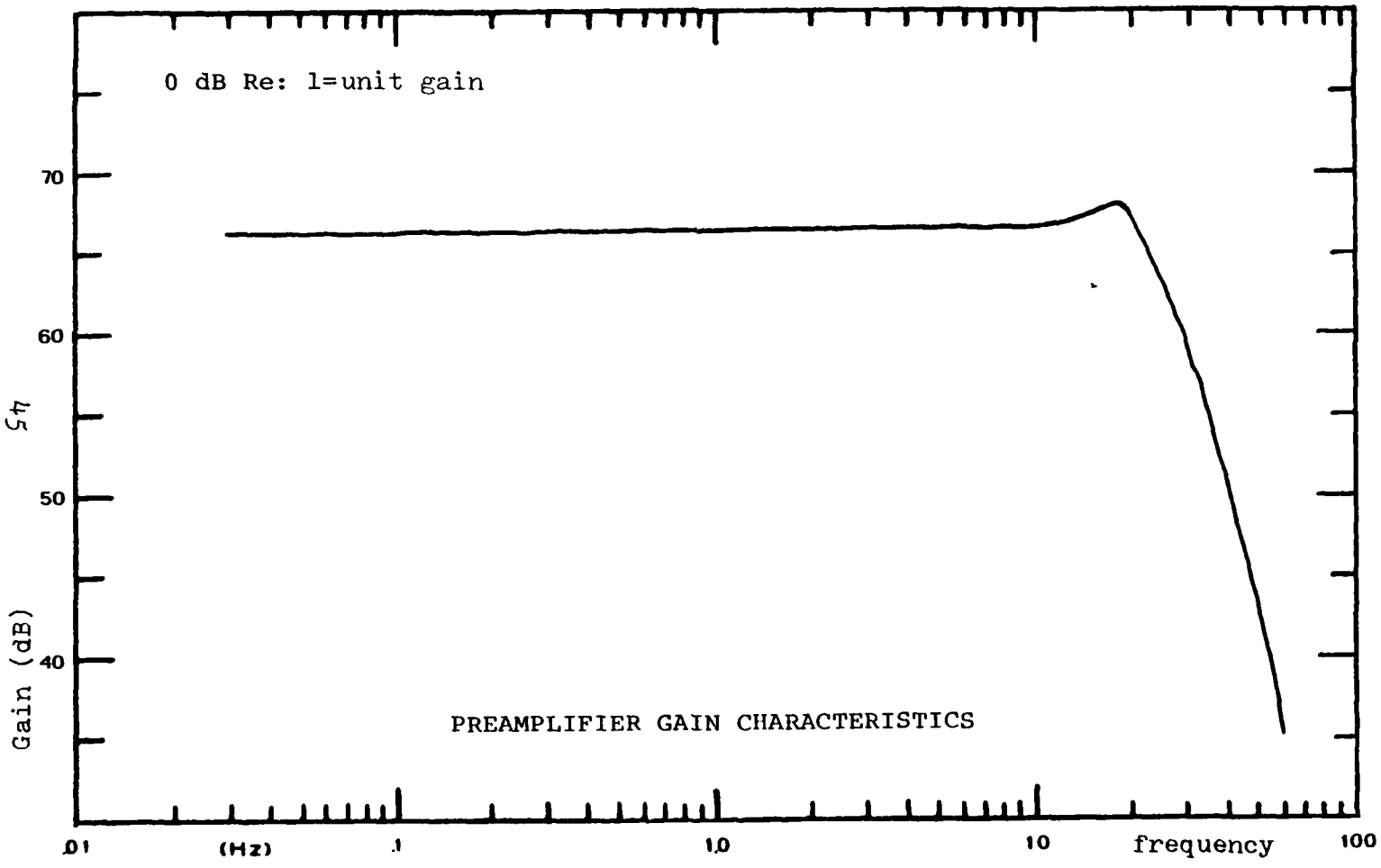
0 dB Re: 1=unit gain
70
60
50
40
Gain (dB)
PREAMPLIFIER GAIN CHARACTERISTICS
.01
(Hz)
.1
1.0
10
frequency
100

Figure 14

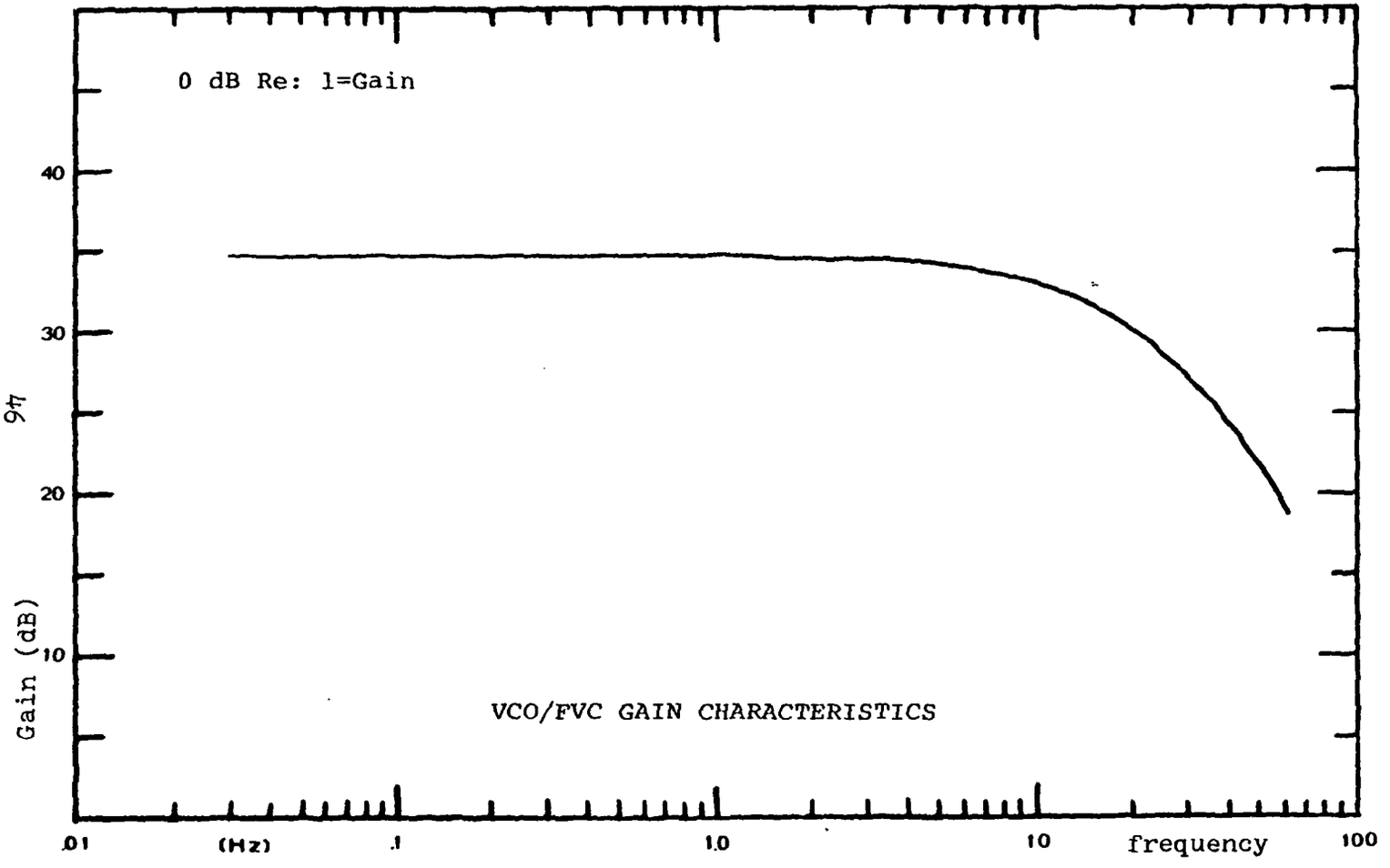
0 dB Re: 1=Gain
40
30
20
10
Gain (dB)
VCO/FVC GAIN CHARACTERISTICS
.01
(Hz)
.1
1.0
10
frequency
100

Figure 15

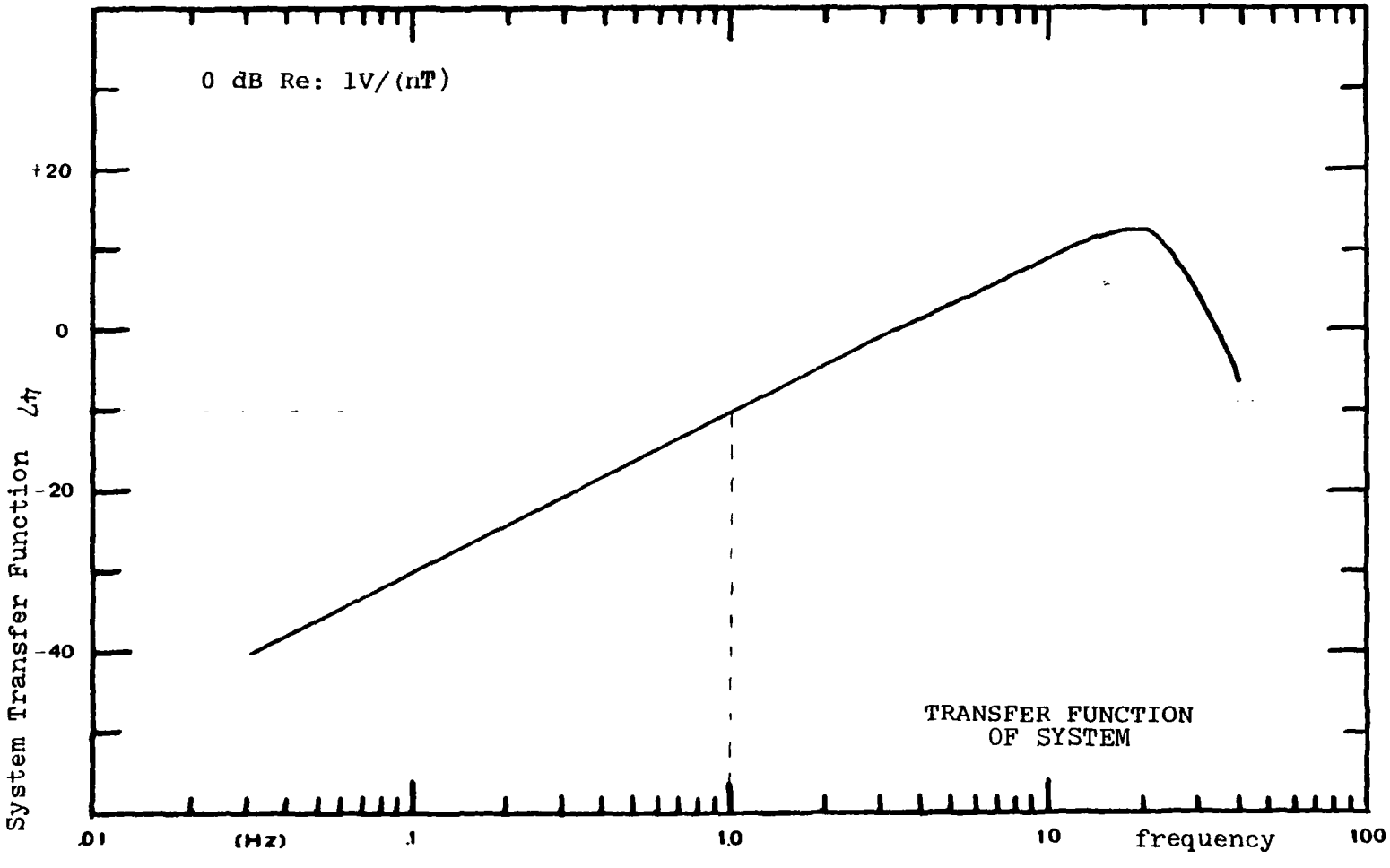
0 dB Re: 1V/(nT)
+20
0
-20
-40
System Transfer Function
.01
(Hz)
.1
1.0
10
frequency
100
TRANSFER FUNCTION
OF SYSTEM

Figure 16

D. SYSTEM NOISE

The best amplifier performance is realized when the amplifier causes the least decrease in the overall signal-to-noise ratio. In many instances the thermal noise generated by the signal source resistance is the dominant factor in determining the input signal-to-noise ratio. Amplifier noise performance can be specified by the amount of noise the amplifier adds to the amplified source thermal noise. Expressed in decibels, and defined as the "noise figure", or NF, it is given by:

$$NF = 20 \log \frac{\text{total rms noise voltage at amp output}}{\text{gain x (source thermal noise voltage)}} \quad (3\text{-}14)$$

where the Source Thermal Noise = $\sqrt{4KTR\Delta f}$ volts rms, and

K = Boltzmann's constant, 1.38×10^{-23} joules/^{o}K

T = absolute temperature in degree Kelvin

f = Equivalent Noise Bandwidth in Hz

R = source resistance in ohms

The total output noise may be converted to an equivalent input noise by dividing by the amplifier gain. Thus the noise figure becomes:

$$NF = 20 \log \frac{\text{total rms noise voltage referred to amp input}}{\text{source thermal noise voltage (rms)}} \quad (3\text{-}15)$$

The equivalent noise bandwidth (Δf) used in determining the source thermal noise is simply $\pi/2$ times the high frequency rolloff.

The system's preamplifier has a 3 dB point on the low pass gain curve at 25 Hz. This yields an equivalent noise bandwidth of

$$\Delta f = 25 \times \pi/2 = 39.27 \text{ Hz}$$

and a source thermal noise of 8.69×10^{-9} rms volts, which is -161 dB re: 1 volt.

A 120Ω resistor was connected across to the preamplifier input while the rms voltage was measured on the spectrum analyzer. By dividing the total output noise by the amplifier gain the Noise Figure at one hertz was obtained as 15 dB (see in Figure 17).

Once the total rms noise voltage referred to the preamplifier's input was determined, the noise introduced by the remainder of the system was determined to be negligible in comparison to the preamplifier noise, with the exception of four very discrete frequency components introduced by the tape recorder. These are centered at 3.4, 6.1, 6.8, and 8.1 Hz and have been deleted from the data curves. The purpose of the reference signal and mixer is to eliminate the tape recorder noise. However, the noise reduction is limited to about 10 dB at these four undesired frequencies.

The total system noise rms voltage level was measured several times at various locations. In particular, it was measured each time data was taken in the environment pre-

sent (i.e. land or sea). On each occasion the total noise was found to be at the level shown in Figure 17 which was exclusively front end preamplifier noise. No other sources introduced noise above this level.

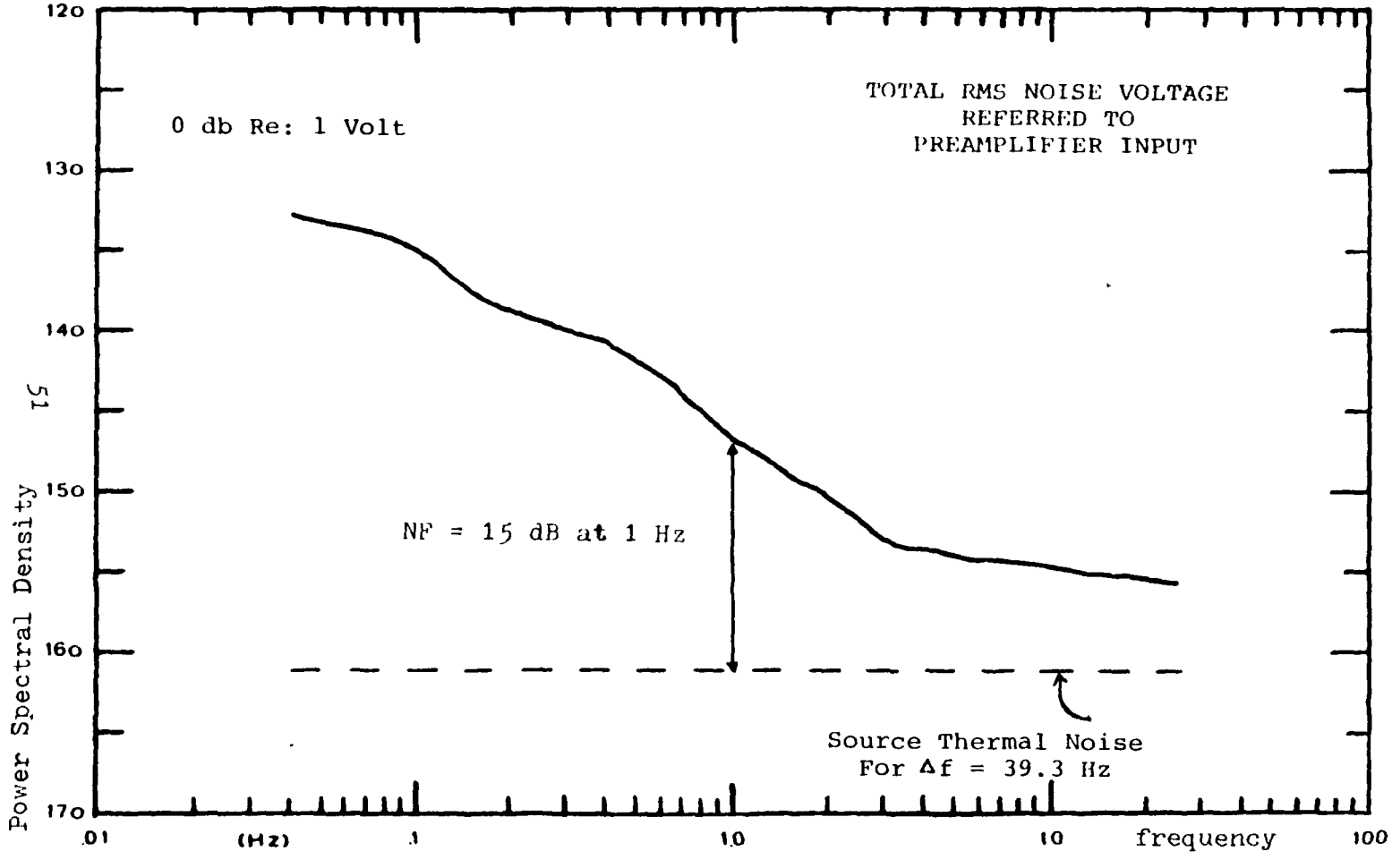
120
130
140
150
160
170
0 db Re: 1 Volt
TOTAL RMS NOISE VOLTAGE
REFERRED TO
PREAMPLIFIER INPUT
NF = 15 dB at 1 Hz
Source Thermal Noise
For Δf = 39.3 Hz
Power Spectral Density
51
.01
(Hz)
.1
1.0
10
frequency
100

Figure 17

IV. EXPERIMENTAL RESULTS

A. UNDERWATER DATA

Of the six hours of total recorded data, half was obtained at sea and half at a remote land site near Chew's Ridge in California. The underwater data was taken at two stations designated as Station #1 (36^{o}-38'N, 121^{o}-52'W) and Station #2 (36^{o}-39'N, 121^{o}-53'W). The depth, local time, date, and frequency band of the measurements are annotated on each figure. The sea floor at both stations has less than 5^{o} of slope and consists mainly of smooth sand. The sensor was arranged so that the central axis of symmetry was parallel to the sea floor at an arbitrary angle referenced to a North/South direction.

Figure 18-19 represent one half hour of recorded underwater data taken in a moderately heavy sea state (10-15 ft. swells) on 14 April 80. The remainder of data taken on 14 April was not usable due to loss of electrical continuity between upper and lower spheres. Figures 20-29 represent 2.5 hours of recorded underwater data taken in calm seas on 18 April 80.

B. LAND DATA

All three hours of land data was recorded on 1 May 80. The location was chosen because of its remoteness and lack of external power sources or power lines. The position of the sensor remained fixed throughout each data run, and

the orientation was as follows:

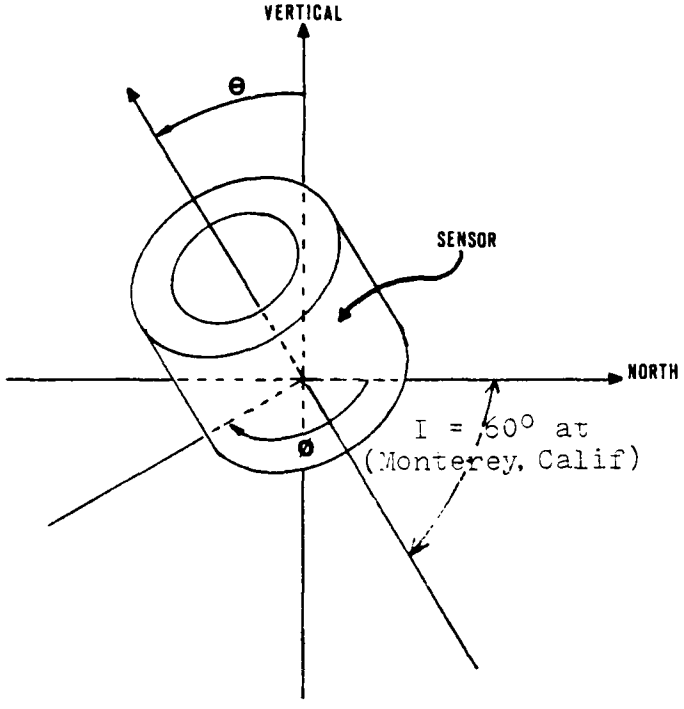

Figure #	θ	Ø
30-31	70°	180°
32	0	NA.
33	90°	90°
34	90°	0°
35	60°	0°
36	30°	180°
37	90°	90°

The only prominent signals observed at less than 1 Hz were on the first run. All subsequent runs revealed preamplifier noise to be dominant at less than 1 Hz.

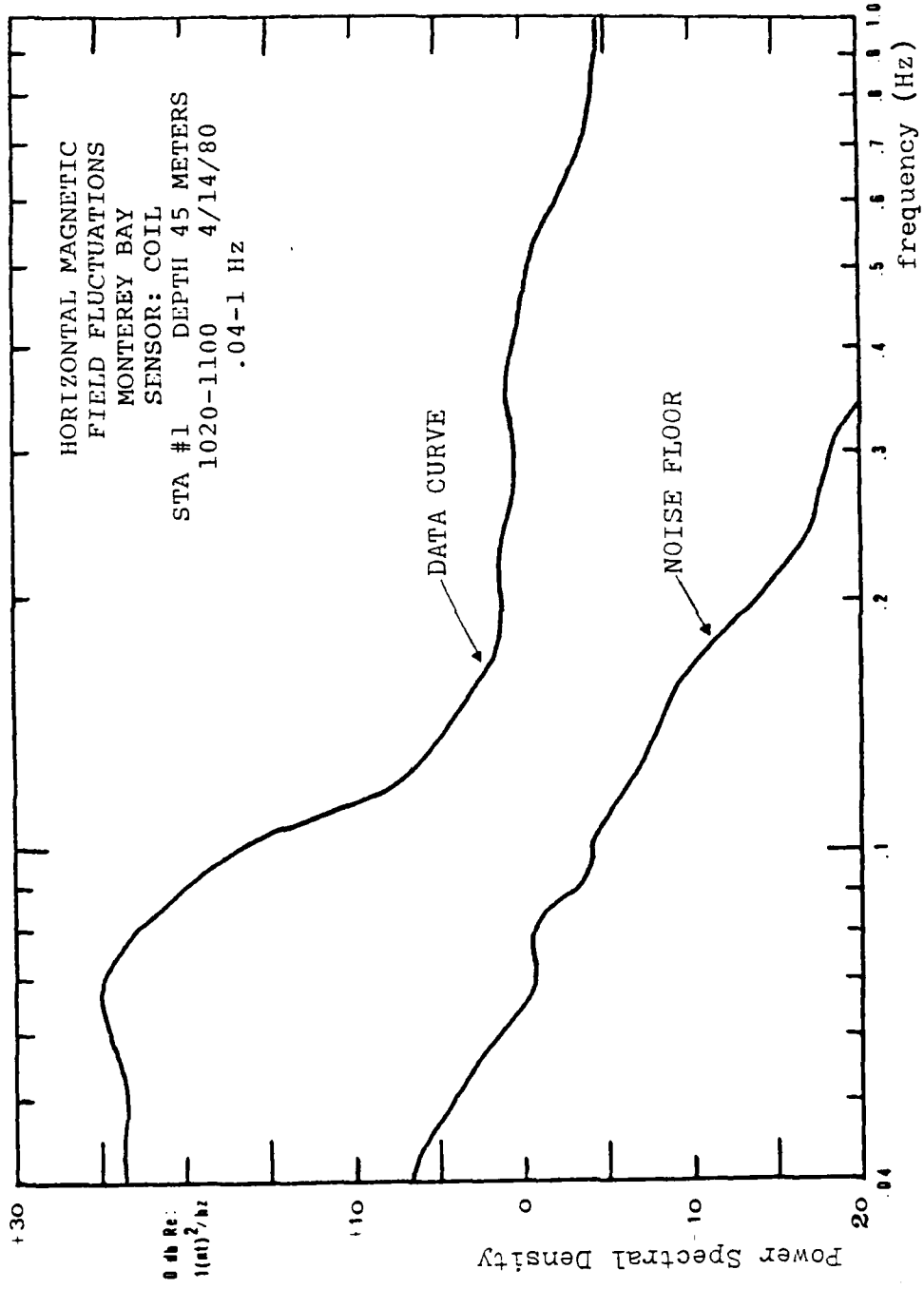
HORIZONTAL MAGNETIC
FIELD FLUCTUATIONS
MONTEREY BAY
SENSOR: COIL
STA #1 DEPTH 45 METERS
1020-1100 4/14/80
.04-1 Hz
DATA CURVE
NOISE FLOOR
Power Spectral Density
Frequency (Hz)

Figure 18

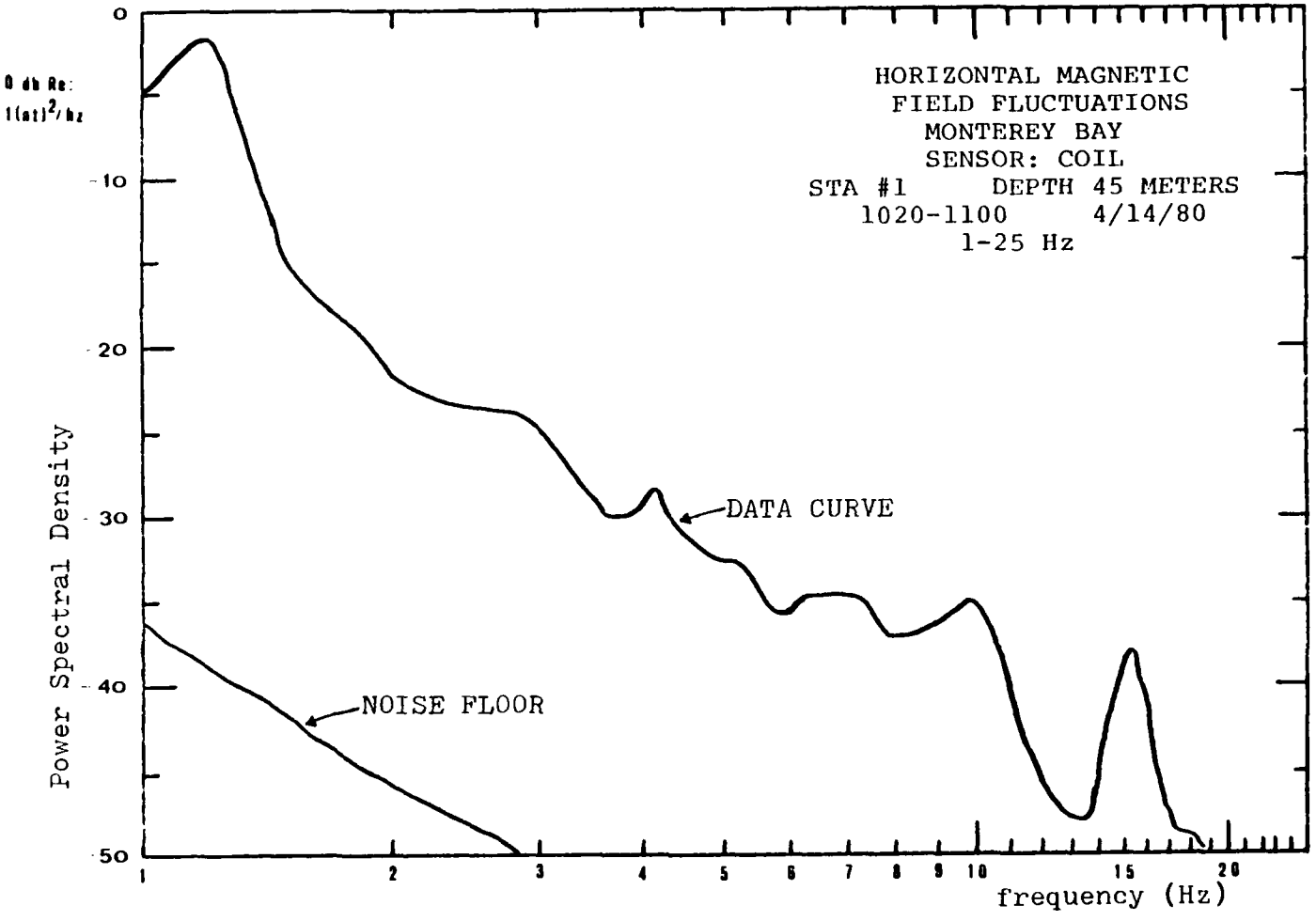
0 db Re:
1(nt)²/hz
0
10
20
30
40
50
Power Spectral Density
HORIZONTAL MAGNETIC
FIELD FLUCTUATIONS
MONTEREY BAY
SENSOR: COIL
STA #1 DEPTH 45 METERS
1020-1100 4/14/80
1-25 Hz
DATA CURVE
NOISE FLOOR
1
2
3
4
5
6
7
8
9
10
15
20
frequency (Hz)

Figure 19

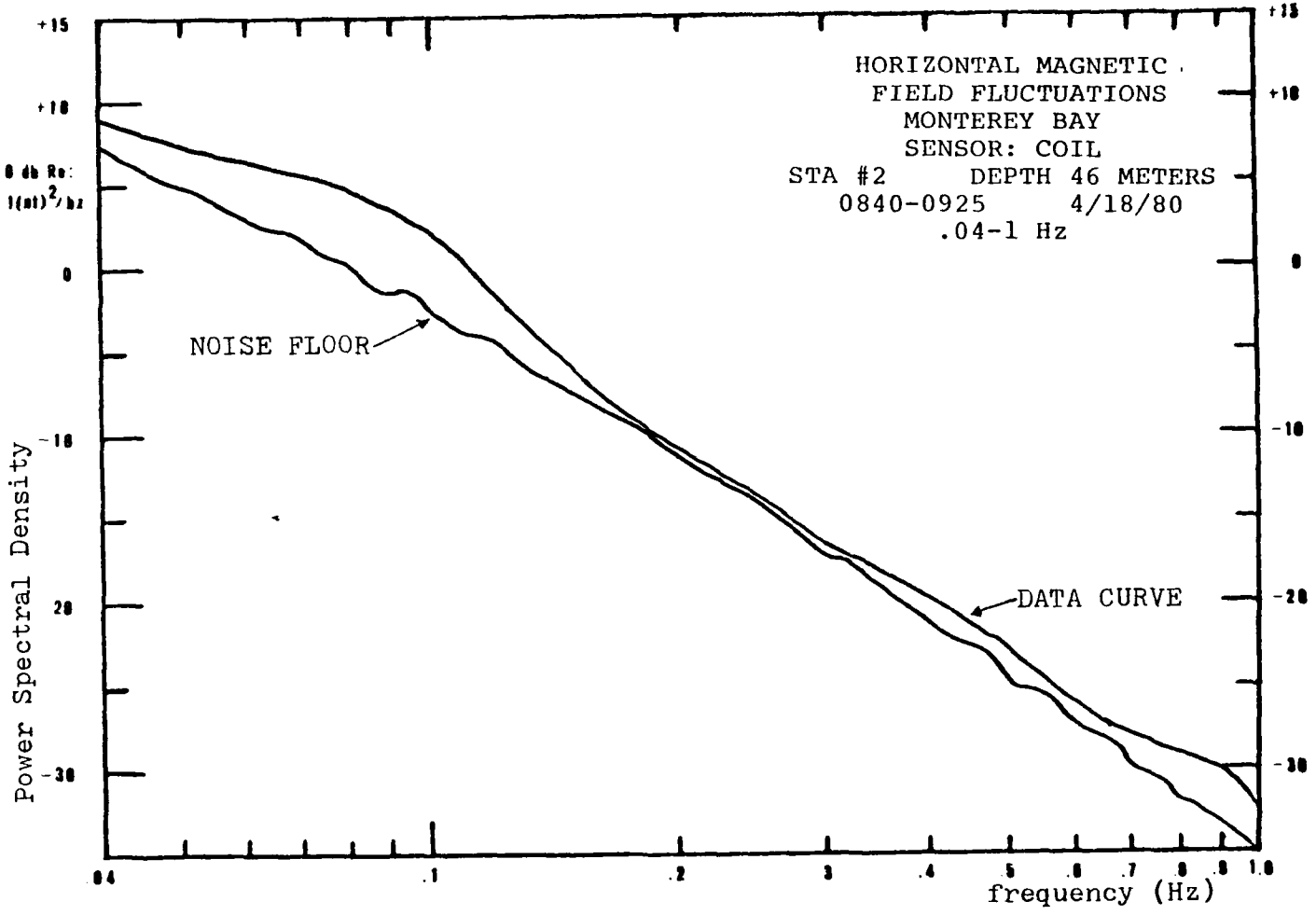
HORIZONTAL MAGNETIC
FIELD FLUCTUATIONS
MONTEREY BAY
SENSOR: COIL
STA #2 DEPTH 46 METERS
0840-0925 4/18/80
.04-1 Hz
NOISE FLOOR
DATA CURVE
Power Spectral Density
frequency (Hz)
+15
+10
0
-10
-20
-30
.04
.1
.2
.3
.4
.5
.6
.7
.8
.9
1.0

Figure 20

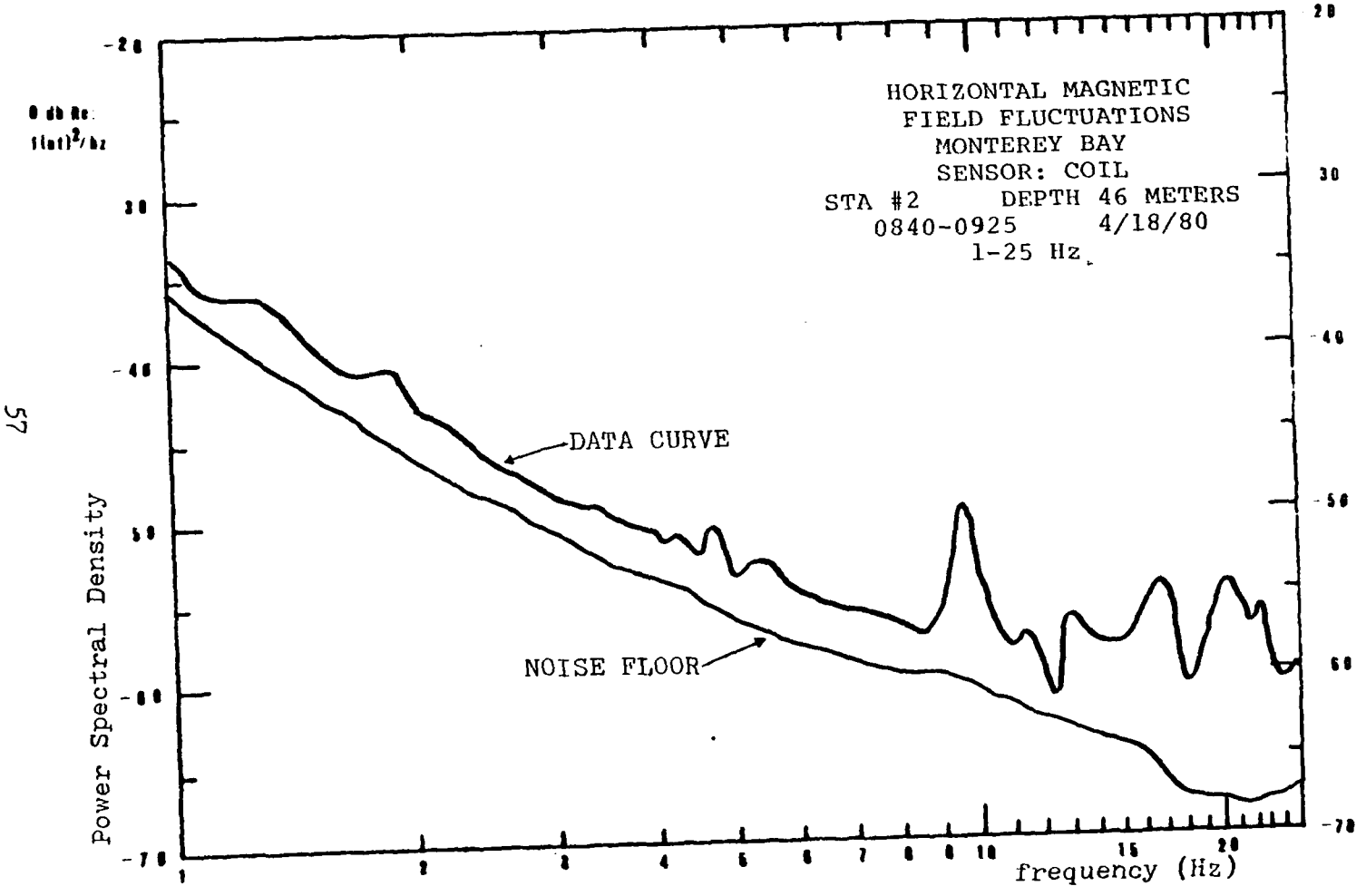
HORIZONTAL MAGNETIC
FIELD FLUCTUATIONS
MONTEREY BAY
SENSOR: COIL
STA #2 DEPTH 46 METERS
0840-0925 4/18/80
1-25 Hz
DATA CURVE
NOISE FLOOR
Power Spectral Density
frequency (Hz)

Figure 21

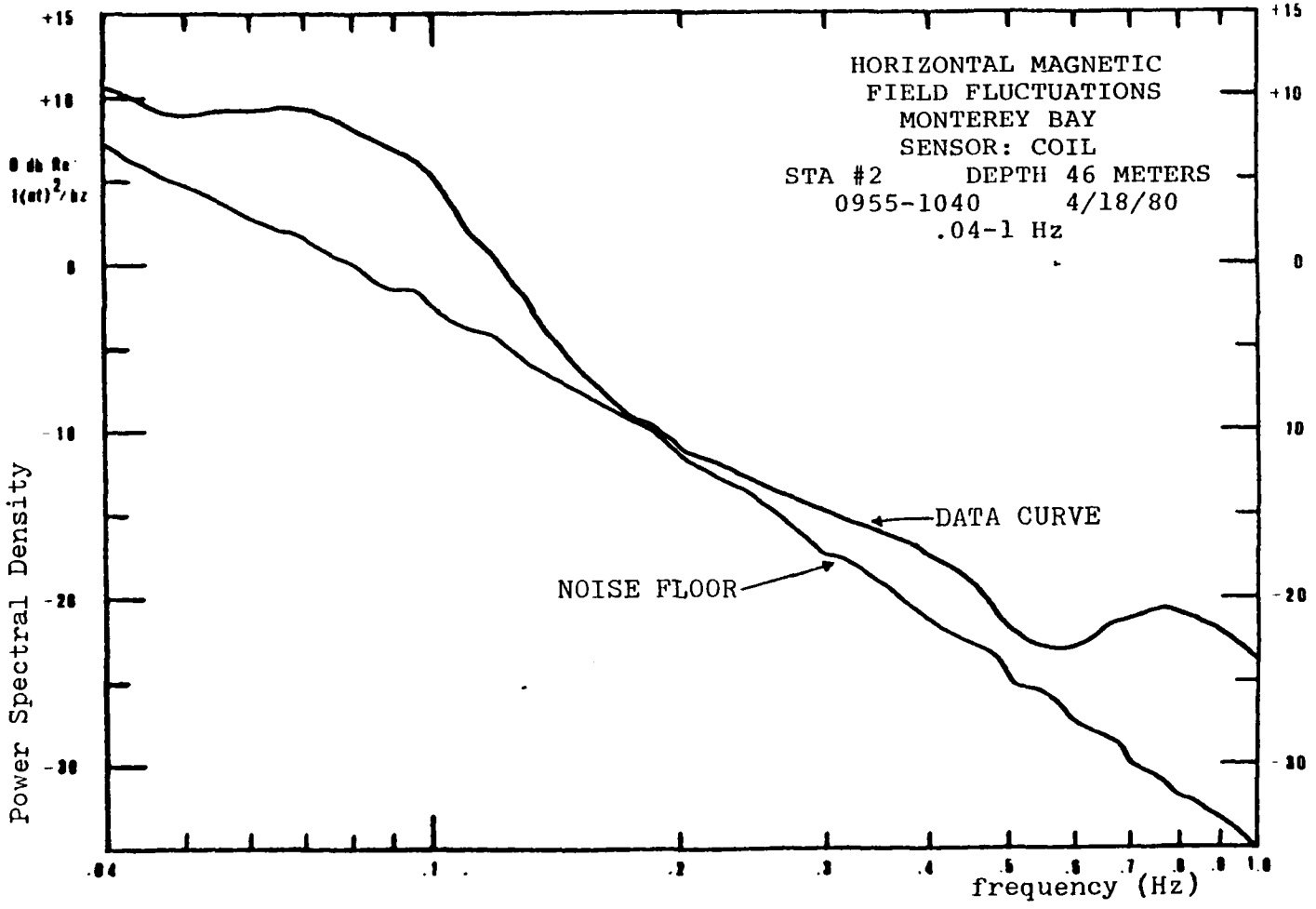
HORIZONTAL MAGNETIC
FIELD FLUCTUATIONS
MONTEREY BAY
SENSOR: COIL
STA #2 DEPTH 46 METERS
0955-1040 4/18/80
.04-1 Hz
DATA CURVE
NOISE FLOOR
Power Spectral Density
frequency (Hz)
+15
+10
0
-10
-20
-30
.04
.1
.2
.3
.4
.5
.6
.7
.8
.9
1.0

Figure 22

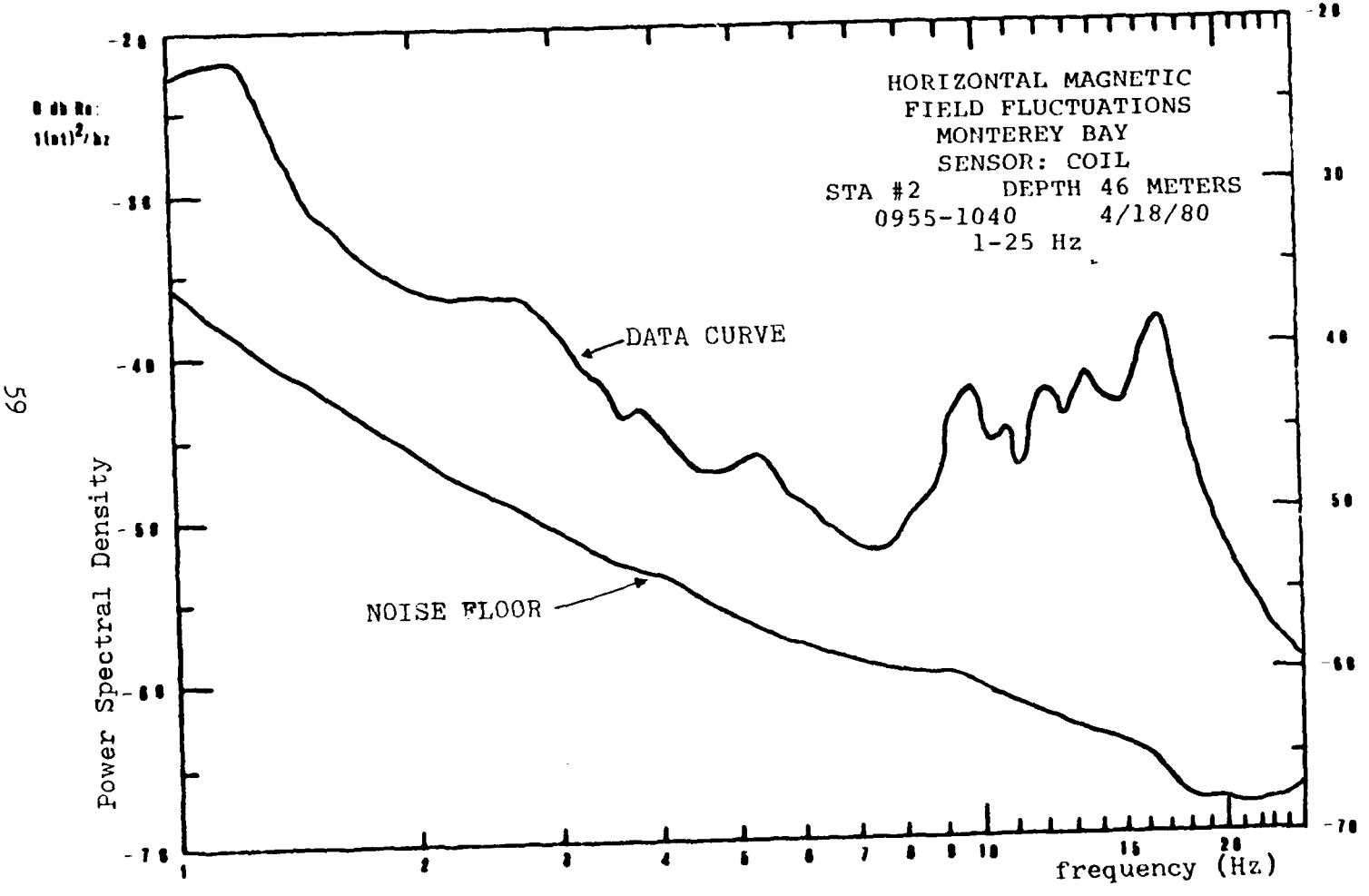
HORIZONTAL MAGNETIC
FIELD FLUCTUATIONS
MONTEREY BAY
SENSOR: COIL
STA #2 DEPTH 46 METERS
0955-1040 4/18/80
1-25 Hz
DATA CURVE
NOISE FLOOR
Power Spectral Density
frequency (Hz)

Figure 23

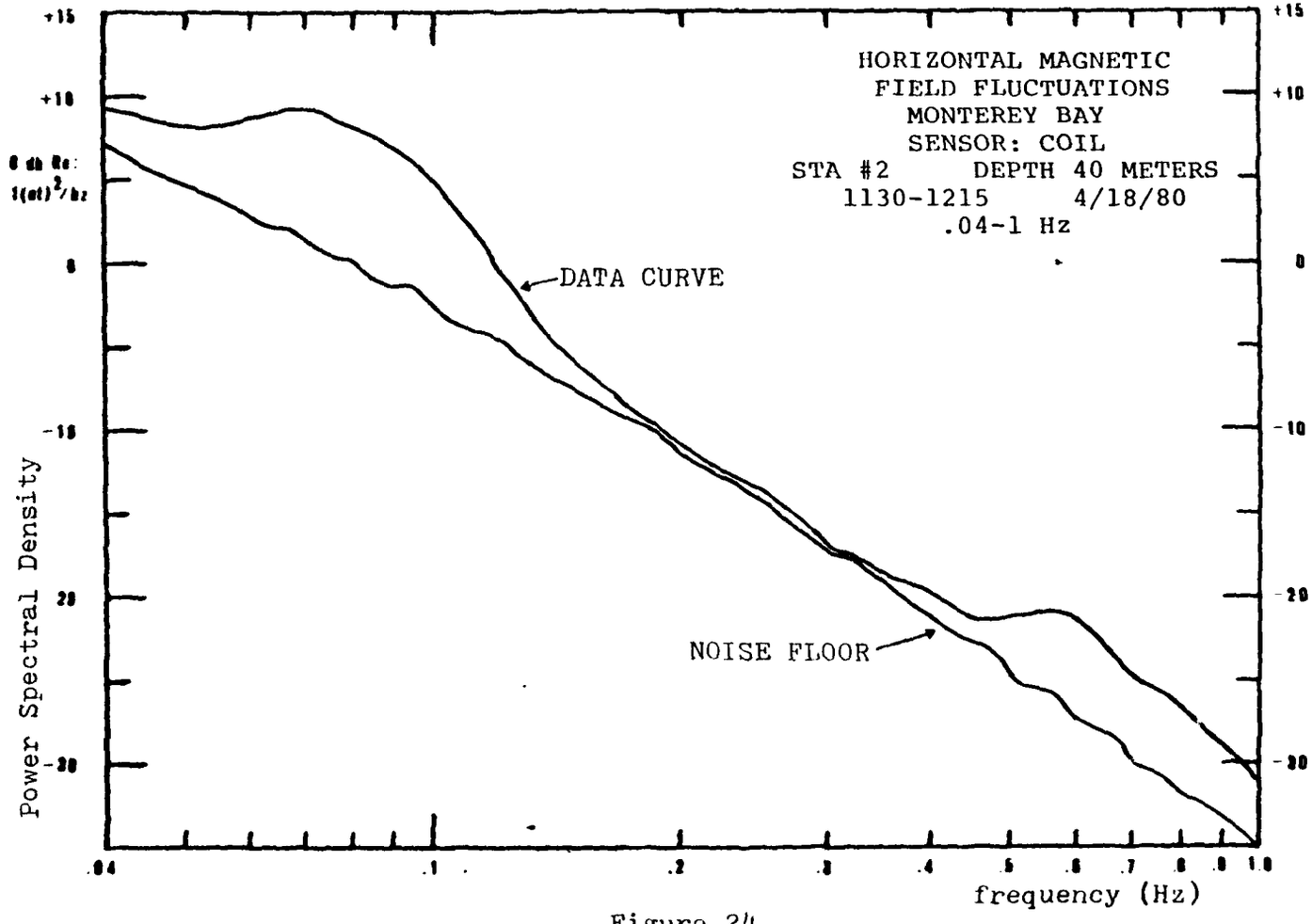
HORIZONTAL MAGNETIC
FIELD FLUCTUATIONS
MONTEREY BAY
SENSOR: COIL
STA #2 DEPTH 40 METERS
1130-1215 4/18/80
.04-1 Hz
DATA CURVE
NOISE FLOOR
Power Spectral Density
frequency (Hz)
+15
+10
0
-10
-20
-30
.04
.1
.2
.3
.4
.5
.6
.7
.8
.9
1.0

Figure 24

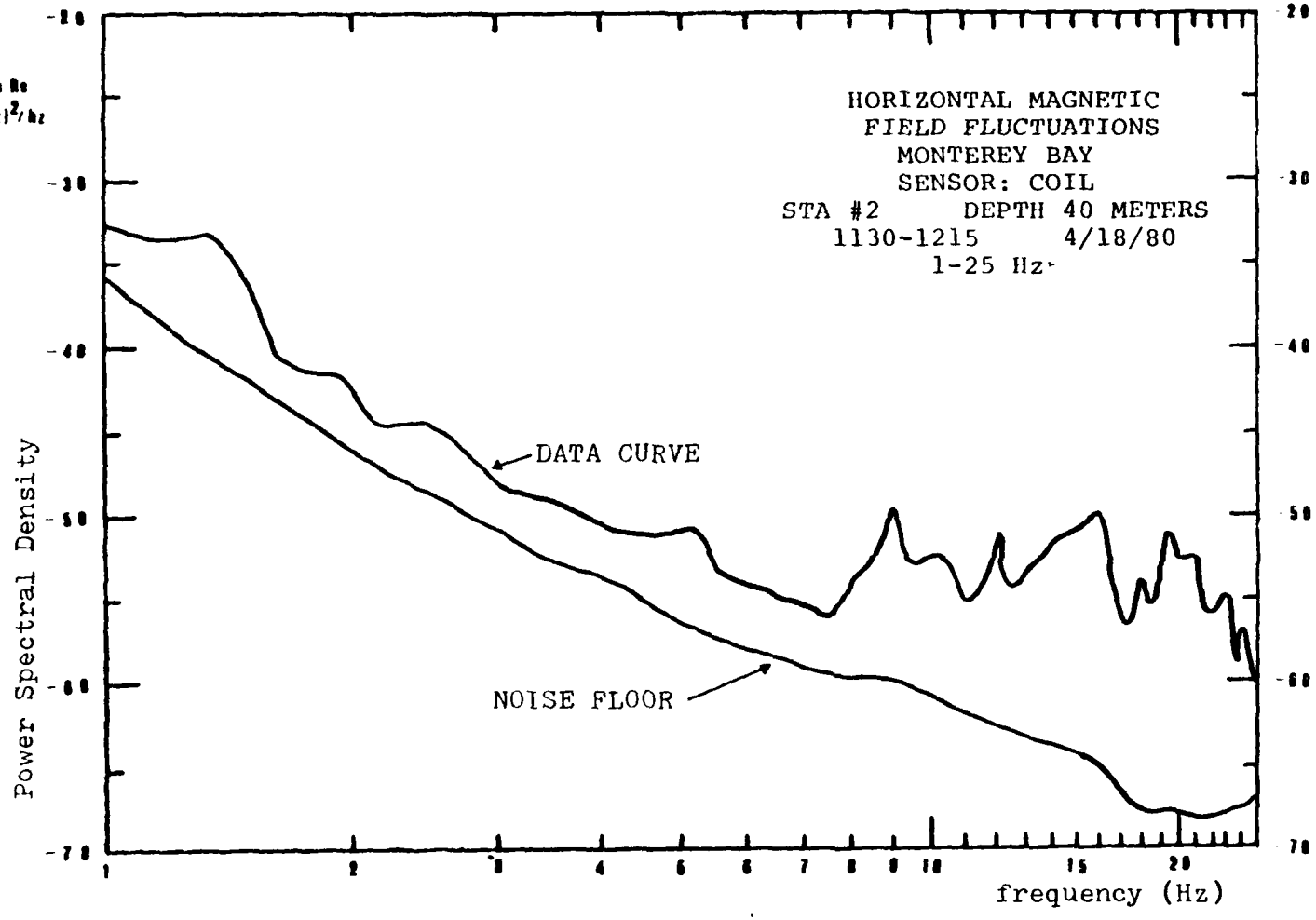
HORIZONTAL MAGNETIC
FIELD FLUCTUATIONS
MONTEREY BAY
SENSOR: COIL
STA #2 DEPTH 40 METERS
1130-1215 4/18/80
1-25 Hz
DATA CURVE
NOISE FLOOR
Power Spectral Density
frequency (Hz)

Figure 25

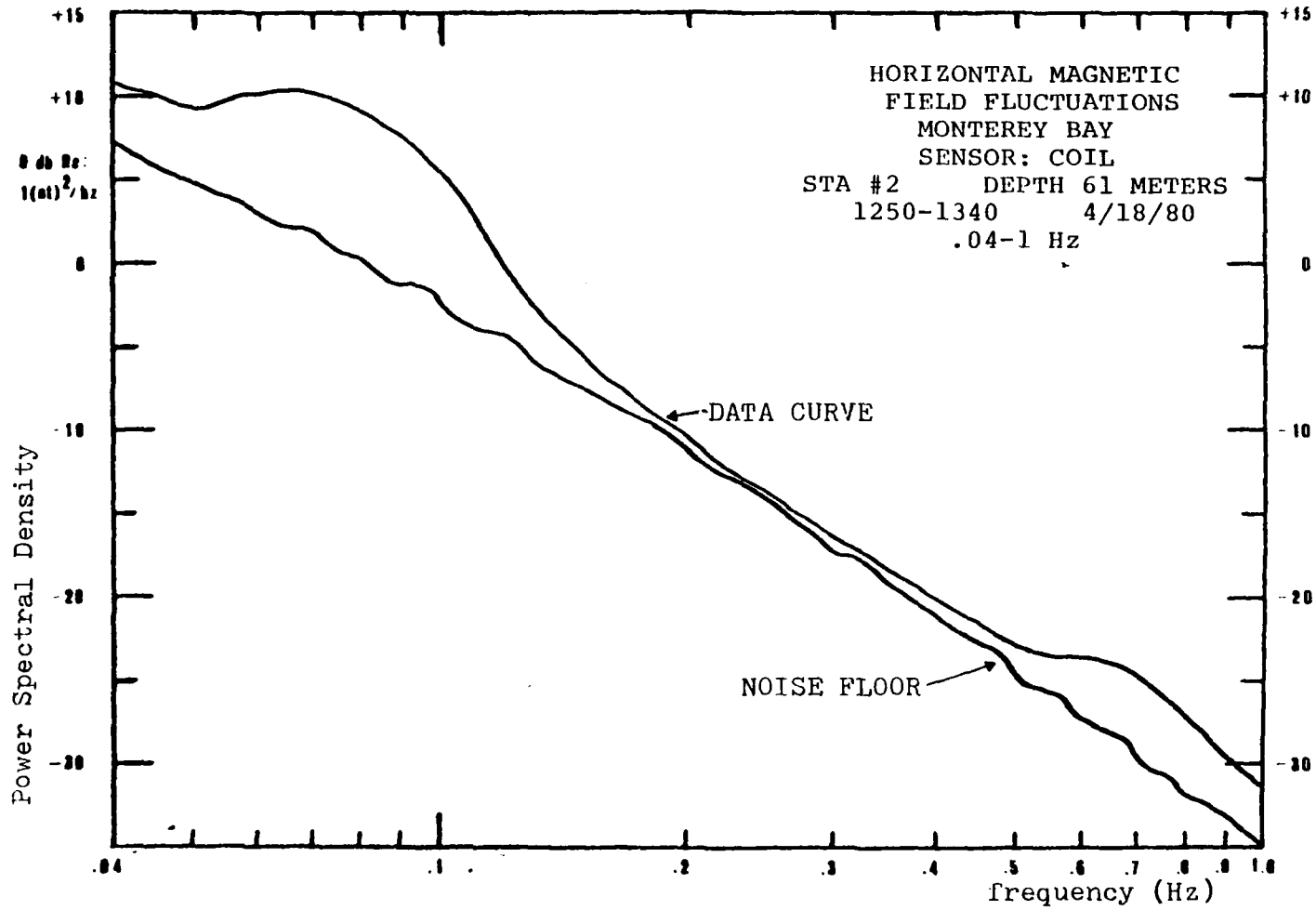
HORIZONTAL MAGNETIC
FIELD FLUCTUATIONS
MONTEREY BAY
SENSOR: COIL
STA #2 DEPTH 61 METERS
1250-1340 4/18/80
.04-1 Hz
DATA CURVE
NOISE FLOOR
Power Spectral Density
Frequency (Hz)
+15
+10
0
-10
-20
-30
.04
.1
.2
.3
.4
.5
.6
.7
.8
.9
1.0

Figure 26

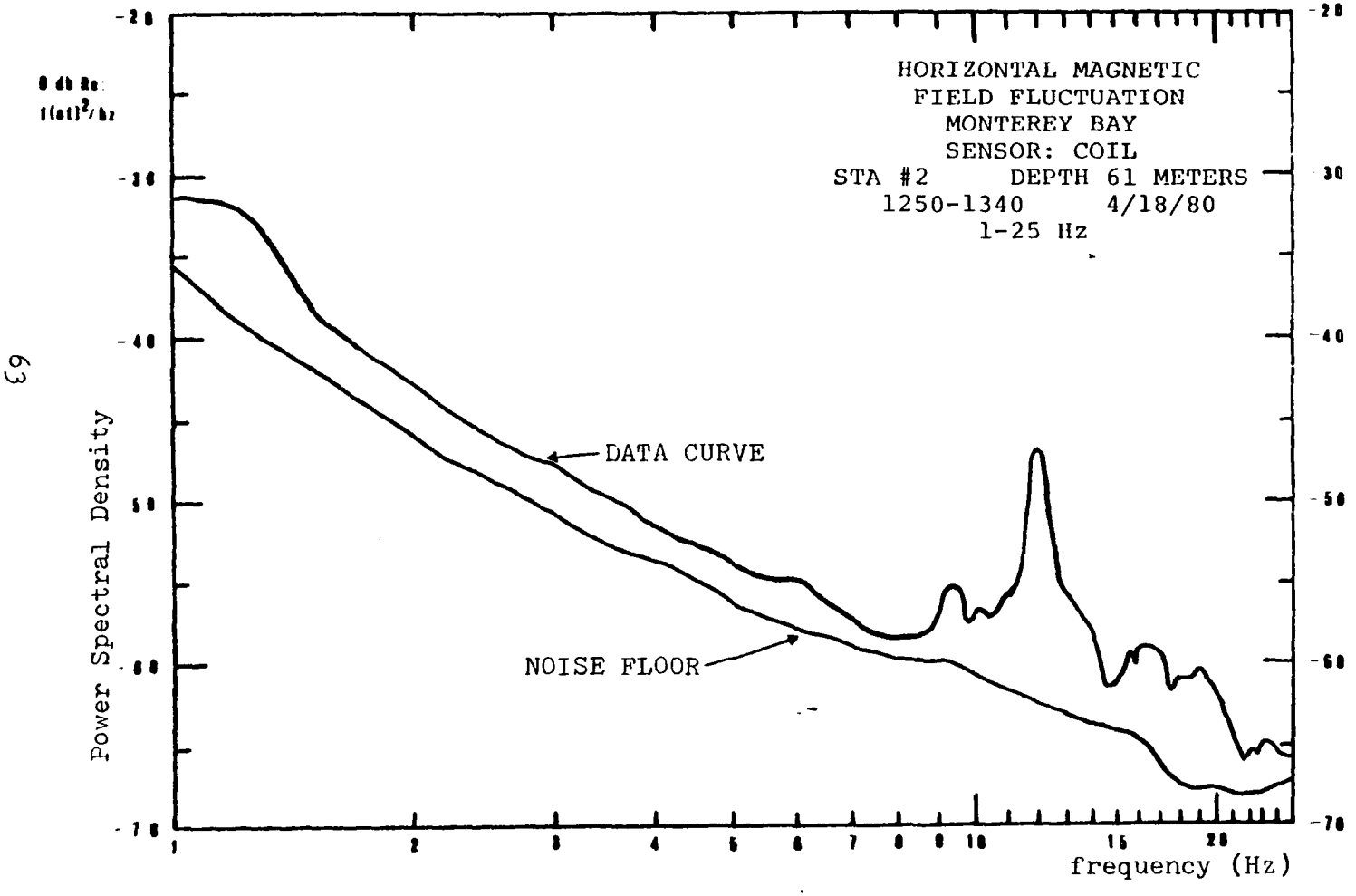
HORIZONTAL MAGNETIC
FIELD FLUCTUATION
MONTEREY BAY
SENSOR: COIL
STA #2 DEPTH 61 METERS
1250-1340 4/18/80
1-25 Hz
DATA CURVE
NOISE FLOOR
Power Spectral Density
frequency (Hz)

Figure 27

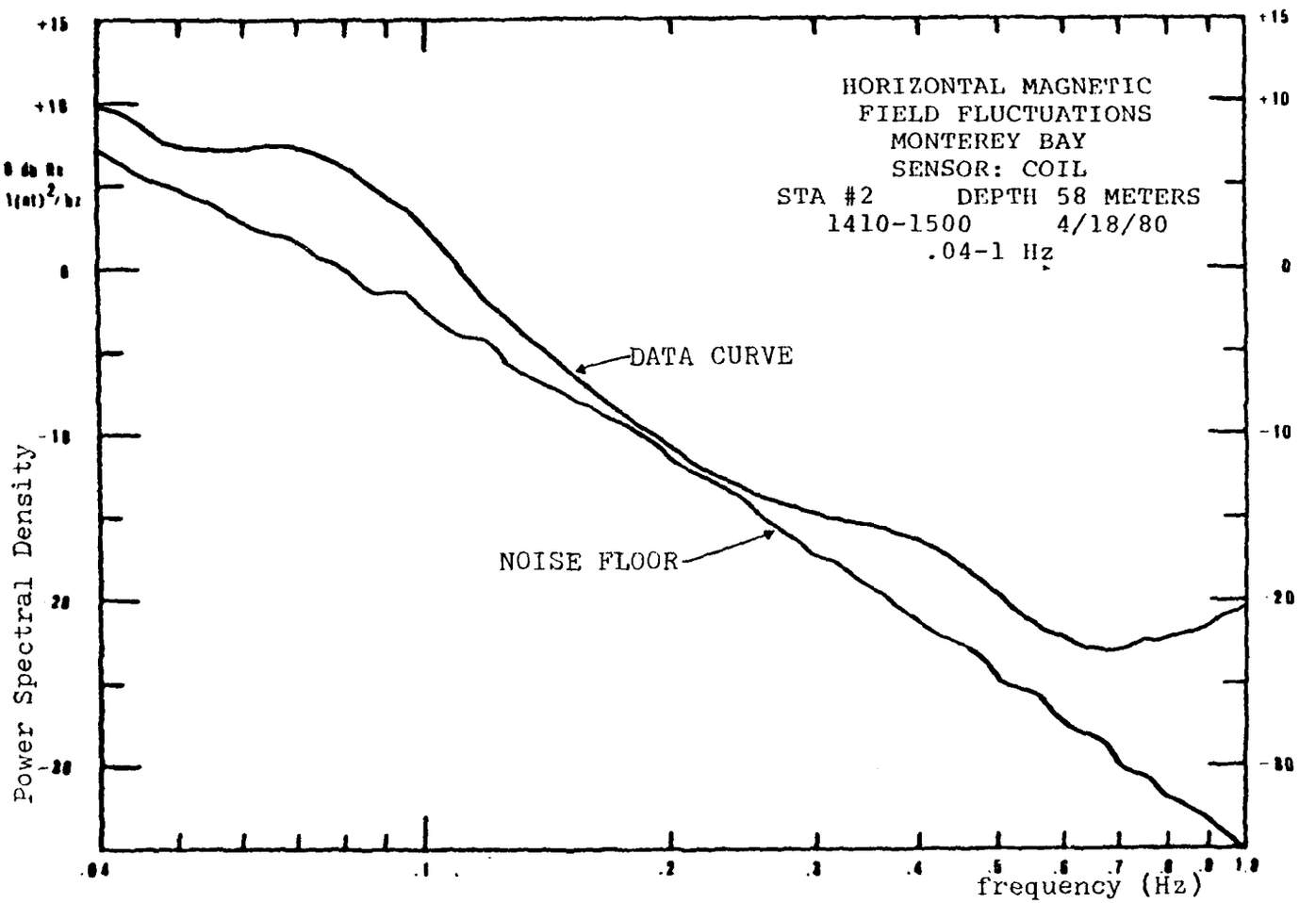
HORIZONTAL MAGNETIC
FIELD FLUCTUATIONS
MONTEREY BAY
SENSOR: COIL
STA #2 DEPTH 58 METERS
1410-1500 4/18/80
.04-1 Hz
DATA CURVE
NOISE FLOOR
Power Spectral Density
frequency (Hz)
+15
+10
0
-10
-20
-30
.04
.1
.2
.3
.4
.5
.6
.7
.8
.9
1.0

Figure 28

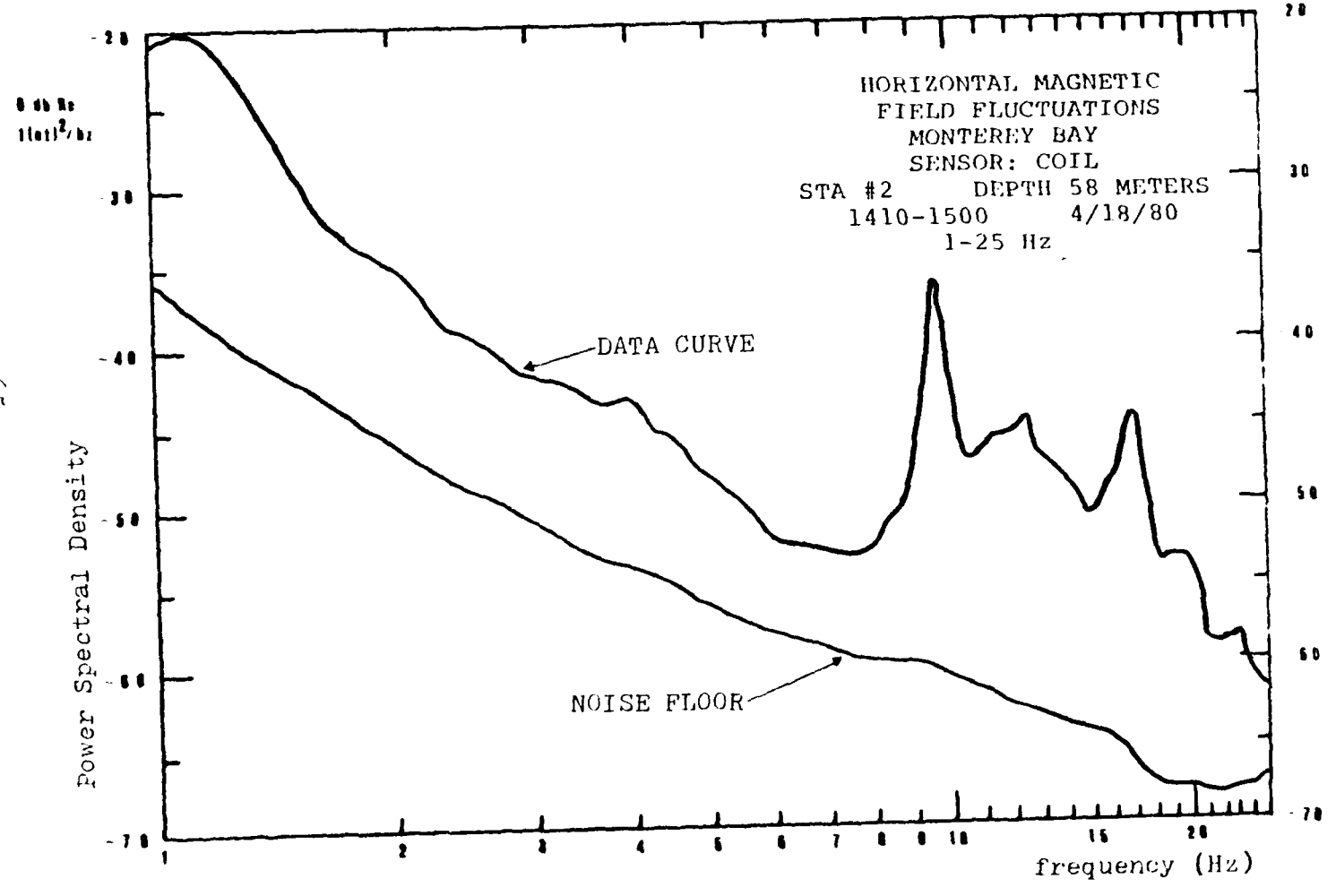
HORIZONTAL MAGNETIC
FIELD FLUCTUATIONS
MONTEREY BAY
SENSOR: COIL
STA #2 DEPTH 58 METERS
1410-1500 4/18/80
1-25 Hz
DATA CURVE
NOISE FLOOR
Power Spectral Density
frequency (Hz)

Figure 29

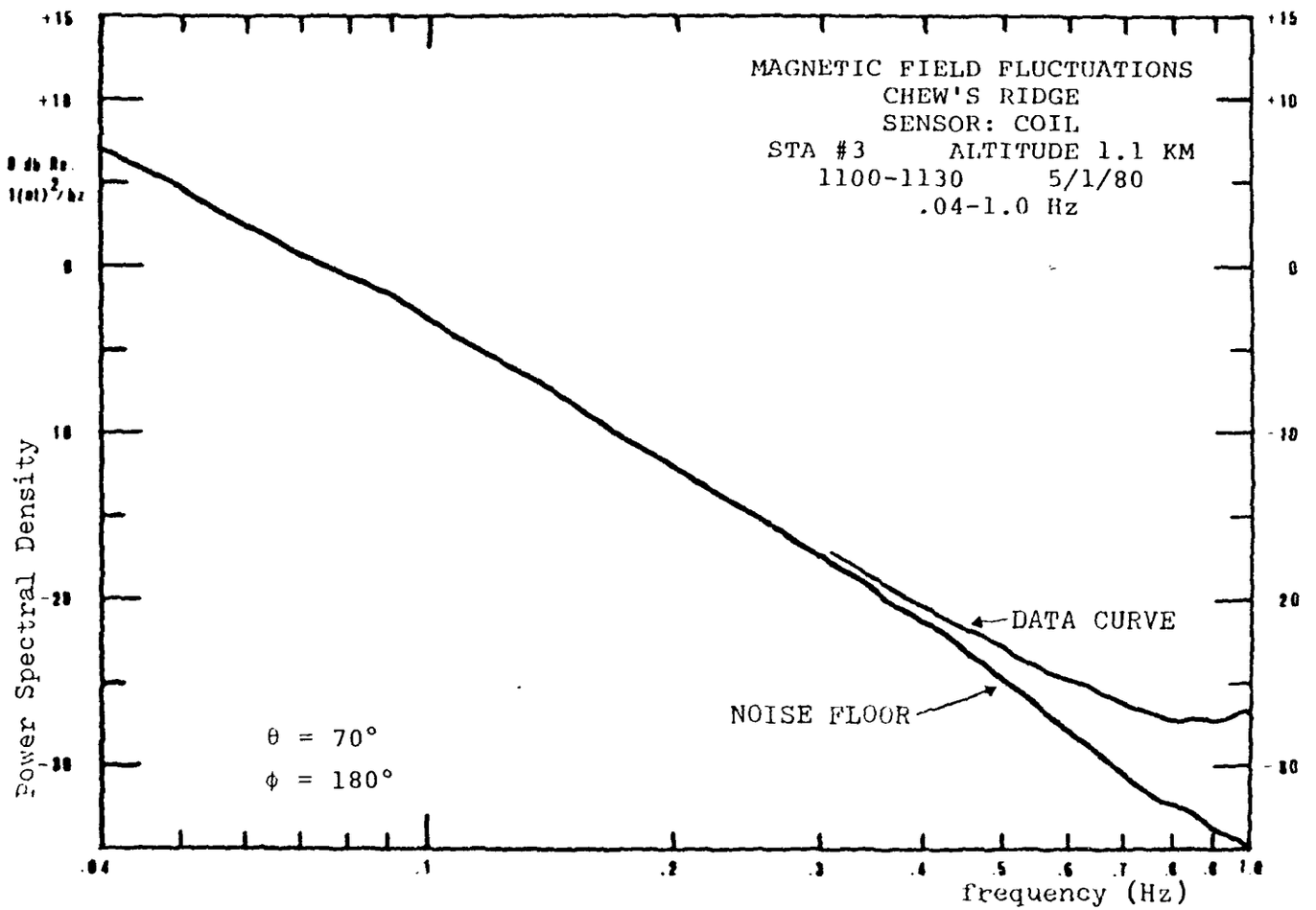
MAGNETIC FIELD FLUCTUATIONS
CHEW'S RIDGE
SENSOR: COIL
STA #3 ALTITUDE 1.1 KM
1100-1130 5/1/80
.04-1.0 Hz
Power Spectral Density
frequency (Hz)
DATA CURVE
NOISE FLOOR
θ = 70°
ϕ = 180°

Figure 30

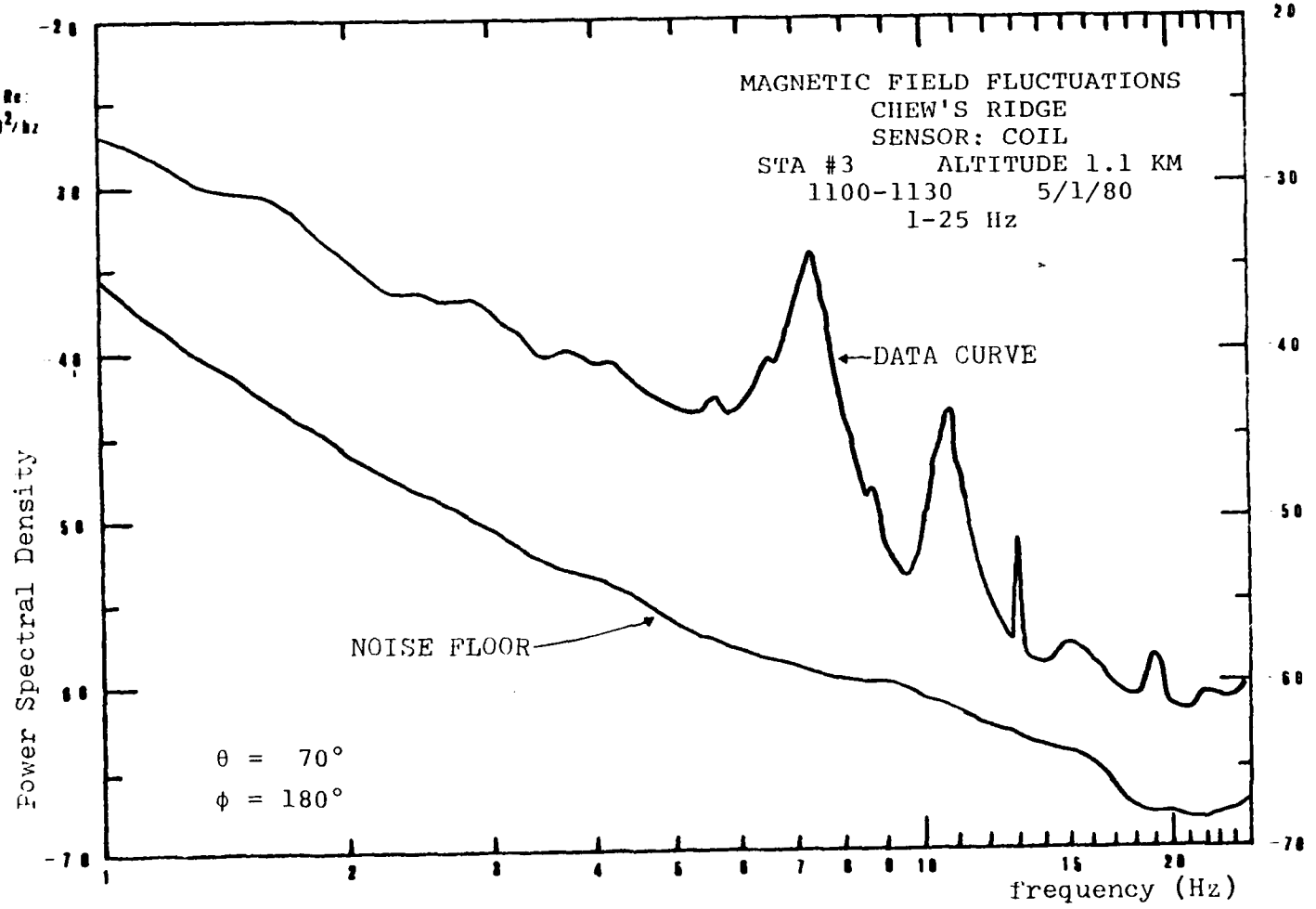
MAGNETIC FIELD FLUCTUATIONS
CHEW'S RIDGE
SENSOR: COIL
STA #3 ALTITUDE 1.1 KM
1100-1130 5/1/80
1-25 Hz
DATA CURVE
NOISE FLOOR
θ = 70°
φ = 180°
Power Spectral Density
frequency (Hz)

Figure 31

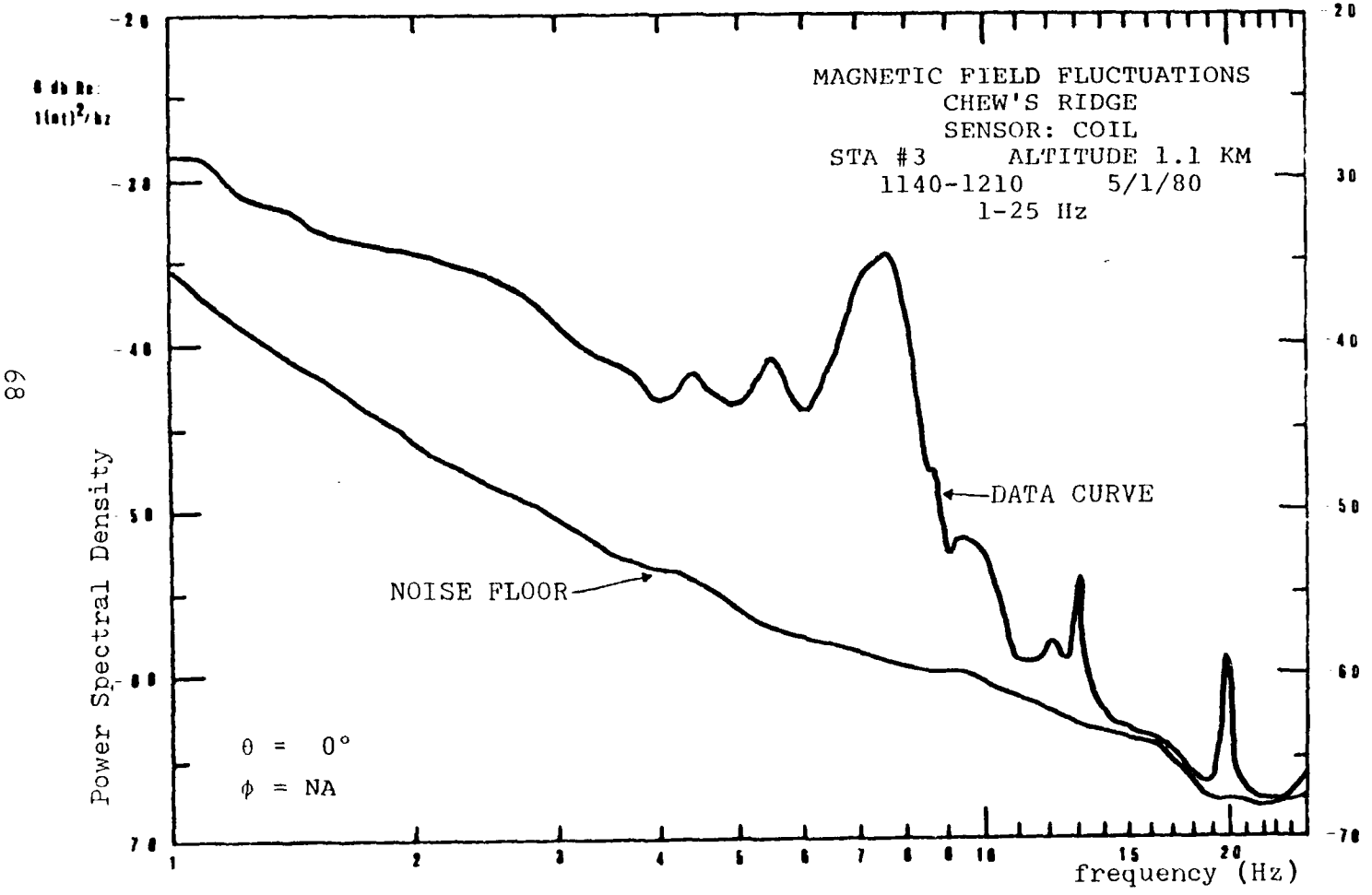
MAGNETIC FIELD FLUCTUATIONS
CHEW'S RIDGE
SENSOR: COIL
STA #3 ALTITUDE 1.1 KM
1140-1210 5/1/80
1-25 Hz
DATA CURVE
NOISE FLOOR
θ = 0°
ϕ = NA
Power Spectral Density
frequency (Hz)

Figure 32

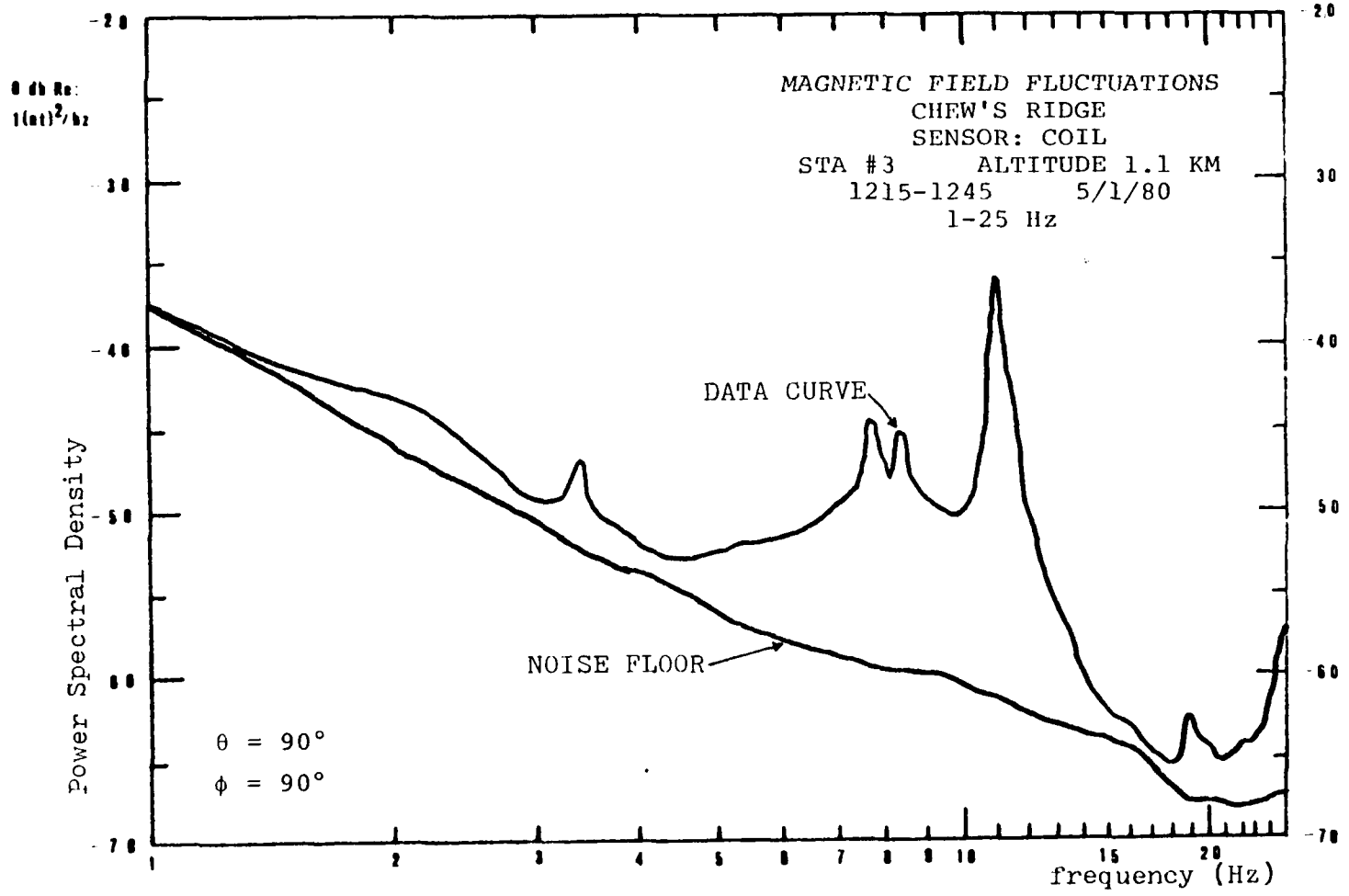
MAGNETIC FIELD FLUCTUATIONS
CHEW'S RIDGE
SENSOR: COIL
STA #3 ALTITUDE 1.1 KM
1215-1245 5/1/80
1-25 Hz
DATA CURVE
NOISE FLOOR
θ = 90°
φ = 90°
Power Spectral Density
frequency (Hz)

Figure 33

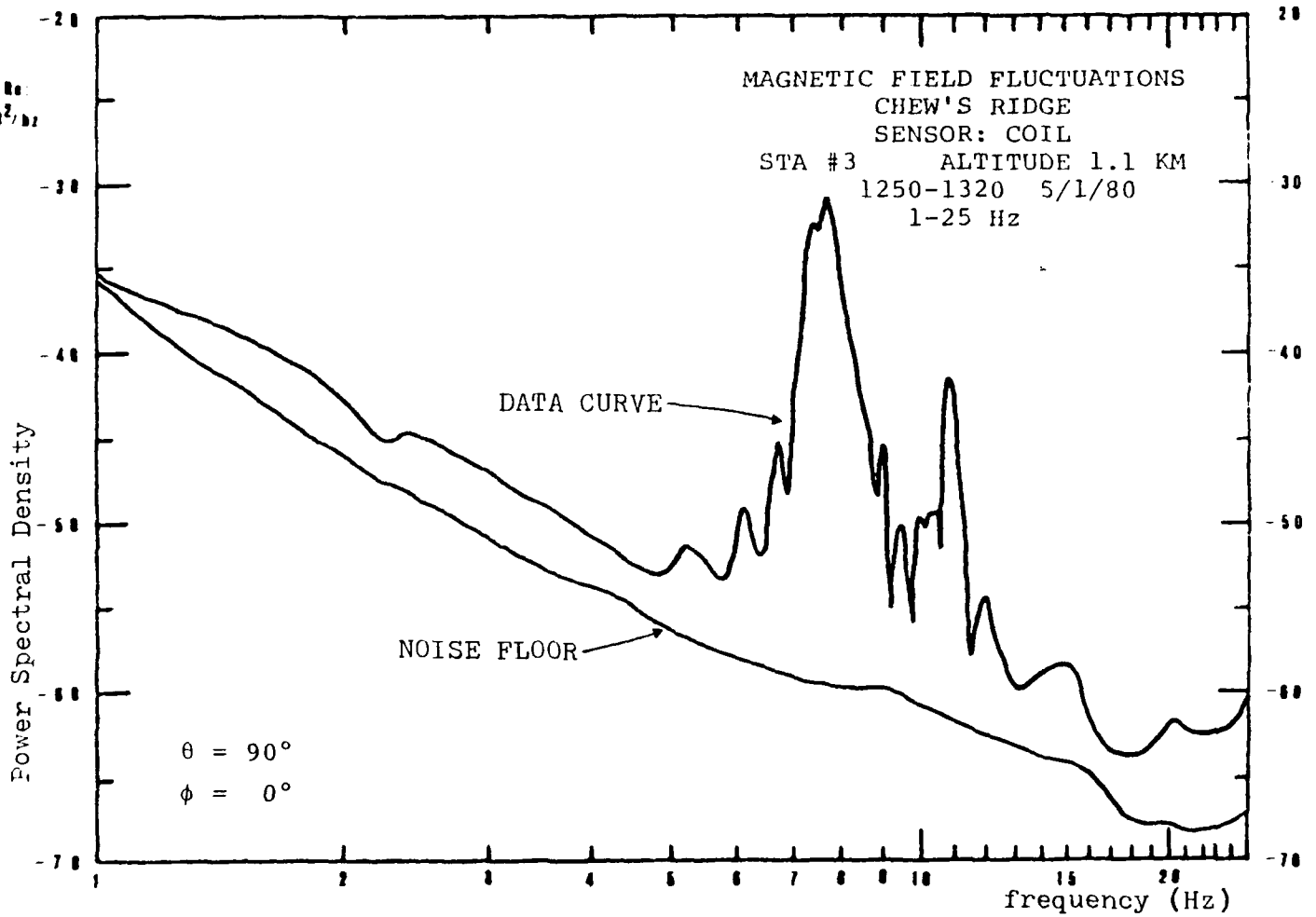
MAGNETIC FIELD FLUCTUATIONS
CHEW'S RIDGE
SENSOR: COIL
STA #3 ALTITUDE 1.1 KM
1250-1320 5/1/80
1-25 Hz
DATA CURVE
NOISE FLOOR
θ = 90°
φ = 0°
Power Spectral Density
frequency (Hz)

Figure 34

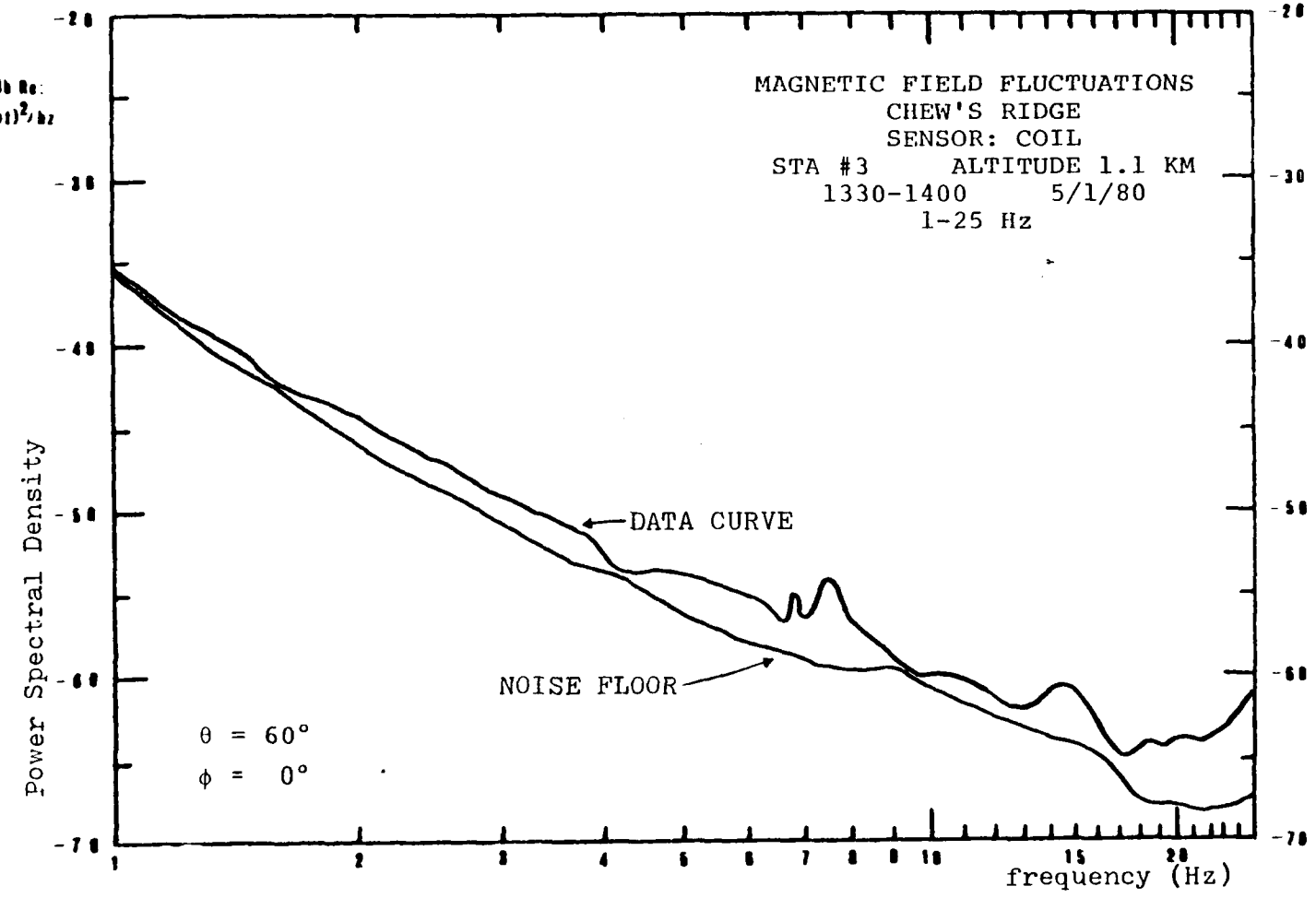
MAGNETIC FIELD FLUCTUATIONS
CHEW'S RIDGE
SENSOR: COIL
STA #3 ALTITUDE 1.1 KM
1330-1400 5/1/80
1-25 Hz
DATA CURVE
NOISE FLOOR
θ = 60°
φ = 0°
Power Spectral Density
frequency (Hz)

Figure 35

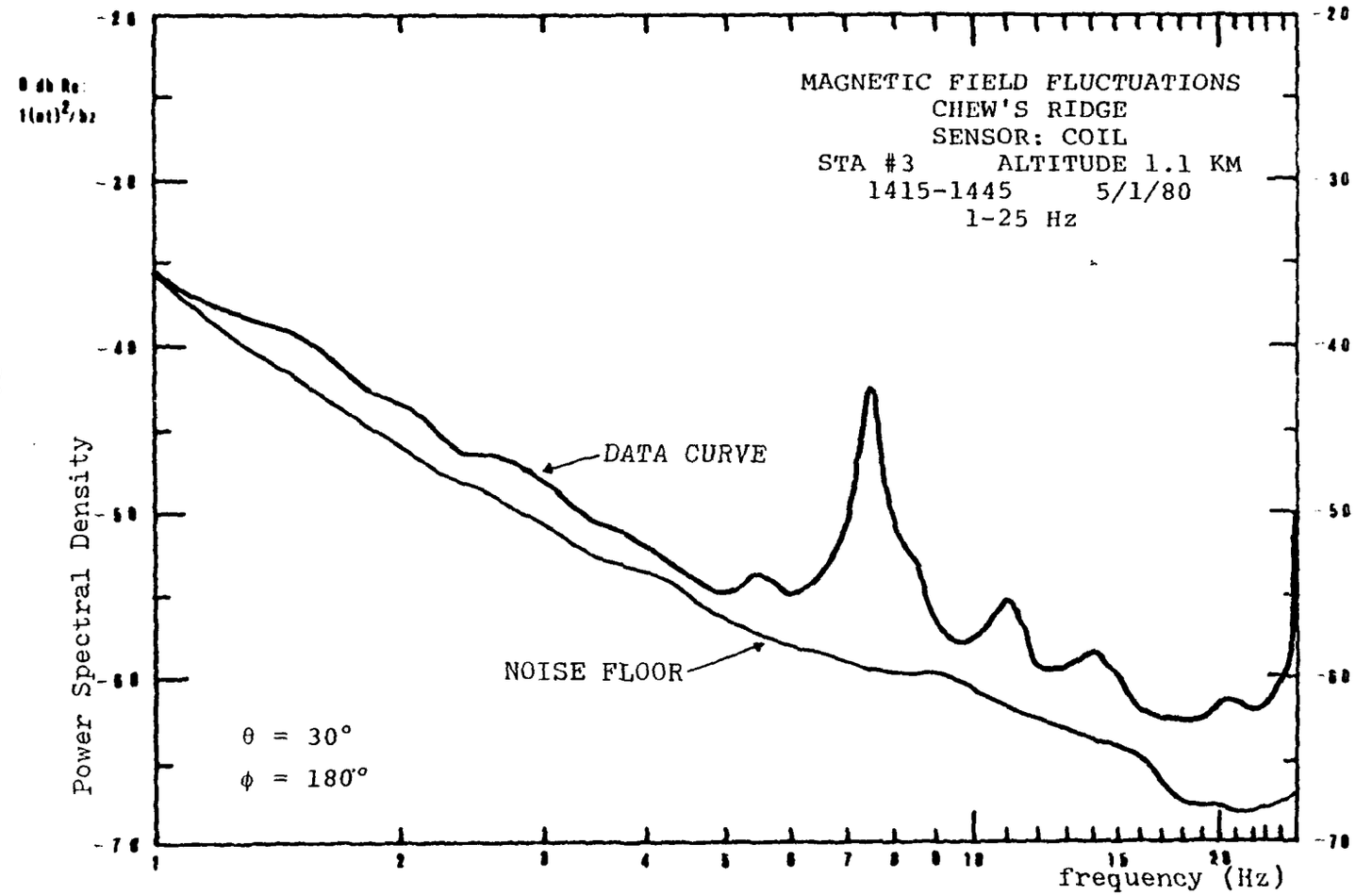
MAGNETIC FIELD FLUCTUATIONS
CHEW'S RIDGE
SENSOR: COIL
STA #3 ALTITUDE 1.1 KM
1415-1445 5/1/80
1-25 Hz
DATA CURVE
NOISE FLOOR
θ = 30°
φ = 180°
Power Spectral Density
frequency (Hz)

Figure 36

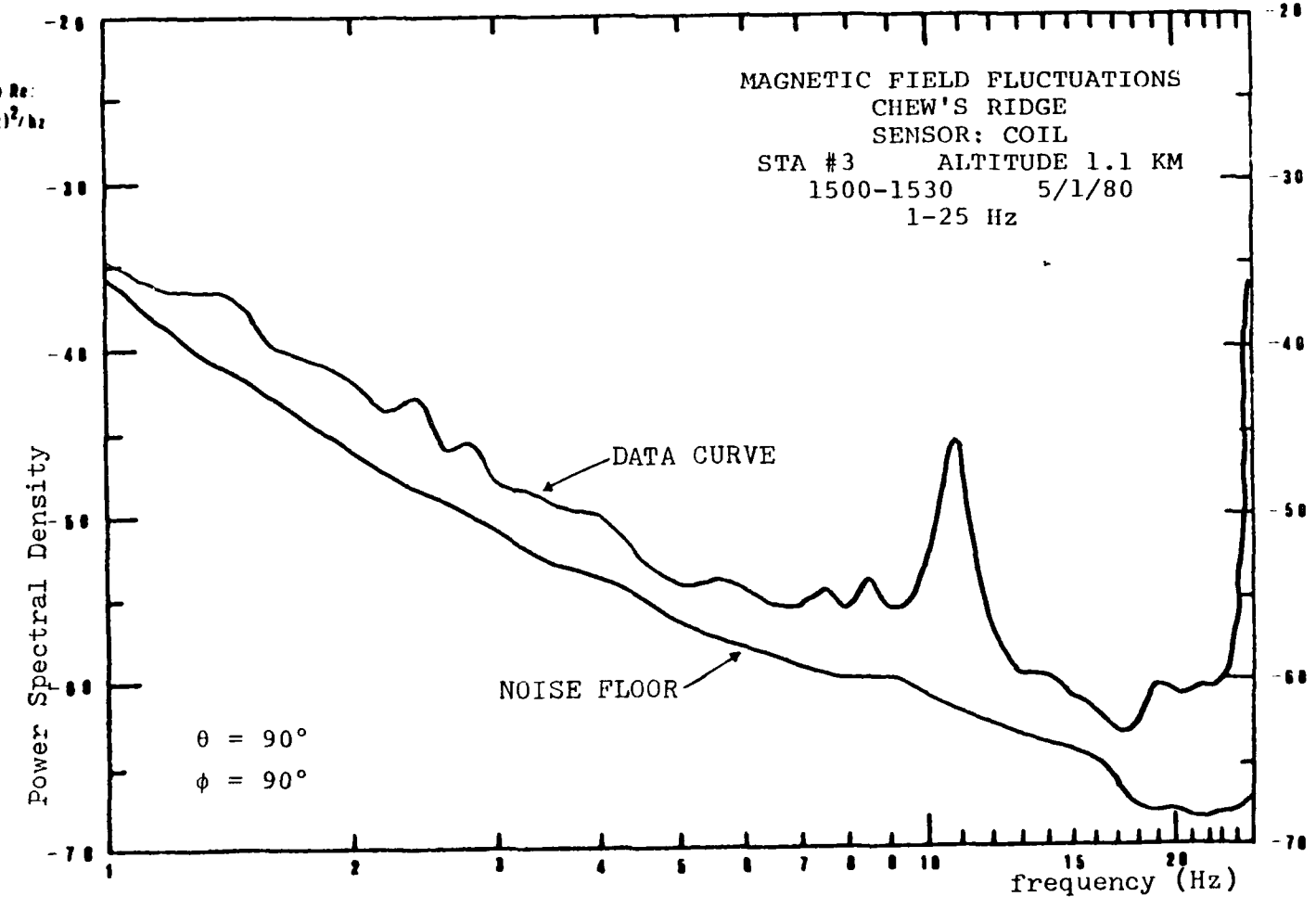
MAGNETIC FIELD FLUCTUATIONS
CHEW'S RIDGE
SENSOR: COIL
STA #3 ALTITUDE 1.1 KM
1500-1530 5/1/80
1-25 Hz
DATA CURVE
NOISE FLOOR
θ = 90°
φ = 90°
Power Spectral Density
frequency (Hz)

Figure 37

C. DISCUSSION AND CORRELATION OF DATA

Many variables influence the level of geomagnetic activity on the sea floor, thus, an unambiguous comparison with the sparce previous data is almost impossible. Three attempts at sea of three hours duration each were made with the coil's axis of symmetry directed upward in order to measure the vertical field component. The data gathered indicated that the geomagnetic activity in the vertical plane was below the noise level of the system. This agrees with theory which predicts that incident plane waves are refracted normal to the surface leaving only a component of the field in the horizontal plane in the sea. The data indicates that a small verticle component in the sea may still be present but was observed to be below preamplifier noise. Thus an upper limit on the vertical component of magnetic field fluctuations can be established as $10^{-3} nT^2/Hz$ at 1 Hz and $10^{-6} nT^2/Hz$ at 10 Hz.

It is also difficult to compare the fluctuations of the total magnetic field as obtained from a total field measuring system and a system which measures only one component of the field. Earlier data obtained with a Cesium magnetometer (Chaffee 1979) on the floor of Monterey Bay indicated that the 1 Hz fluctuations as measured in a 5 hour period were -30 dB referenced to 1 nT^2/Hz at a depth of 70 meters. The average value obtained with the coil on 18 April at 1 Hz was -28 dB referenced to 1 nT^2/Hz at a depth of 45 meters. This appears to be in very good agreement.

The most interesting frequency range observed was above 1 Hz. The level of geomagnetic activity was observed to be quiet between 1-6 Hz but became active at 9.6, 11.9, 16.5, and 19 Hz for the sea measurements. The land measurements indicated similar characteristics with predominant frequencies centered at 7.3, 10.7, and 24.9 Hz. Polk and Fitchen (1962) made measurements of the N-S, E-W horizontal magnetic components and showed that the fundamental mode of Schumann resonance is not constant in frequency with time. They were able to determine the spectral frequency range as 7 Hz to 11 Hz. The spectral frequencies at 7.3 Hz and 9.6 Hz as measured on land and in the sea respectively, correlate well with the fundamental Schumann resonance frequency.

The spectral frequencies of 10.7 Hz and 11.9 Hz as measured on land and in the sea respectively have the typical time development for Schumann resonances as reported by Polk and Fitchen. The second resonant mode should occur at 14 Hz as observed by Balser and Wagner (1960). Since the data in this research does not correlate well in frequency as a second resonant mode, but does indicate typical waveshapes for Schumann resonance, furthur investigation is recommended.

The 7.3 and 10.7 Hz spectral lines appeared to have different polarizations as different coil orientations produced varying levels of either frequency. This observation could not be established on the sea floor, as no control

over the angle with respect to North/South was available, but was quite evident in the land measurements. The 24.9 Hz spectral line was observed to increase toward the afternoon and was apparently independent of orientation. Furthur investigation of these frequencies is required to determine polarization as the methods utilized for determining orientation were inaccurate ($\pm$ 5°) but the data was still reproducable and quite convincing.

The sea floor data taken on 14 April was higher in magnitude than the data taken on the 18 April. In part this can be attributed to a higher A-index (9) on 14 April compared to an A-index (4) on 18 April. Internal and surface wave motion was higher on 14 April as evidenced by separation of the cable. No wave height correlation could be made, since a wave height measuring device was not available in the vicinity of the data gathering region.

V. EQUIPMENT/SYSTEM IMPROVEMENTS AND RECOMMENDATIONS

The system utilized for this project was well suited to a shallow sea water environment (200 meters). The system and equipment have been demonstrated to operate as conceived. To deploy this system in a deep ocean environment will require several modifications.

The following discussion on system improvements is presented as recommendations to make the system more reliable and usable in the ocean environment. The tape recorder is probably the single, major source of equipment troubles in the system. Although the record heads and capstan drive were meticulously cleaned and demagnetized, the recorded information still appeared noisy and distorted. The mixer circuit was able to attenuate and filter some of these distortions, but not to the degree that totally eliminated them. Initial investigation revealed that the longer the tapes, the more prominent the noise. Shorter tapes were utilized with some success. Further investigation revealed that the single capstan drive motor and associated circuitry were of inferior design and failed to adequately compensate for the changing tape reel speeds. As discussed in a previous section, the distortions were finally determined to be present at certain discrete frequencies.

Another obvious requirement for a more reliable recorder is the reduction of recording time brought about

by the shorter tapes. Even though digitizing the data would increase data gathering time, the present recording system's operation in this role is highly questionable. Therefore, it is recommended that this tape recorder be replaced by a more reliable instrument.

Coils used as sensors require less power to operate than the more complicated total field measuring magnetometers. However, coil type sensors have lower sensitivities (sensitivity is proportional to frequency) and are unable to measure the dc component of the earth's main field. The present coil size is restricted by the largest glass sphere, as discussed in Section III. The sensitivity of the sensor can be increased by increasing the area and/or the number of turns of the coil. However, this is not possible in the present system. Thus the sensor is limited in its capabilities to detect geomagnetic fluctuations because of its lack of sensitivity at low frequencies.

In addition, higher frequencies are attenuated more than lower frequencies in sea water (see Section II). Hence, the use of a coil in a deep ocean environment is questionable but not completely ruled out. Modifications to the preamplifier (to be discussed below) would increase the sensitivity of the system and, possibly make it quite feasible for deep ocean use. However, it is recommended that continued use of the present system be restricted to shallow water deployment or the system be redesigned for

land measurements. That is, a larger sensor be designed and constructed for increased sensitivity and used to gather geomagnetic fluctuations on land. If three such sensors were produced, then all components of the earth's magnetic field fluctuations could be measured. In addition, the polarization of the horizontal component could be further investigated by connecting two such coils and determining the coherence between the two measurements.

State of the art devices limit the design of a pre-amplifier which operates at low frequencies. In the present system, the noise figure of the preamplifier is 15 dB at one hertz. More recently an improved preamplifier has been designed and built by Dr. Alan Phillips whose noise figure is about 10 dB better. This improvement will greatly enhance the sensitivity of the system and make its use in a deep ocean environment more feasible.

In the present system, no means exist for determining the horizontal orientation of the sensor axis when deployed in the ocean. Observed data indicates that the horizontal component of geomagnetic field variations may be polarized. (See Section IV on discussion of data). It is recommended that an aiming device be designed and constructed so the exact orientation of the sensor is known when deployed in the ocean.

An improvement in the splicing of cable and connectors is recommended. Presently the Research Department at

the Naval Postgraduate School splices the connector pigtails to the cable and sphere penetrators. This method was satisfactory for shallow water employment, however, a more reliable method is required for deep ocean usage. It is recommended that cables, connector pigtails, and penetrators be commercially spliced for greater reliability.

Presently the only means of data correlation are with past data collected at the Naval Postgraduate School and the indices (see Section II) reported by Fredericksburg, Virginia. Since surface and internal ocean waves are known to be a source of field fluctuations, it is recommended that a wave gauge (various types are available) be purchased and utilized as another means of correlating geomagnetic variations.

It is recommended that the various electronic component chassis's be integrated into one or two units and a more practical method of connecting power be provided to enhance the system's compactness and increase its reliability.

APPENDIX A

EQUIPMENT SCHEMATICS

Numerous preamplifiers were tested and utilized during the extent of this project. Figure 38 was the most recent "State of the Art" amplifier which provided the quietest operation, i.e., greatest signal-to-noise ratio.

Figure 39 is the schematic for the mixer circuit used at the output of the analog cassette recorder for data analysis. Figure 40 is the 2 KHz oscillator reference signal generator used in the analog recording system to reduce tape "wow and flutter". Figure 41 is the VCO unit used in this experiment.

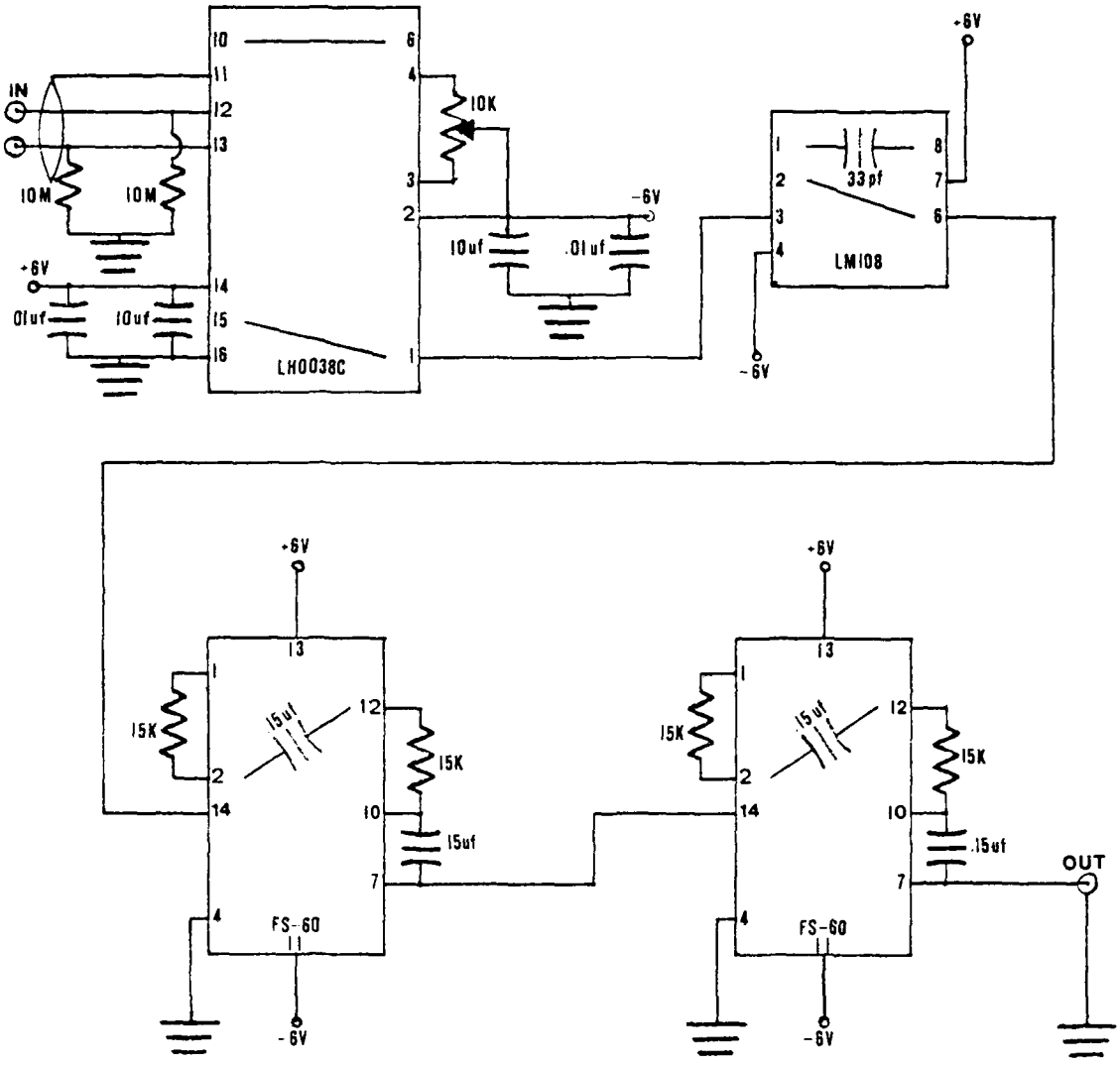

PREAMP

Figure 38

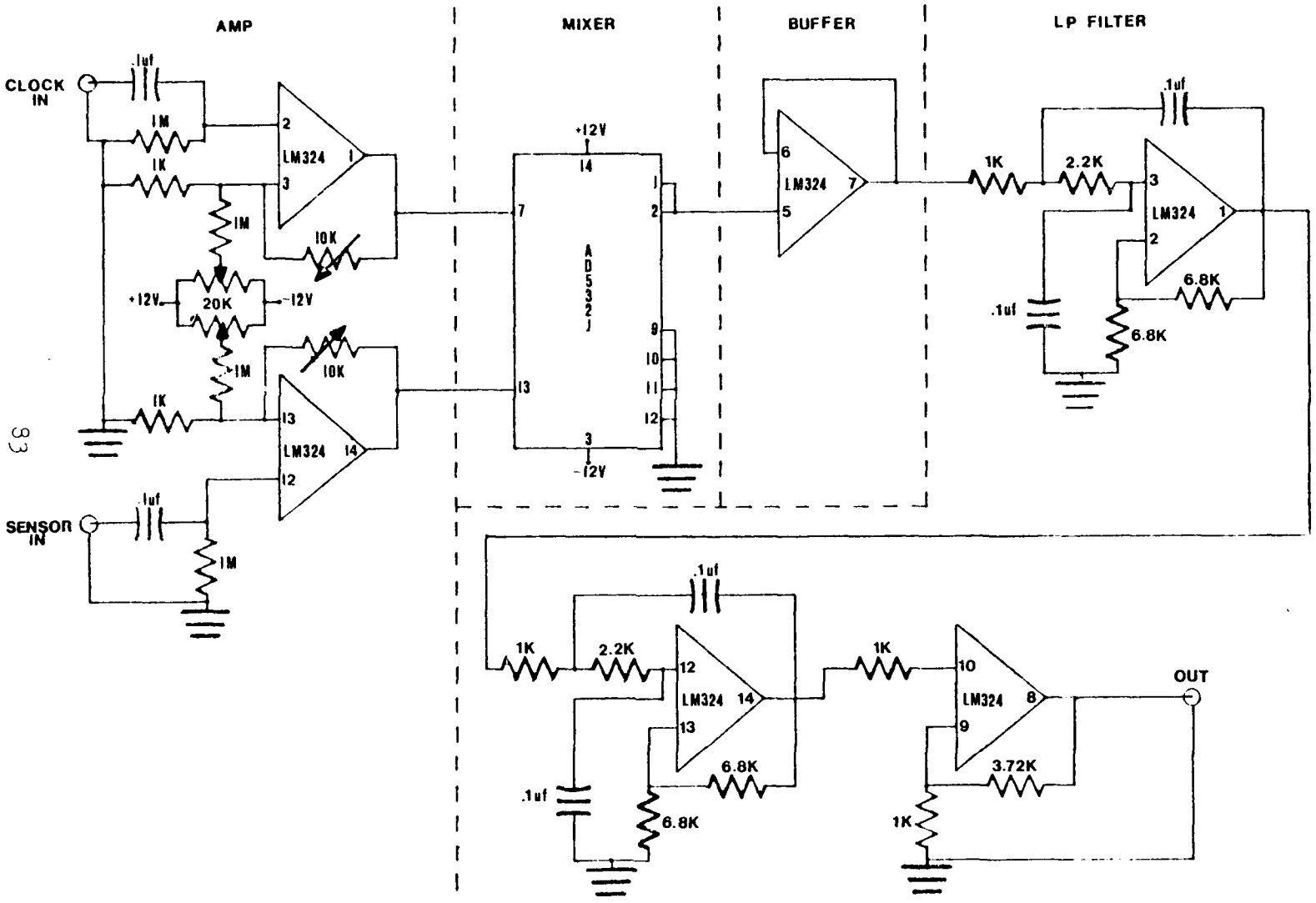

Figure 39

MIXER

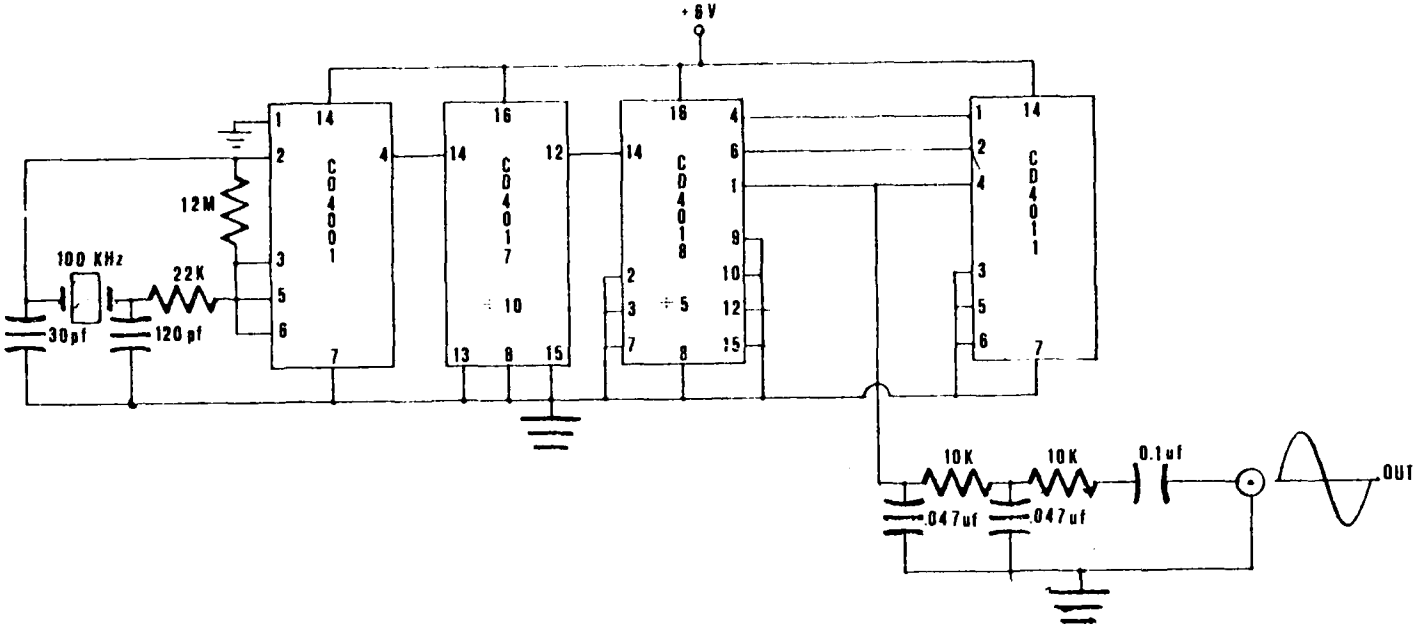

2KHz CLOCK

Figure 40

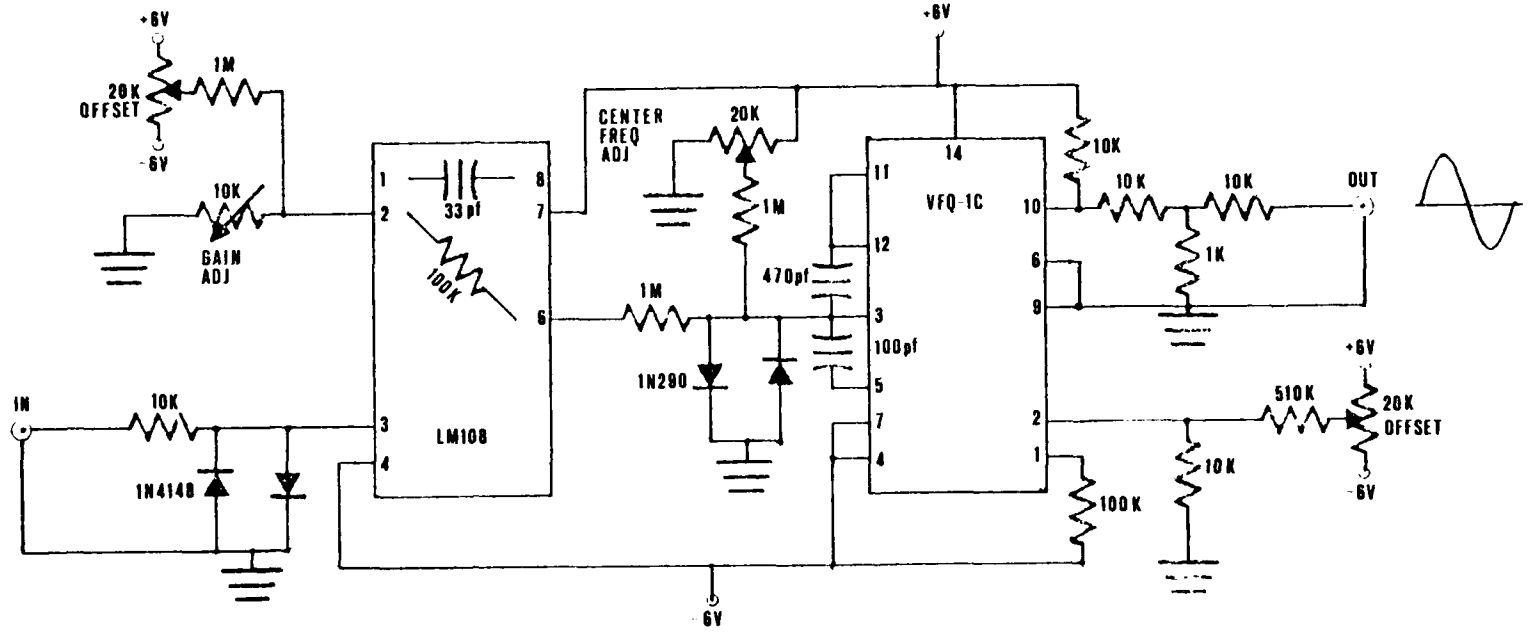

VCO

Figure 41

APPENDIX B

EQUIPMENT USAGE

Equipment utilized to measure, record, and analyze magnetic field fluctuations requires a certain amount of maintenance and handling. Below is a suggested list of hints which might help prevent equipment damage and prolong its usefulness.

A. Benthos glass spheres - much care should be exercised when handling the hemispherical shells because they are highly susceptible to chipping around the ground glass edges when exposed. The shell halves are serialized and appropriately marked for proper mating. When exposed to a deep water environment, the spheres are subjected to lower temperatures. Retreaval from the ocean depths results in the condensation of water. A heat gun may be necessary to dry the surfaces and return the spheres to ambient temperature. Temperature differences may also cause the glass housings to become vacuum locked. Evenly applied heat about the sphere surface will assist in releasing the vacuum.

The strip sealant used for sealing the shells should be applied on a meticulously cleaned surface at or near room temperature. Failure to properly seal the spheres will result in leakage and possibly, equipment damage. Toulene and alcohol are the recommended glass

cleaning solutions. Caution: Toulene is both toxic and poisonous. It should be applied with rubber gloves in a well ventilated area.

B. Electronic Equipment - of particular concern here is proper application of power supply voltages. Improperly applied voltages may result in integrated circuit and/or printed circuit board damage. The suggested application of dc power is to first, connect the non-common lead (s), being careful not to short the common lead against the equipment chassis, and finally, connect the common lead. Circuit power should not be applied unless there is a load on the input.

C. Portable Cassette Tape Recorder - The tape recorder heads and capstan drive should be cleaned and demagnetized after each recording. Failure to do this may result in noise spikes that could ruin a hard days work. It is also recommended that all tapes be "fast forwarded and rewound" before being utilized for data taking. High quality 60 minute tapes are recommended, since longer tapes appear to impose greater drag on this type recorder. Before sealing the instrumentation sphere, ensure the record button is depressed and the record levels are properly adjusted.

D. Voltage controlled oscillator (VCO) - the center frequency of the VCO should be adjusted to 1500 Hz prior to sealing the instrumentation sphere. This can be accomplished by adjusting the center frequency poteniometer with the input shorted.

E. Mixer - an amplifier stage is provided for the sensor and reference oscillator (clock) inputs to the mixer. With inputs from the clock and sensor, adjust the gain poteniometers for a 6-10 V peak-to-peak output difference frequency. A 6-10 V peak-to-peak output is necessary to drive the frequency-to-voltage converter. Verify that the output difference frequency is what it should be. Note that this procedure may have to be performed prior to each data analysis, since record levels may vary from one recording to the next.

F. Gelyte batteries - the batteries should be charged prior to taking data. Each battery is labeled and a record of charge is maintained in the laboratory. Presently there are 2 ampere-hour ratings being utilized in the system. The recommended charge procedure is:

18 ampere-hour: charge at 1 ampere for approximately 20 hours for full charge. Do not overcharge for more than 24 hours in excess of the ampere-hour rating.

2.6 ampere-hour: charge at 0.2 amp for approximately 15 hours for full charge. Do not overcharge for more than 24 hours in excess of the ampere-hour rating.

G. Connectors/cable: before and after each use in a corrosive environment, all connectors should be scrupulously cleaned to prevent deterioration. Alcohol and cotton-tipped applicators should be used. Further, all male connectors should be lightly lubricated with silicon grease to ensure

an adequate seal and prevent water intrusion. The locking sleeves on the connectors are there to prevent stress and are not part of the pressure system. The connectors are adequately marked and care should be exercised in mating them. The cable and connector pigtails should not be subjected to undue strains and sharp bends. Intermittent and/or complete signal loss may result as well as cable separation.

APPENDIX C

Geomagnetic Indices and Forecasts can be a valuable aid in data correlation and interpretation. In this Appendix we include an explanation of the type of geomagnetic information which is available on a weekly basis from NOOA (Boulder, Colorado) and which we have found to be very helpful in our research.

A UNITED STATES DEPARTMENT OF COMMERCE PUBLICATION

PRELIMINARY REPORT AND FORECAST OF SOLAR GEOPHYSICAL DATA

published daily

by the

[illegible]

SESC PRF 244
6 May 1970

Space Environment Services Center
Space Environment Laboratory, ERL
National Oceanic and Atmospheric Administration
Boulder, Colorado 80302

Basking in the warmth, feeding on its energy, planned by its originators, man ponders the mysteries of the sun.

NOAA-SESC photograph of Galen McFadyen atop Boulder's Flatiron Mountains by Joe Jasenik, December, 1968.

DESCRIPTIVE TEXT

Contents of

Preliminary Report and Forecast of
Solar-Geophysical Activity

1 May 1980

The Preliminary Report and Forecast of Solar-Geophysical Activity (PRF) is composed each Tuesday and issued the next day by the joint National Oceanic and Atmospheric Administration, Space Environment Laboratory (NOAA)/Air Force Air Weather Service (AWS), Space Environment Services Center (herein denoted as SESC), Boulder, Colorado 80303. It is a continuation of the series of weekly reports which began in 1951 and were issued jointly by the High Altitude Observatory and NOAA and its predecessors. The current series began with serial number PRF 001 on 09 September 1975.

This is a preliminary report based on data available at the time of publication and, therefore, cannot reliably be cited for reference purposes. It is intended for rapid distribution and of primary use to commercial and real time operations. Many of the data contained here are subject to later revision or refinement. There are no copyright or other restrictions in photocopying this report. Archival quality data, suitable for more extensive studies, are published in the monthly publication "Solar Geophysical Data" (SGD) available from the National Geophysical and Solar-Terrestrial Data Center (World Data Center A), Environmental Data and Information Service, Dó NOAA, Boulder, CO 80303. At a still later date, definitive publication for much of the data is made in the IAU Quarterly Bulletin of Solar Activity. Special reports are also issued from time to time by the World Data Center for Solar-Terrestrial Physics.

This report is made possible through the combined efforts of several groups providing data on a fast time basis. A complete list of data sources is given in Note 4 at the end of this descriptive text. Comments concerning the content of or possible improvements in the Report are invited.

Frontispiece

The frontispiece contains the title of the publication, publication number and date, and a photograph symbolizing man's dependence upon the radiative output of the sun. The photograph is a frame from the time-lapse 35 mm patrol movie taken with the hydrogen-alpha patrol telescope of the Space Environment Services Center in Boulder, Colorado. The photograph was taken December 9, 1968 by Joe Sutorik, chief solar observer, in collaboration with student observer and mountaineer Galen McFadyen. The two observers carefully charted the positions of the setting sun along the profile of the rugged Flatiron Mountains three miles west of the observatory and anticipated the date when the sun would set behind an accessible rock

A.

outcropping. On the selected date, Mr. McFadyen scaled the mountain and positioned himself so that his full figure would appear silhouetted against the sun.

First page

The first page summarizes the highlights of solar-geophysical activity during the past seven days and contains forecasts of expected activity during the next 27-day interval.

In the activity summary and forecasts, solar active regions are identified by the SESC-assigned region number, latitude, Carrington (heliographic) longitude, and modified Zurich region classification/ sunspot area in millionths of the solar hemisphere on the date of maximum sunspot area.

Significant solar activity is discussed in terms of the characteristics of the region of origin, x-ray classification of flares (C, M, or X), optical importance of flares (SN, 1B, etc.), radio emission, energetic particle emission, and geophysical effects. The characteristics of near-Earth proton events as detected by both satellites and ground-based sensors are discussed. Geomagnetic storms and disturbances are described. Observations of visual aurora are described when available. Whenever feasible, solar and geomagnetic activity will be summarized and forecast within the framework of the following routinely used terms:

Solar activity:

Very low - usually only quiet regions on the solar disk and no more than five of these; fewer than ten C-class subflares without important centimetric radio bursts or sudden ionospheric disturbances during a 24-hour period.

Low - usually more than five but less than ten quiet regions on the solar disk; only C-class subflares without important centimetric radio bursts or sudden ionospheric disturbances during a 24-hour period.

Moderate - eruptive regions on the solar disk; fewer than five M-class x-ray events with important centimetric radio bursts or sudden ionospheric disturbances during a 24-hour period.

High - active regions on the solar disk; several M-class x-ray events with important centimetric radio bursts and strong sudden ionospheric disturbances and/or one or two importance 2 chromospheric flares or X-class x-ray events during a 24-hour period.

B.

Very high - one or more regions on the solar disk capable of producing proton events; one or more chromospheric flares of importance 2 or greater with outstanding centimetric radio bursts (500 flux units above background, or greater), X-class x-ray events, and major sudden ionospheric disturbances observed or expected within a 24-hour period.

The x-ray classification of solar flares was initiated by the Space Environment Services Center on 01 January 1969. This classification attempts to classify solar activity by its energy output, and offers at least two distinct advantages compared to the standard optical classifications. It gives a better measure of the geophysical significance of a solar event, and it provides an objective means of classifying almost all geophysically significant activity regardless of its location on the solar disk or at (or beyond) the solar limb. The definitions of class C, M, and X events are based upon the peak x-ray flux in the 1 to 8 Ångstrom wavelength range, as follows:

Class	Peak 1-8Å flux (ϕ in watt m^{-2})	(ϕ in erg $cm^{-2}sec^{-1}$)
C	$\phi < 10^{-5}$	$\phi < 10^{-2}$
M	$10^{-5} \leq \phi < 10^{-4}$	$10^{-2} \leq \phi < 10^{-1}$
X	$\phi \geq 10^{-4}$	$\phi \geq 10^{-1}$

For descriptive purposes, a one digit number from 1 to 9 may be appended to these letter designations. The letter then acts as a multiplier. For example, a C3 burst indicates an x-ray burst with peak flux in the neighborhood of $3x10^{-6}$ watt m^{-2}. Similarly, an X5 event would indicate an x-ray burst with peak flux near $5x10^{-4}$ watt m^{-2}. This expanded classification is generally used only for description of events; forecasts are usually issued in terms of the broad C, M, and X categories. C0 designation may be used for events smaller than $1x10^{-6}$ watt m^{-2}.

Geomagnetic activity:

In the definitions of the following adjectives used to describe geomagnetic activity, A refers to the 24-hour A-index observed at a mid-latitude observatory such as Fredericksburg, VA; not the planetary A-index, Ap. The K-indices are, likewise, mid-latitude values.

Quiet = $A \leq 7$, usually no K-indices > 2.

Unsettled = $7 < A < 15$, usually no K-indices > 3.

Active = $15 \leq A < 30$, a few K-indices of 4.

Minor storm = $30 \leq A < 50$, K-indices mostly 4 and 5.

Major storm = $A \geq 50$, some K-indices 6, or greater.

C.

Sudden commencements are indicated by beginning times given to the nearest minute. Gradual commencements are indicated by beginning times to the nearest hour.

Immediately following the summary of activity and the forecasts is a computer-generated display of classical solar-geophysical indices for the dates indicated. The column headings are defined as follows:

OTT 2800 MHz: The Ottawa NRC 10 centimeter (2800MHz) radio flux observed at approximately 1700Z on that date.

SSP NBR: The official SESC sunspot number reported for that date in the Joint USAF/NOAA Solar Region and Activity Summary issued at 0200Z the next day by SESC. Sunspot reports are received daily from as many as half a dozen observatories. The SESC staff reviews these reports and forms a composite picture of each individual region, taking into account such factors as the time of observation and the quality of seeing. The composite information for all regions is then incorporated in the 0200Z message. The sunspot number is computed according to the formula R=10G+N where G is the number of sunspot groups (regions) and N is the total number of individual spots comprising all groups. A sunspot number of zero indicates there were no visible sunspots on that date, while a blank indicates that no observations were possible.

Fredericksburg and Anchorage A- and K-indices: The daily 24-hour A-index and 3-hourly K-indices from the Fredericksburg VA (mid-latitude) and Anchorage AK (high-latitude) stations monitoring the Earth's magnetic field. K-indices range from 0 (very quiet) to 9 (extremely disturbed). A-indices range from 0 (very quiet) to 400 (extremely disturbed) with an A-index of 30 or greater, indicating geomagnetic storm conditions.

Additional pages

Additional pages are included in the Preliminary Report as solar activity requires, and are comprised of computer-generated displays which are described below in their normal sequence. The sequence and page numbering may vary occasionally depending upon the level of activity, reports of special events, or the inclusion of data for past days which could not be published at the usual time.

Alerts Issued This Week

A summary of all events which exceeded the SESC alert thresholds during the previous week. Listed are the dates, times and the activity that resulted in the issuance of the alert. This summary will enable alert customers to have a complete listing of alerts and may adequately fill the needs of some customers currently contacted by telephone.

D.

AD-A092 399 NAVAL POSTGRADUATE SCHOOL MONTEREY CA F/G 8/14
LOW FREQUENCY GEOMAGNETIC FLUCTUATIONS (.04 TO 25 HZ) ON LAND A--ETC(U)
JUN 80 G R MCDEVITT, B B HOMAN

UNCLASSIFIED NL

2 OF 2
AD
A092 399

END
DATE FILMED
8 1
DTIC

Weekly Energetic Event Summary

A summary of all energetic (x-ray intensity greater than or equal to $1x10^{-5}$ watt m^{-2}) events occurring during the seven days preceding the Report composition date. Reported are:

Month and Day: Date event occurred.

Begin, Maximum and End: Begin, maximum and end times of the x-ray burst. The begin time is often well defined due to the impulsive beginning of most flare associated x-ray events. In the past, x-ray events were ended when the flux levels decayed to a point halfway between the maximum level and the pre-flare background level. This definition occasionally resulted in unterminated events. For operational purposes the end time of an x-ray burst is now determined by both the peak flux and the decay rate. An X-class event is ended when flux levels decay to less than M5 levels and remain stable for a minimum of four minutes or when flux levels decay to less than the M1 level, regardless of stability. All bursts smaller than X-class are now ended when flux levels decay to the C5 level or when flux levels decay to a point halfway between the maximum level and the pre-flare background level and remain stable for a minimum of four minutes. The typical x-ray signature dictates that the end time of a burst will be less well defined than the begin time.

X-ray Class: As defined earlier in this descriptive text.

OPT: Optical information (if available) as follows:

Type of Activity:
- FLA - Solar flare
- EPL - Eruptive prominence on the solar limb
- BSL - Bright surge on the limb
- SPY - Spray (including ejecta)
- LPS - Loops
- DSF - Disappearing solar filament
- UNK - Unknown activity

Importance:
- S = Subflare
  area < 2.0 square degrees
- 1 = Importance 1
  2.0 ≤ area ≤ 5.1 square degrees
- 2 = Importance 2
  5.2 ≤ area ≤ 12.4 square degrees
- 3 = Importance 3
  12.5 ≤ area ≤ 24.7 square degrees
- 4 = Importance 4
  24.8 ≤ area in square degrees

E.

Brightness qualifiers F, N or B are generally appended to the importance character to indicate Faint, Normal or Brilliant, respectively.
Location: Flare location in heliographic coordinates.
Region: SESC-assigned region number.

Radio: Flux unit peak value above pre-burst background of associated radio bursts at frequencies of 245, 415, 606, 1415, 2695, 8800 and 15400 MHz.
1 Flux Unit = 10^{-22} watt m^{-2} Hz^{-1}.

Sweep: Sweep frequency radio event associated with the energetic event, as follows (generally only II, IV and CTM are reported:

Type:
- I - Noise storm
- II - Slow drift burst
- III - Fast drift burst
- IV - Broad-band smooth continuum burst
- V - Brief continuum burst generally associated with Type III bursts
- CTM - Long-lived continuum associated with storms of Type IV bursts
- STM - Storm of Type III bursts
- MWB - Short microwave continuum
- SDF - Decimeter slow drift burst

Importance: Relative importance on a scale of 1 to 3. An importance 1 sweep event would be considered small or minor. An importance 3 event is a major or significant event.

SID: Sudden Ionospheric Disturbance information, as follows:

Type: SWF - Short-wave fadeout
Frequency: Highest frequency SWF was detected.
Importance: Subjective measurement of the relative importance of the event on a scale of 1 to 3 (much the same as already described for sweep frequency radio events).

Flare List

A listing of solar flares (optical importance and/or x-ray class) reported during the previous seven days. The list has been edited on a daily basis by the duty solar forecaster to delete multiple reports of the same event. Criteria used in determining which report, or combination of reports, will be used include: Quality of the observation (observing conditions, was flare observed in its entirety?), type of report (real time or film review), and the consensus of reporting observatories. The list includes the following information:

F

Month and Day: Date event occurred.

Begin, Maximum and End: Begin, maximum and end times of the optical flare. If the start of the flare was not observed, a "B" is appended to the begin time indicating the flare started "Before" that time. If the maximum was not observed, the space is left blank. If the end of the flare was not observed, an "A" is appended to the end time indicating the flare ended "After" the end time.
Location: Flare location in heliographic coordinates.
IMP: Importance of the optical flare, as defined earlier in this descriptive text.
REG: SESC-assigned region number or left blank for unassociated x-ray events and for flares which occasionally occur in undefined regions.
Class: Denotes x-ray class of the event according to the C, M and X classification described earlier in this descriptive text.

Weekly Region Summary

A summary of all regions visible on the solar disk during the previous seven days. Each date's assessment of a region is based upon observations made during the 24-hour UT day and the location is corrected to 2400Z on the date indicated.

This summary information is compiled from the Joint AFGWC/SESC Solar Region and Activity Summary which is a composite picture of each region from all sunspot reports received at Boulder during the UT Day. The Weekly Region Summary contains the following information:

MO and DA: Month and day

Region Location: Location of the "midpoint of the latitudinal and longitudinal extremeties" of the white-light sunspot group in heliographic coordinates at 2400Z on the date reported. The position of the center of H-alpha plage associated with the region is given if sunspots were not visible.

Sunspot: Sunspot information is as follows:
Area: Total area of the region's sunspots in millionths of the solar hemisphere.
Z: Modified Zurich (McIntosh) three letter (Zpc) classification as follows:

Z = Modified Zurich Brunner classes, A through H
p = Penumbra type of largest spot in group: x - no penumbra, r - rudimentary, s - small symmetric, a - small asymmetric, h - large symmetric, and k - large asymmetric
c = Relative sunspot distribution or compactness of group: x - single spot, o - open, i - intermediate, and c - compact

G.

NR: Total number of individual sunspots in the group or region.

MAG: Magnetic classification, as shown below:

A = Alpha (single polarity spot)
B = Beta (bipolar spot configuration)
G = Gamma (atypical mixture of polarities)
BG = Beta-Gamma (mixture of polarities in a dominantly bipolar configuration)
BD = Beta with Delta configuration
BGD = Beta Gamma with a Delta configuration
D = Delta (opposite polarity umbrae within single penumbra)

H-Alpha Plage: Indicates no sunspots visible but region still visible in H-alpha spectroheliograms.

Calcium: Calcium spectroheliogram data from Manila, Philippines, as follows:

Area: Total region area of calcium plage in millionths of the solar hemisphere.

BRT: Calcium plage brightness on a subjective scale of 1.0 (low) to 5.0 (high).

Blank space indicates no calcium plage report available for that region on that date.

Flares: Tabulation of the number of C, M and X-Class x-ray bursts, number of subflares and number of importance 1, 2 and 3 flares observed on that date.

At the bottom, the average Carrington longitude of the region and the x-ray burst and flare totals are listed. Finally, a comment on the fate of the region is included. This indicates whether the region crossed over the solar limb, died on the solar disk, or was still an active region on the disk at the end of the reporting period.

Boulder Geomagnetic Substorm Log

This is a tabulation of substorm occurrences as observed by ground magnetometers in the North American International Magnetospheric Studies (IMS) network. This network is comprised of twenty-six stations; extending from north of the auroral oval to the equatorial zone. A substorm is a localized geomagnetic disturbance which usually occurs near local midnight and is restricted in longitude. However, the current systems developed during a substorm may affect ground magnetometers in the entire nighttime sector. Additionally, individual substorms may occur at local times, away from midnight, and may be as large as 24 hours (global) in longitudinal extent. By noting the time, location and scale of a substorm; one may estimate the effect of a substorm at a specific location. Among the many substorm effects are ionospheric effects (which influence radio communications) and telluric effects (which may disturb long distance electric power and communications systems). The familiar aurora is a visible manifestation of the geomagnetic substorm.

H.

Currently, the Log provides the date, onset time (UT) and direction (from Boulder) of each substorm. The direction is listed as "east", "west" or "centered" (at Boulder's geomagnetic longitude). The comment section further describes the geomagnetic field for a particular day. Occurrences such as sudden commencements (sc), sudden impulses, magnetic storm periods, multiple substorms and substorm (relative) strengths are included.

Recent Monthly Solar Indices (Preliminary)

This is a listing of monthly preliminary solar indices for the past year (updated within one week after the end of each month). The daily sunspot numbers appearing on the first page of the Report, which are a consensus of observations from as many as half a dozen observations, are simply averaged and is reported as "SESC Observed".

Official Zurich sunspot numbers are reported as "Zurich" as they become available. The ratio of Zurich to SESC sunspot numbers are listed under "Ratio Zurich/SESC"; these can be used to determine an SESC "k" (correction) factor. In order to provide the best early estimate of the Zurich sunspot number, e.g. near the end of the month when the number is not yet available, an SESC corrected number will appear in parentheses in the "Zurich" column.

The monthly mean value of 10.7 centimeter radio flux (1 flux unit = 10^{-22} watt m^{-2} Hz^{-1}) is listed for comparison with monthly mean sunspot numbers for comparable periods. These radio flux values have been adjusted to 1 A.U., except where values appear in parentheses. Parenthetical values are the average of the daily values transmitted to SESC in real time. Adjusted values are those which appear in Solar Geophysical Data (SGD).

Special pages

To some extent the Preliminary Report is regarded as an experimental publication by the NOAA/SEL Space Environment Services Center. The Center publishes new data, often on a trial basis; within the following limitations:

1. There must be reason to believe that new data will be of interest to a broad range of Report subscribers.
2. Inclusion of new data must not have a substantial impact on the costs of producing the Report (as would, for example, publication of photographs).

Some items added to the Report are of a "one-time-only" nature. Among these are special drawings, descriptions or reports of unusual solar-geophysical features or events. Other data forms, such as the tabulation of monthly mean sunspot numbers, are candidates for permanent inclusion in the Report. Because a full discussion of special items is not possible in this descriptive text; explanations will accompany new data forms. Subscribers are encouraged to comment on the utility of various new data provided in the Report. Suggestions regarding new items to be placed in the Report will be carefully considered.

SMS/GOES X-ray and Particle Plots

The Synchronous Meteorological Satellites (SMS-1 launched in June 1974 and SMS-2 launched in February 1975) and the Geostationary Operational Environmental Satellites (GOES-1 launched in October 1975, GOES-2 launched in June 1977 and GOES-3 launched in June 1978) carry 0.5 - 4Å and 1 - 8Å solar x-ray detectors and seven proton sensors covering the range 0.8 to 500 MeV. These sensors, as well as a number of other sensors, are currently monitored continuously (except during eclipse periods) in real time by the NOAA/SEL Space Environment Services Center in Boulder. GOES-2 and GOES-3, in geostationary orbit at 110° West and 135° West, respectively, are now in use; and SMS-1 and -2 and GOES-1 are in standby mode.

Preliminary graphs of SMS/GOES x-ray and proton data are printed in the Report as solar activity warrants, with noteworthy x-ray events being generally more frequent than solar protons events.

The top line of the display identifies the satellite, the sensors, and the traces, as follows:

Satellite:	Either GOES-1 or GOES-2
Sensors:	Either XRA (x-ray) or EPS (energetic particles)
Traces:	XRA_____(line) 1 - 8Å
	.....(points) 0.5 - 4Å
	EPS_____(line) Flux > 10 MeV

The second line indicates the date and time of the start of the plot. The number appearing in parentheses, either (1) or (5) indicates whether the plots are based on 1-minute or 5-minute averages of the data.

The ordinate units of the XRA plots are in watt m^{-2} and the corresponding C, M and X x-ray classification threshold is labelled on the right margin of the plot. The ordinate units of the EPS plots are in P cm^{-2} sec^{-1} $ster^{-1}$. The abscissa is a time scale in minutes or hours, indicating the time elapsed since the beginning of the plot at the specified start time.

Bad data have been deleted wherever possible.

Last page

The last page contains the current preliminary H-alpha synoptic chart. These maps depict the large-scale distribution of solar magnetic fields as inferred from the positions of filaments (cross-hatched), plage corridors (solid lines through stippled areas), filament channels (solid lines outside active regions) and sunspots (large dots, drawn very schematically). The stippled areas represent the H-alpha plages. Dashed lines are interpolations and estimates required to obtain consistency with polarities and patterns observed on previous solar rotations. The numbers identify active regions. The "plus" and "minus" signs indicate the polarity of the solar magnetic field. The heliographic latitude is given along the left-

and right-hand side of the map, the Carrington longitude is printed along the bottom, and the date of the central meridian passage of a given longitude appears at the top. Some portions of the maps may be inaccurate; however, every effort is made to correct and refine the maps as more detailed study and comparison of time sequences of H-alpha photographs and solar magnetograms permit. Edited charts for complete Carrington rotations appear later in Solar Geophysical Data (SGD).

Notes:

1. All times used within the Preliminary Report are Universal Times or Greenwich Mean Times (as indicated by UT, GMT or Z).

2. The highlights on the first page and all data listings cover the seven-day period Monday through Sunday. The 27-day forecast period begins on the following Wednesday.

3. All data listings are prepared by computer. Occasionally, inaccurate data will be reported and included. SESC appreciates notification of any questionable data.

4. The following are observatories whose reports are included in the SESC data base and utilized for preparing the Preliminary Report and Forecast of Solar-Geophysical Activity:

K.

STATION	WMO ID	URSI ID	LOCATION
Anchorage, Alaska, USA	70273	25601	N61 W150
Athens, Greece	16716	32401	N38 E 23
Boulder, Colorado, USA	72469	20401	N40 W105
College, Alaska, USA	-----	25602	N64 W147
Culgoora, Australia	-----	85303	S30 E149
Ft. Yukon, Alaska, USA	70194	-----	N67 W145
Fredericksburg, Virginia, USA	72405	18403	N38 W 77
GOES-2 (USA satellite)	-----	-----	W109 geostationary
GOES-3 (USA satellite	-----	-----	W135 geostationary
Hiraiso, Japan	-----	44401	N36 E141
Holloman AFB, New Mexico, USA	72269	21305	N33 W106
Irkutsk, USSR	30710	40501	N52 E104
Kitt Peak, Arizona, USA	-----	21304	N32 W111
Learmonth, Australia	94302	81202	S22 E114
La Posta, California, USA	72287	22301	N34 W118
Manila, Philippines	98429	42101	N14 E121
McMath Obs., Pontiac, Michigan, USA	72537	18404	N42 W 83
Moscow, USSR	27612	34502	N55 E 37
MSFC (Huntsville), Alabama, USA	-----	19301	N35 W 87
Ottawa, Canada	72628	18406	N45 W 76
Palehua, Hawaii, USA	91178	26204	N21 W158
Poitiers, France	07335	30511	N46 E 0
Ramey, Puerto Rico	78514	17201	N18 W 67
Sacramento Peak, New Mexico, USA	-----	21301	N32 W105
Sagamore Hill, Massachusetts, USA	72509	17401	N42 W 70
Sheep Mountain, Alaska, USA	70269	-----	N62 W148
Sydney, Australia	94768	85304	S34 E151
Thule, Greenland	04202	17801	N76 W 68
Tokyo, Japan	47662	44406	N36 E140
Vostok, Antarctica	89606	81801	S78 E105

L.

SUMMARY OF SERVICES FROM THE NOAA SPACE ENVIRONMENT SERVICES CENTER

* The weekly publication "Preliminary Report and Forecast of Solar and Geophysical Activity." A summary of activity indices and event data for the preceding week and a prediction for the next 27 days.

* A tape recorded message of solar and geophysical activity and indices for the most recent 24 hours and for the next 24 hours. Telephone numbers are: Commercial: (303) 499-8129 or FTS: 323-3235.

* A 40-second message with similar information on WWV at 18 minutes past each hour.

* Primary Report of Solar and Geophysical Activity issued each day at 2200UT. Contains activity summary, solar and geomagnetic activity indices for previous 24 hours and predictions for the next 72 hours. Available by teletype with recipient expected to pay cost of transmission.

* HF Radio Propagation Report issued each day at 0600UT (with secondary messages at 0000UT, 1200UT, 1800UT). Distribution is also by teletype with recipient expected to pay costs.

* Direct inquiries to the duty forecaster (0700 to midnight, seven days per week, Mountain Time). Call (303) 499-1000 extension 3171 or FTS 323-3171 (We do not accept collect calls).

* Event notification by phone or Teletype. Persons or organizations requiring immediate notification of the prediction or occurrence of various solar geophysical phenomena are contacted when their alert thresholds are met.

* Direct access to the SELDADS (Space Environment Laboratory Data Acquisition and Display System). Using standard computer terminals, customers may access the SELDADS and obtain printouts of solar, interplanetary and geomagnetic variations data.

Descriptive leaflets of each of these are available. For more information, please write to:

Space Environment Services Center
NOAA R43
325 Broadway
Boulder, Colorado 80303, USA

The Space Environment Services Center is a real time service organization for serving those people needing real time or near-real-time operational support. If you need archival data for research studies, you should write to:

National Geophysical and Solar-Terrestrial Data Center
Environment Data Services
D6 NOAA
325 Broadway
Boulder, Colorado 80303, USA

M.

APPENDIX D

TRANSFER FUNCTION USAGE

The spectrum analyser when in the dBV display mode reads:

$$N(dBV)=20\log \frac{A \text{ volts}}{1 \text{ volt}} .$$

0 dB referenced to 1 nT and not 1 volt is desired. Thus:

$$\left(\frac{A \text{ volts}}{1 \text{ volt}}\right)\left(\frac{X \text{ volts/nT}}{X \text{ volts/nT}}\right)=\left(\frac{A \text{ volts}}{X \text{ volts/nT}}\right)\left(\frac{X \text{ volts}}{1 \text{ volt nT}}\right)$$

where B (the field measured by the system) is:

$$B=\left(\frac{A \text{ volts}}{X \text{ volts/nT}}\right)$$

so referenced to 1 nT we have:

$$N(dB)=20\log \frac{B}{1 \text{ nT}} + 20\log X .$$

X is the system transfer function given in units of volts/nT. Since spectrum analysers use various averaging windows and have various numbers of bins the following correction must be applied:

$$B^2=\Phi(BW),$$

and:

$$(BW)=\left(\frac{\text{frequency range}}{\text{number of bins}}\right)\left(\frac{\text{window}}{\text{correction}}\right).$$

Now we have:

$$N(dB)=20\log[\Phi^{1/2}(BW)^{1/2}]+20\log x$$

and finally after rearranging:

$$10\log\Phi = N(dB) - 20\log X - 10\log(BW) \ ,$$

where $10\log\Phi$ is the corrected reading or the power spectral density. Φ has the units of nT^2/Hz.

LIST OF REFERENCES

1. Balser, M. and Wagner, C.A., Observations of Earth-Ionosphere Cavity Resonances, Nature, v. 188, p. 638, 1960.

2. Barry, J.M., Power spectra of Geomagnetic Fluctuations Between 0.1 and 10 Hz, M.D. Thesis, Naval Postgraduate School, Monterey, 1978

3. Bitter, F., Currents, Fields, And Particles, 2d ed., p. 226-229, Technology Press of M.I.T. and Wiley, 1956.

4. Campbell, W.H. and Matsushita, S., Physics of Geomagnetic Phenomena, v. 1,2, Academic Press, 1967.

5. Chaffee, E.J., Low Frequency Geomagnetic Fluctuations (.01 to 3 Hz) On The Floor of Monterey Bay, M.S. Thesis, Naval Postgraduate School, Monterey 1979.

6. Clayton, F.W., Power Spectra of Geomagnetic Fluctuations Between 0.1 and 40 Hz, M.S. Thesis, Naval Postgraduate School, Monterey, 1979.

7. Davidson, M.J., Average Diuranl Characteristics of Geomagnetic Power Spectrums in the Period Range 4.5 to 1,000 seconds, Journal of Geophysical Research, v. 69, p. 5116, 1964

8. Fitchen, F. and Polk, C., Schumann Resonances of the Earth-Ionosphere Cavity - Extremely Low Frequency Reception at Kingston, R.I., Journal of Research, v. 660, p. 313, 1962.

9. Fraser-Smith, A.C., Prediction of Geomagnetic Activity (Abstract), EOS Trans. AGU, v. 53, p. 1106, 1972.

10. Fraser-Smith, A.C., Short-Term Prediction and a New Method of Classification of Pc 1 Pulsation Occurances, Paper Prepared for Radioscience Laboratory, Stanford Elec. Lab., Stanford University, Ca., December 1979.

11. Fraser-Smith, A.C. and Buxton, J.L., Superconducting Magnetometer Measurements of Geomagnetic Activity in the 0.1 to 14 Hz Frequency Range, Journal of Geophysical Research, v. 80, n. 22, p. 487, 1962

12. Horton, C.W. and Hoffman, A.A.J., Magnetotelluric Fields in the Range .03 to 7 cycles per kilosecond, 1, Power Spectra, J. Res. Nat. Bur. Stand. Sect. D, v. 66, p. 487, 1962.

13. Jacobs, J.A., Geomagnetic Micropulsations, p. 179, Springer, New York, 1970.

14. Jefimenko, O.D., Electricity and Magnetism, Appleton-Century-Crofts, p. 346, 379-380, 1966.

15. Larsen, T.R. and Egeland, A., Fine Structure of the Earth-Ionosphere Cavity Resonances, Journal of Geophysical Research, v. 73, p. 4986, 1968.

16. Lee, D.T. and Fraser-Smith, A.C., Long-Term Prediction of Pc 1 Geomagnetic Pulsation Occurences, Planetary and Space Science, v. 23, p. 431-436, 1975.

17. Matveyeva, E.T., Troitskaya, V.A., and Gul'Elmi, A.V., The Long-Term Statistical Forecast of Geomagnetic Pulsations of Type Pc 1 Activity, Planetary and Space Science, v. 20, p. 637, 1972.

18. Maxwell, E.L., and Stone, D.L., Natural Noise Fields From 1 cps to 100 kc, IEEE Trans. Antennas Propagat, v. 11, p. 339, 1963.

19. Santirocco, R.A. and Parker, D.G., The Polarization and Power Spectrums of Pc Micropulsations in Bermuda, Journal of Geophysical Research, v. 68, p. 5545, 1963.

20. Skilling, H.H., Fundamentals of Electric Waves, p. 80, Krieger, New York, 1948.

21. Westerlund, S., Preliminary Results of Magnetotelluric Soundings in the Range .01-10,000 Hz, Rep. 706, Kiruna Geophys. Obs., Kiruna, Sweden, December 1970.

INITIAL DISTRIBUTION LIST

		No. Copies
1.	Defense Technical Information Center Cameron Station Alezandria, VA 22314	2
2.	Library, Code 0142 Naval Postgraduate School Monterey, CA 93940	2
3.	Department Chairman, Code 61 Department of Physics and Chemistry Naval Postgraduate School Monterey, CA 93940	1
4.	Professor O. Heinz, Code 61Hz Department of Ph sics and Chemistry Naval Postgraduate chool Monterey, CA 93940	2
5.	Professor Paul H. Moose, Code 61Me Department of Physics and Chemistry Naval Postgraduate School Monterey, CA 93940	2
6.	LT Robert M. Santos USN SMC 1164 Naval Postgraduate School Monterey, CA 93940	1
7.	LT Gary M. McKinley USN SMC 2039 Naval Postgraduate School Monterey, CA 93940	1
8.	Master Research Vessel Acania Coast Guard Piers Monterey, CA 93940	1
9.	LT B. Bert Homan 179 Wells Rd. Orange Park, FL 32073	1
10.	LCDR Gerald R. McDevitt USN Personnel Support Activity Detachment Point Loma 140 Sylvester Rd San Diego, CA 92106	1

11. Dr. A.C. Fraser-Smith — 1
Radio Science Laboratory
Stanford Electronics Laboratories
Stanford University
Stanford, CA 94305

12. Chief of Naval Research
Department of the Navy
800 North Quincy Street
Arlington, VA 22217
Code 100C1 — 1
Code 460 — 1
Code 464 — 3
Code 480 — 1

13. Commanding Officer — 1
Office of Naval Research Branch Office
1030 E. Green Street
Pasadena, CA 91106

14. Director — 1
Naval Research Laboratory
Code 2627
Washington, D.C. 20350

15. Office of Research, Development, Test, and Evaluation — 1
Department of the Navy
Code NOP-987J
Washington, D.C. 20350

16. Director — 1
Defense Advanced Research
Projects Agency
1400 Wilson Boulevard
Arlington, VA 22209

17. Air Force Office of Scientific Research — 1
Department of the Air Force Directorate of Physics (MPG)
Building 410
Bolling Air Force Base
Washington, D.C. 20332

18. Army Research Office — 1
Department of the Army
Geosciences Division
Box 12211
Research Triangle Park, N.C. 27709

19. William J. Andahazy 1
Department of the Navy
Naval Ship Research and Development
Center
Annapolis Laboratory
Annapolis, Maryland 21402

20. Roger Booth 1
Arms Control and Disarmament Agency
MA/AT
The State Department
Washington, D.C. 20451